Tracing the Distribution of Heavy Metals in Sediments of the Pearl River Estuary

WOODS, ASHLEY,MARTIN

Tracing the Distribution of Heavy Metals in the Sediments of the Pearl River Estuary

by Ashley Woods

Thesis submitted for the degree of:

Master of Science (by research) in Geography

Durham University

Department of Geography

November 2009

Declaration

This thesis is the result of my own work. Data from other sources which are referred to in this thesis are acknowledge at the appropriate point in the text.

Abstract

The Pearl River Delta is the socio-economic hub of southern China. The region has experienced rapid industrialisation, particularly since the start of the Chinese Reform Programme in 1979. This rapid industrial development has been coupled with increased pressures on the natural environment environment from pollution and waste associated with this development. These pollutants are transported from within the Pearl River catchment and deposited in sediments of the Pearl River Estuary (PRE).

Geospatial and principal component analysis of the heavy metals Al, Cd, Co, Cr, Cu, Fe, Ni, Pb, Ti and Zn in surface sediments identifies four patterns of spatial distribution that are attributed to three separate heavy metal sources. After normalisation for the effects of the fine particle size affinity, the same spatial distribution patterns remain, but with much less localised variability. Anticlockwise estuarine circulation and the interaction of marine and river water, where distributaries of the North and West Rivers enter the PRE, account for higher concentrations of all metals except Al in the west of the estuary. Pb and Zn are identified as the heavy metals displaying significant enrichment from non-natural sources. Their concentrations which peak at 168 and 699.9mg/Kg respectively along the North River, are found to be associated with higher baseline concentrations resulting from the erosion of metal sulphide bearing carbonates within the catchment. These higher baseline concentrations have then been further enriched by Galena (PbS) and Sphalerite (ZnS) mining operations, atmospheric deposition from fossil fuel burning and some point sources associated with urban and industrial waste.

Temporal analysis of heavy metals and stable Pb isotope variability again highlights Pb and Zn as being significantly enriched from anthropogenic sources, with maximum enrichment factors of 2.6 and 1.8 respectively. The enrichment of these two metals is shown to begin in the 1950s and acceleration of their enrichment in the early 1990s. This second phase of enrichment in the 1990s is also associated with slight enrichment of Cr, Cu and Ni that is also attributed to anthropogenic sources.

Acknowledgements

First and foremost I would like to thank my supervisors Cheng and Jerry who gave up a lot of their time and provided invaluable guidance throughout my research. I would also like to thank Martin and Amanda in the labs for all their help with HF digests and running of my samples through the various machinery. Thanks to Chris and Nima who gave me some invaluable help when programming Matlab computations.

I would also like to thank Joanna for being so supportive of my work over this year, the guys at Fat Buddha for some great laughs whilst working weekend nights and the guys at Durham City Hockey Club.

Table of Contents

List of Figures

List of Tables

1. Introduction

1.1 Background

The Pearl River Delta (PRD) is one of the most densely populated agricultural regions in Asia. The region has also been China's gateways for foreign trade over the last 500 years, not just because of its geography but also because it has been a major trading post with the West through the Special Administrative Regions (SARs) of Hong Kong and Macau (Sit, 1984).

The PRD has experienced the most intensive industrial and economic development over the last 30 years, coupled with rapid population expansion. This development and expansion has resulted in increasing volumes of untreated waste-water and other pollutants being expelled into the regions waterways, directly impacting the environment (Ip *et al.,* 2004).

Sedimentary sequences in estuaries have been widely studied because of their ability to preserve a chronology of environmental change (Chagué-Goff *et al.,* 2000) and are frequently found in close proximity to dense human population centres (Schrőder-Adams, 2006). The effects of natural and anthropogenic processes are reflected in the geochemistry of Pearl River Estuary (PRE) sediments (Zhang and Wang, 2001), and therefore by understanding the distribution of certain contaminants, it is possible to gain an insight into the pollution regimes operating within the river catchment. In addition to this, estuarine sediments are recognised widely as an important sink for heavy metals and other pollutants (Li *et al.,* 2001) due to their high fine-grained sediment affinity (Ip *et al.,* 2004). However, whilst estuarine sediments act as a sink for heavy metals, this removal may only be temporary and these pollutants may be remobilised within the water column due to changes in environmental conditions (Lee and Cundy, 2000; Li *et al.,* 2001).

Remobilisation processes can be both natural (e.g. bioturbation, erosion) and anthropogenic (e.g. land reclamation, dredging) (Lee and Cundy, 2000). Anthropogenic factors are of particular significance in the PRE due to large scale land reclamation projects (Seto *et al.,* 2002; Chen *et al.,* 2005; Fan *et al.,* 2007) and dredging (Luo *et al.,* 2007) that occur within its waters. Future environmental hazards may be posed by

heavy metals stored within the sediments of the PRE; an understanding of the spatial and temporal distribution of these heavy metals is essential in mitigating their future environmental impact.

1.2. Physical Geography

The Pearl River (*Zhujiang*) is 2214km in length, draining a catchment area of 0.45×10^6 km^2 and transporting an annual sediment load of some 8.34×10^7 m^3 tons to the estuary each year. The Pearl River drains a latitude-orientated basin 26-22°N and 112-115°E (Zhang *et al.,* 2008), with an average annual temperature across the basin of 14-22°C and precipitation of 1200-2200mm (Lu *et al.,* 2007), resulting in an annual discharge of 3.33×10^{11} m^3 (Xia *et al.,* 2004). This warm, humid climate with high precipitation promotes strong physical and chemical weathering process' and high rates of erosion, leading to the huge volumes of terrigenous sediment being transported through the river system. Through the PRD, the Pearl River is comprised of three main river channels of which, the West River (*Xijiang*) is the main channel in the network and is confluent with the East (*Dongjiang*) and North (*Beijiang*) Rivers in the lowers reaches of the PRD (Lou *et al.,* 2007) (see fig. 1.1).

The PRE has a bell-shaped outline oriented along a north-south axis approximately 49km long and between 4km and 58km wide (Ip *et al.,* 2004), encompassing an area of approximately 2100 km^2 (Zhou *et al.,* 2004) (see fig. 1.1). The three main channels of the Pearl River drain into the South China Sea through 8 major distributaries or 'gates' (*men* translates as gate in Mandarin), of which four (*Humen, Jiaomen, Hongqimen* and *Hengmen*) course into the PRE, and account for 55% of the total discharge and 40% of the suspended sediment load of the Pearl River (Zhao, 1990 in Xia *et al.,* 2004). The PRE is mesotidal (Mao *et al.,* 2004), with an average tidal range of 0.9-1.7m (Xia *et al.,* 2004) and maximum tidal current velocity of 3m s^{-1} (Zhou *et al.,* 2004). The PRE is hydrodynamically characterised as being well mixed during the dry season and stratified during the wet season (Dong *et al.,* 2004). From West to East across the estuary, the bathymetry can be characterised by the West Shoal, West Channel, Central Shoal, East Channel and East Shoal (Xia *et al.,* 2004). The average water depth is 4.8m, but the East and West Channels are maintained to a depth of 10m for navigation.

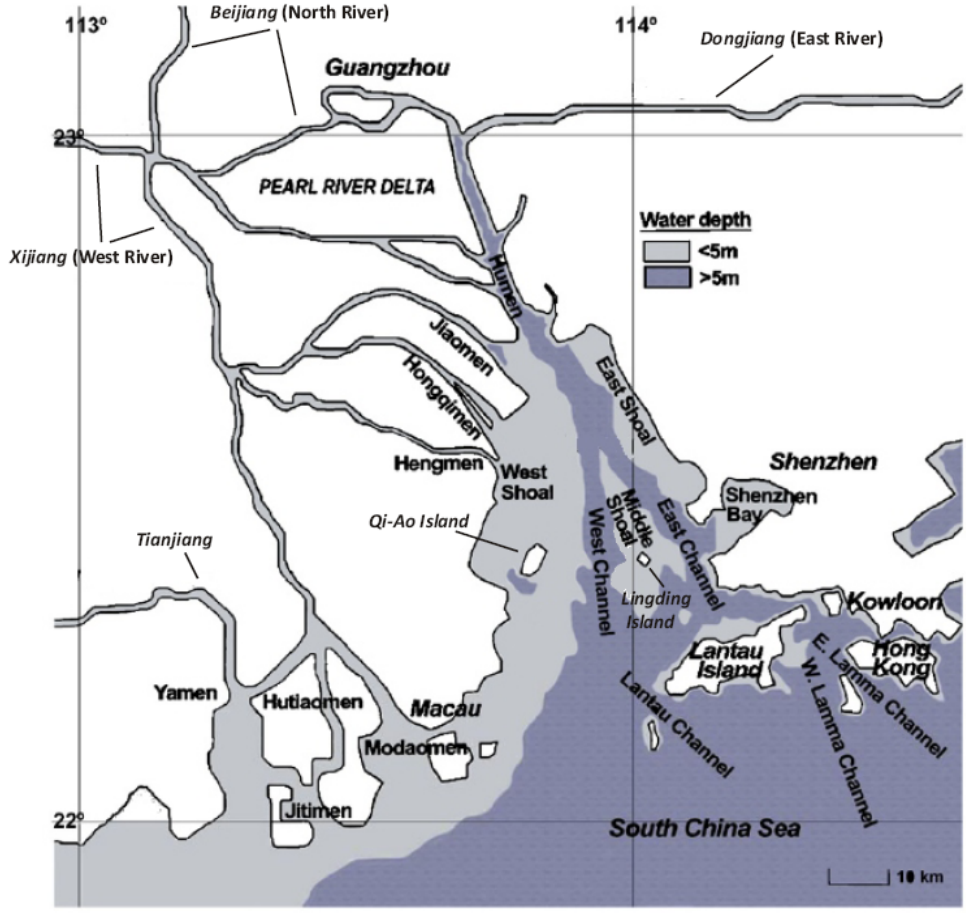

Figure 1.1 Map of Pearl River Estuary (adapted from Harrison *et al.,* 2008).

1.3 Economic Development

Since the start of the Chinese reform programme in 1979, the Pearl River Delta Economic Zone (PRDEZ) has been the most economically dynamic region of mainland China (Enright *et al.,* 2006). This economic prosperity and development is the result of the Central Government of the People's Republic of China (PRC) allowing the the formation of Special Economic Zones (SEZs) in the PRDEZ, that had less restrictive economic policies and attracted domestic and international investment through incentives such as Tax Holidays and low *Enterprise* income tax rates. As a result the region's GDP has grown from US$8 billion in 1980 to US$89 billion in 2000, and US$221.2 billion in 2005 (Enright *et al.,* 2006) and Guangzhou has asserted itself as the largest light industrial base in China (Wong *et al.,* 2002). The breakdown of GDP within industrial sectors shows that *Primary* and *Secondary* industry accounted for 53.7% in

2005.

Population growth has come hand-in-hand with this economic growth, reaching 45.47 million in 2005 (27.63 million officially registered) (Enright *et al.,* 2006). As with many developing nations, this growth has come at the expense of the natural environment (Leung *et al.,* 2005) and in particular water quality as a result of human activity in the region (Chau, 2006).

1.4 Research Questions

A trace/heavy metal pollution signature of the rapid socio-economic development within the PRDEZ, Hong Kong SAR and Macau SAR is stored within the estuarine sediments of the Pearl River. However, this signature is affected by many natural processes (surface and subsurface geology, hydrological and marine regimes etc.) which make the anthropogenic signature more difficult to distinguish. In addition to this, it is important to understand the *availability* of these pollutants stored within the estuarine sediments as this give a better insight into the potential risk they pose.

Coastal fluvio-marine sediments have become the subject of increased interest due to the environmental history that is preserved and the future risks that the sediments may pose to the environment (Chagué-Goff *et al.,* 2000; Lee and Cundy, 2001; Álvarez-Iglesais *et al.,* 2007; Cantwell *et al.,* 2007; Markie *et al.,* 2007; Tylmann *et al.,* 2007).

The next chapter will review the research that has already been conducted across the globe and more specifically in the PRE. The emphasis of this review is to guide the development of research aims and objectives based upon the findings of previous research. The specific emphasis on the review will be focused on the spatial and temporal heavy metals trends, the techniques used to investigate and understand them, and the separation of the natural and anthropogenic signatures. The review will also attempt to place the PRE in a global context by comparing pollution levels to other industrialised estuaries.

Tracing the Distribution of Heavy Metals in the Sediments of the Pearl River Estuary

by Ashley Woods

Thesis submitted for the degree of:

Master of Science (by research) in Geography

Durham University

Department of Geography

November 2009

Declaration

This thesis is the result of my own work. Data from other sources which are referred to in this thesis are acknowledge at the appropriate point in the text.

Abstract

The Pearl River Delta is the socio-economic hub of southern China. The region has experienced rapid industrialisation, particularly since the start of the Chinese Reform Programme in 1979. This rapid industrial development has been coupled with increased pressures on the natural environment environment from pollution and waste associated with this development. These pollutants are transported from within the Pearl River catchment and deposited in sediments of the Pearl River Estuary (PRE).

Geospatial and principal component analysis of the heavy metals Al, Cd, Co, Cr, Cu, Fe, Ni, Pb, Ti and Zn in surface sediments identifies four patterns of spatial distribution that are attributed to three separate heavy metal sources. After normalisation for the effects of the fine particle size affinity, the same spatial distribution patterns remain, but with much less localised variability. Anticlockwise estuarine circulation and the interaction of marine and river water, where distributaries of the North and West Rivers enter the PRE, account for higher concentrations of all metals except Al in the west of the estuary. Pb and Zn are identified as the heavy metals displaying significant enrichment from non-natural sources. Their concentrations which peak at 168 and 699.9mg/Kg respectively along the North River, are found to be associated with higher baseline concentrations resulting from the erosion of metal sulphide bearing carbonates within the catchment. These higher baseline concentrations have then been further enriched by Galena (PbS) and Sphalerite (ZnS) mining operations, atmospheric deposition from fossil fuel burning and some point sources associated with urban and industrial waste.

Temporal analysis of heavy metals and stable Pb isotope variability again highlights Pb and Zn as being significantly enriched from anthropogenic sources, with maximum enrichment factors of 2.6 and 1.8 respectively. The enrichment of these two metals is shown to begin in the 1950s and acceleration of their enrichment in the early 1990s. This second phase of enrichment in the 1990s is also associated with slight enrichment of Cr, Cu and Ni that is also attributed to anthropogenic sources.

Acknowledgements

First and foremost I would like to thank my supervisors Cheng and Jerry who gave up a lot of their time and provided invaluable guidance throughout my research. I would also like to thank Martin and Amanda in the labs for all their help with HF digests and running of my samples through the various machinery. Thanks to Chris and Nima who gave me some invaluable help when programming Matlab computations.

I would also like to thank Joanna for being so supportive of my work over this year, the guys at Fat Buddha for some great laughs whilst working weekend nights and the guys at Durham City Hockey Club.

2. Estuarine Sediments

The rapid industrial and population growth the PRDEZ has experienced since the start of the 1980's has been shown to have directly affected the natural environment and may pose environmental hazards for years to come (Ridgeway and Shimmield, 2002). To mitigate the potential secondary impact that recycled heavy metals from estuarine sediments could have on the environment, it is important to understand their distribution, depositional history, mobility, biological availability and the effect that the hydrological and marine regimes have on them within the estuarine system.

The PRD has been subject to a number of studies aiming to quantify the concentrations of trace metal pollutants present within the sediments of the PRE and its tributaries (Li *et al.,* 2000; Li *et al.,* 2001; Zhang and Wang, 2001; Zhou *et al.,*2004; Wong *et al.,* 2007), agricultural soils (Wong *et al.,* 2002), the atmosphere (Wong *et al.,* 2003; Lee *et al.,* 2005; Lee *et al.,* 2007) and in Pacific Oysters and common fish (Liu and Deng, 2007; Cheung *et al.,* 2008). It is recognised that there are many different sources of heavy metal contaminants into the PRE, including atmospheric deposition, surface run-off, leachates and untreated waste water (Li *et al.,* 2000). However, the geology of the region will also contribute to the enrichment and depletion of various chemical elements in PRE sediments, due to erosion and transportation of sediments by the Pearl River and its' tributaries.

2.1 Geology

The three main tributaries of the Pearl River drain geologically different catchment areas (see fig. 2.1), and as such have characteristic baseline geochemistries. A simplified overview of the respective tributaries shows that the East River sediments are elevated in concentrations of Rare Earth Elements (REEs) and alkali metals. These are enriched in sediments of this tributary because of the high concentrations of REE's, (specifically including the very immobile elements Zr and Hf), and alkali metal found within granites and granodiorites (Taylor and McLennen, 1995) which are the dominant bedrock type in the catchment of the East River (Zhang and Wang, 2001) (see fig. 2.1). The North River flows across a mixed geology of clastics and limestone and the West

River predominantly flows over limestone, possibly leading to elevated levels of alkali earth metals which are a by-product of limestone weathering (Zhang and Wang, 2001).

Across the whole Pearl River basin, carbonates account for 39% of the area. Acid to intermediate composition Granites are the dominant type of igneous rocks and are restricted to Guangdong province, and a scattering Pyrite and Evapourite formations are found in the upper reaches of the *West River*. The lower alluvial and delta plains of the Pearl River are composed of Quaternary fluvial sediments (Lu *et al.,* 2007, Zhang *et al.,* 2007).

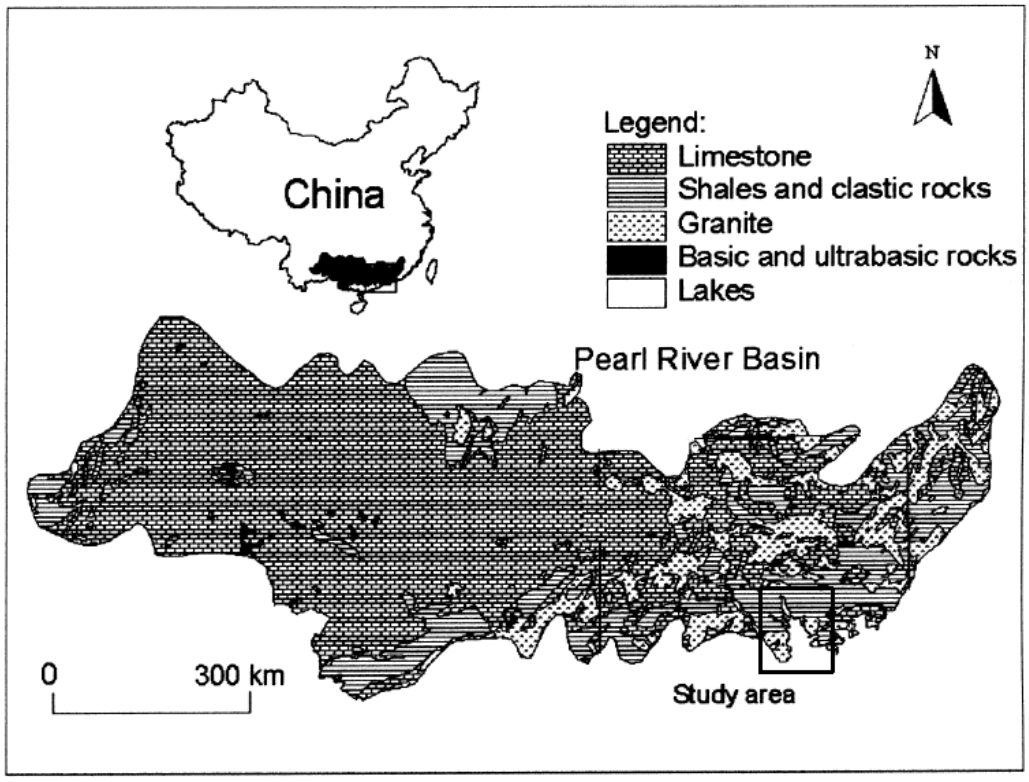

Figure 2.1. Geology of the Pearl River Basin (Zhang and Wang, 2001)

2.2 Estuarine Sediments

A number of studies have previously investigated the temporal trends of certain heavy metal pollutants within PRE sediments. A study of 30 cores taken from the PRE in June 2000 found top enrichment of trace metals when compared to sub-surface samples, with significant increases in Cu, Pb and Zn fluxes since the 1970's based on ^{210}Pb dating of the sediment cores (Ip *et al.,* 2004). Li *et al.,* (2000) also found that

sediments of the PRE were enriched in Cu, Pb and Zn from 21 cores, with the concentrations generally increasing over the last two decades. However, these results only confirm *a priori* expectations given that significant industrial development in the region only began after the start of the Chinese reform programme in 1979.

Investigations by Li *et al.,* (2001) and Zhou *et al.,* (2004) deduced that top-enrichment of certain heavy metals (Cu, Pb and Zn) predominantly occurred in the western parts of the PRE and that concentrations were much lower in the eastern section. In addition to this top-enrichment, a further 2 depth distribution patterns (see fig. 2.2) were found to exist within the estuary. A complicated distribution was found to the north of the PRE just above the *Humen* gate is the same area as PE15 (this study), and a uniform distribution was found in the central and central-southern parts of the estuary based upon a core extracted near to PE74 (this study). These 3 patterns of distribution are attributed to the different hydrological conditions that exist in these sections of the estuary (Li *et al.,* 2000; Zhou *et al.,* 2004). Top-enrichment in the west being the result of direct pollution input from the *Xijiang* and *Beijiang* tributaries (Zhou *et al.,* 2004) and a stable, low energy sedimentation environment (Li *et al.,* 2000). An irregular distribution with respect to depth is found in the north of the PRE and is explained by variable sedimentary conditions as a result of variable freshwater fluxes, land reclamation and dredging (Zhou *et al.,* 2004). The final pattern is one of uniform distribution and occurs in the central and lower regions of the PRE. Both Li *et al.,* (2001) and Zhou *et al., (*2004) attribute this to strong mixing of fresh- and marine-water where the high energy environment may re-suspend older estuarine sediments and mix them with younger ones before re-deposition.

Zhou *et al.,* (2004) found that Pb and Co were the trace metals that were heavily influenced by anthropogenic activity. A caveat of Pb distribution is that within the PRE a major input is from atmospheric deposition (Wong *et al.,* 2003) rather than directly from industrial effluents. A low correlation coefficient of just 0.315 was calculated using Pearson's correlation matrix between the two elements further suggesting that their sources are quite different, with Co fluxes coming from industrial waste-water (Li *et al.,* 2000). Many of the other heavy and trace metals (Cr, Cu, Ni, Ti, V and Zn) were found to be associated with the biological and chemical weathering of

the soils and bedrock within the PRD (Zhou *et al.,* 2004).

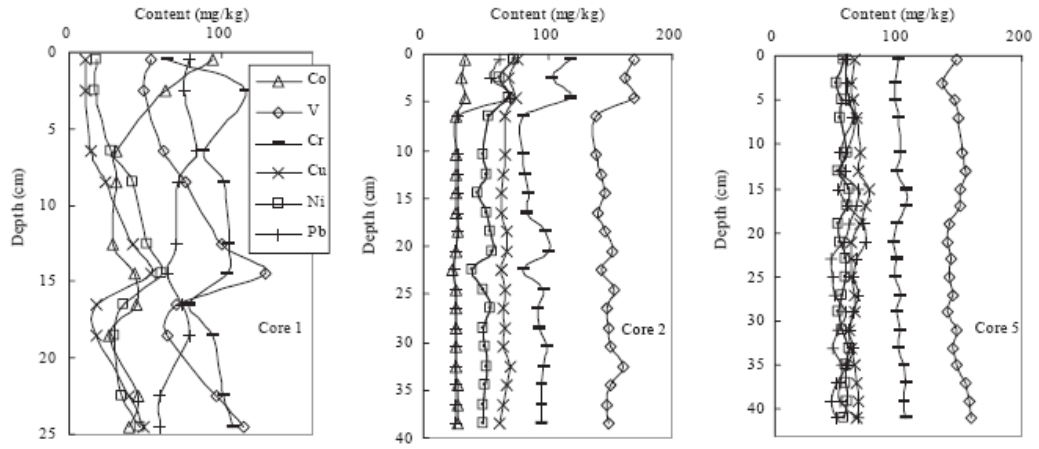

Figure 2.2. Complicated (left), Top enriched (middle) and uniform distribution (right) profiles from three cores taken in the PRE (Zhou *et al.,* 2004). Only 3 cores shown here to demonstrate the generalised heavy metal profiles of the 3 distribution patterns identified.

Concurrent findings from geochemical analysis of sediments from the three main tributaries of the Pearl River also support these conclusions, with weathering of Limestone within the West River (*Xijiang*) catchment resulting in enrichment of a suite of trace elements similar to those found in the PRE sediments (Zhang and Wang, 2001).

Ip *et al.,* (2004) dated certain PRE sediment profiles using the ^{210}Pb technique and calibrated the unsupported ^{210}Pb activity with the Constant Rate Sedimentation (CRS) model. Increased sedimentation rates in the PRE since the 1970s could themselves account for this increase in trace metal concentrations, as they may indicate increased weathering within the river catchment and therefore a higher sediment load. However, Ip *et al.,* (2004) noted that there has been no significant increase in levels of Fe or Al in the last 30 years (rock-forming elements) which would be indicative of increased weathering. This is further verified by a decreasing ^{206}Pb/^{207}Pb isotope ratio towards the top of cores taken from the estuary, indicating anthropogenic sources for at least the increased presence of Pb (Li *et al.,* 2001; Ip *et al.,* 2004). The complementary use of ^{137}Cs profiles would help to constrain certain depth-ages within sediment profiles and allow a more accurate time-line of deposition to be produced; a technique that has yet to be employed in the region. A compounding problem that may affect the accurate dating of sediment profiles are the *Lechang* and *Fankou* Pb mines and a Pb smeltery at *Shaoguan,* located on the upper reaches of the

North River (Zhang and Wang, 2001), which may artificially alter the isotopic composition of Pb found the PRE sediments and make calibration more problematic.

In addition to understanding historical trends in heavy metal pollution fluxes to the estuary, an understanding of the spatial distribution of these pollutants is also needed. This distribution will not only be affected by industrial sources of various trace metals, but also by the fluvial and tidal regimes that are in operation in the PRE. Zhou *et al.,* (2004) found from 12 sampling locations that for many trace metals including Co, Pb and Zn, maximum values where found in the middle and mid-western areas of the estuary to the north west of Lantau Island (see fig. 2.3). This distribution pattern is in accordance with analysis of enrichment patterns within the three major tributaries entering the PRE (Zhang and Wang, 2001), where higher concentrations of Pb were found in the sediments of the North River and to a lesser extent, the West River, which enter the PRE through the *Humen, Jiaomen, Hongqimen* and *Hengmen* gates. In addition to the riverine sources, the enrichment pattern is also attributed to the industrial activities in Shenzhen Bay (Zhou *et al.,* 2004) (see fig. 1.1). This interpretation is partially verified by the work of Ouyang *et al.,* (2006) who found that the highest concentrations of dissolved heavy metals were in the waters of the East and Shenzhen rivers[1]. However, this research also found the North and West rivers have much lower dissolved concentrations of heavy metals; results that generally conflict with spatial distribution of heavy metals in surface sediments of the PRE presented by Zhou *et al.,* (2004). These conflicting findings suggest that the deposition of trace elements is much more complex than the aforementioned conclusions suggest, and that many variables must taken into account when explaining their distribution in the estuary.

2.3 Heavy Metal Availability

Once deposited, metals become subject to a variety of physical, chemical and biological processes that could potentially rework them back into the water column. The processes can be both natural (e.g. bioturbation, erosion) and anthropogenic (e.g. land reclamation, dredging) (Lee and Cundy, 2000). Anthropogenic factors are of particular significance in the PRE due to large scale land reclamation projects (Seto *et*

1 Although not marked on the map of the PRE (fig. 1.1) the Shenzhen River separates Hong Kong SAR from mainland China, coursing through Shenzhen city and into Shenzhen Bay along an east-west axis.

al., 2002; Chen *et al.,* 2005; Fan *et al.,* 2007) (see fig. 2.4) and dredging (Luo *et al.,* 2007) that occurs within its waters.

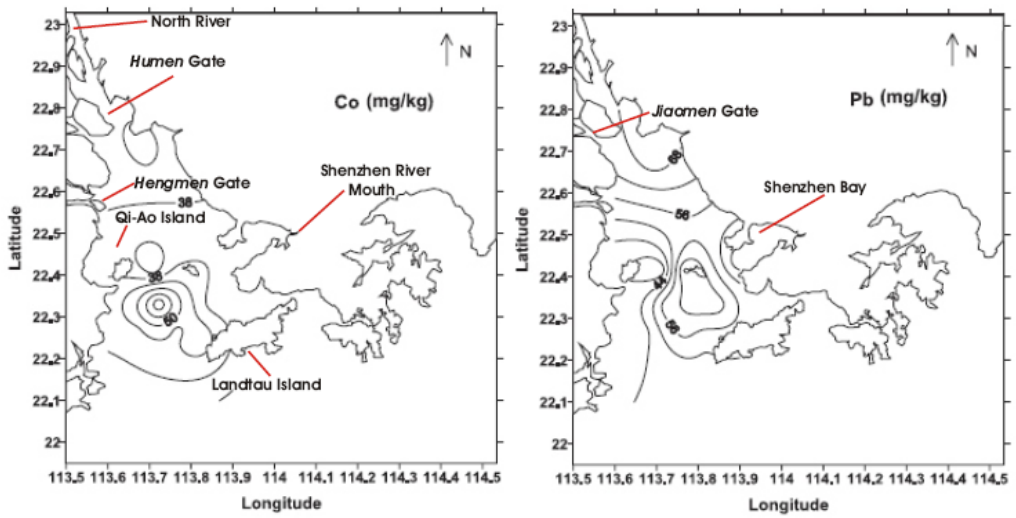

Figure 2.3. Spatial distribution of Co (left) and Pb (right)adapted from Zhou *et al.,* (2004).

2.3.1 Heavy Metal Speciation

The potential bioavailability of heavy metal is key to understanding the risk they pose to the environment. Some studies have suggested that total content and speciation of heavy metals can determine their availability (Li *et al.,* 2007), others have used a weak chemical reagent to extract the trace metals in a readily exchangeable ionic form (Li *et al.,* 2000), and others still have stated that only heavy metals found within organic matter are considered to be biologically available (González *et al.,* 2007). In the PRE, very few studies have attempted to determine the *availability* of heavy metals within the estuarine sediments to biological organisms. Li *et al.,* (2007) in their study of wetlands across the PRE suggest that metal speciation studies offer the most realistic estimation of the environmental impact of pollutants.

The findings of the Li *et al.,* (2007) study are similar to those of a previous study by the same author on the chemical partitioning of Cu, Pb and Zn in the PRE sediments (Li *et al.,* 2001). In both, it was found that Pb and Zn fractionation occurred primarily in the Fe-Mn oxide and residual fractions and Cu occupied the organic and residual fractions. Top-enrichment of these metals within the cores taken came from an increase in the non-residual fractions, indicating their source being anthropogenic and

that their bioavailability might be greater than initially thought. Moreover, using the weak chemical reagent method, Li *et al.,* (2000) found that less than 1% of the total concentration within sediments were in a readily exchangeable ionic form but may provide a potential source to the water column through the sediment-water interface.

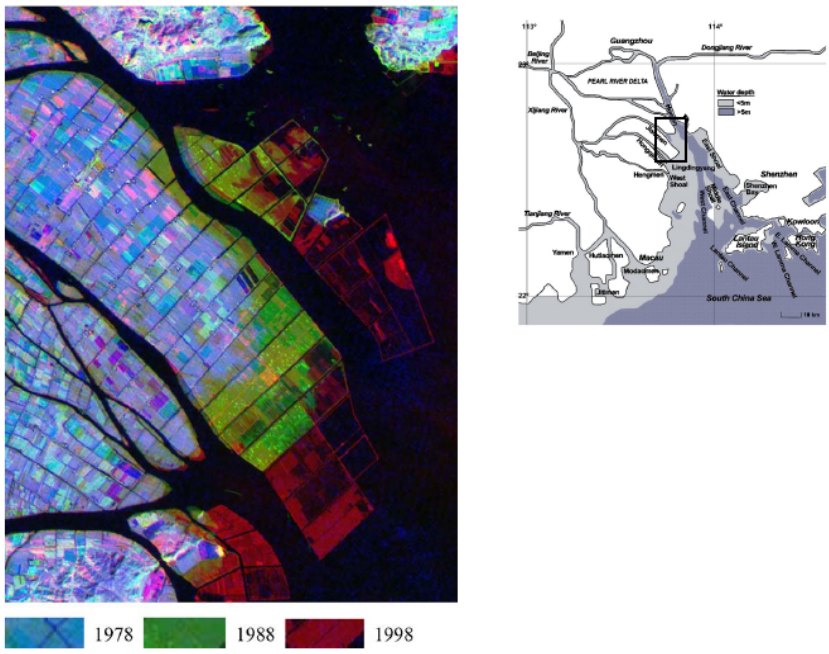

Figure 2.4. Land reclamation in the north of the PRE (near Humen gate) compiled from MSS (1978), TM (1988) and ETM+ (1998) satellite imagery (Chen *et al.,* 2005)

With such a small amount of literature pertaining to heavy metal speciation in the sediments of the PRE, it is difficult to make an assessment on the availability of these pollutants.

2.3.2 Ecotoxicology

Using biological indicators to assess natural environmental conditions and changes has been employed in a wide range of studies within marine, estuarine and freshwater environments across the globe (Ruiz *et al.,* 2004; Caurant., *et al.,* 2006; Durou *et al* 2007; Ip *et al.,* 2005; Malloy *et al.,* 2007; Nieto *et al.,* 2007 and Speelmans *et al.,* 2007). In addition to this, ecotoxicological investigation can assess the availability of heavy metal pollutants by directly sampling their ecological impact, particularly in benthic organisms. In the PRE two such ecotoxicological assessment of heavy metal pollution have been undertaken using Pacific Oysters (Liu and Deng, 2007) and come common fish species (Cheung *et al.,* 2008). In the Pacific Oysters study, the morphology

and dry weight of the shells were analysed in addition to digestions of oyster soft tissues for analysis of Cd, Cu, Pb, Zn concentrations using Inductively Coupled Plasma Atomic Emission Spectrometry (ICP-AES). The results show that the highest concentration of Pb is found in the western PRE, whereas Cd, Cu and Zn concentrations were found to be highest in oysters from the east of the estuary. A distribution pattern that is very different to the sedimentary investigations conducted within the estuary. Another caveat with this research (Liu and Deng, 2007), is the very low number of sampling points within the estuary, making comparisons with other research tentative at best. The study of some common freshwater and marine fish species found that As, Cd and Pb were enriched in some freshwater species based on findings from ICP-OES (Cheung *et al.,* 2008). In this study however, many of the fish examined for heavy metals were bought from markets and therefore there origin with in Pearl River system is not known and there is no way to assess any post-catch contamination during transportation to market.

2.3.3 Foraminifera

For an ecotoxicological assessment, it appears prudent to chose fauna that occur relatively ubiquitously across the estuary rather than being constrained to specific environmental niches. Benthic foraminifera are a very suitable fauna as they constitute the most diverse group of shelled micro-organisms in the oceans (Sen Gupta, 2002). Individual species of foraminifera live within different environmental parameters (e.g. salinity, temperature, organic content etc.) and therefore can be used as a proxy for certain environmental conditions; where changes in the species and population distribution can be used to infer environmental change. Foraminifera have also been shown to be sensitive to various types of pollution (Yanko *et al.,* 2002) and have been the subject of a number of pollution studies (see Nigam *et al.,* 2006 for a review).

Foraminifera have a reproduction time of between 6 months and a year and their tests are readily preserved in sediments. They therefore produce a biofacies that is indicative of a very short time period (just a few years) (Albani *et al.,* 2007). Another advantage of using foraminifera is that even in very restricted or polluted environments, a relatively large number of just a few opportunistic species may be

found (Albani *et al.,* 2007)..

One method of analysis is by using a 'presence-absence-relative dominance' approach of investigation (Albani *et al.,* 2007). With many species of foraminifera being specific to certain prevailing environmental conditions, the presence of certain species within a community can be used to construct a biotope for a region. Changes in these biotopes in a region over time can therefore be used to indicate changes in the prevailing environmental conditions (Albani *et al.,* 2007). In regions where species diversity is normally low (such as in a estuarine environment), the appearance or absence of species over time can be of the same significance to environmental changes, as can analysis of total population present (Nigam *et al.,* 2005). A study of Rangitopuni Estuary and Waitemata Harbour in Auckland, New Zealand (Hayward *et al.,* 2004) shows two step change in foraminifera assemblages between 1950 and 1970 attributed to a lowering in salinity as a result of increased run-off caused by urbanisation. A similar study using foraminifera species and population distribution in Naples Harbour (Southern Italy) found that certain species of foraminifera such *Quinqueloculina seminulum and Ammonia tepida* are more appropriate for monitoring high pollution concentrations due to their absence in the most polluted sediments (Ferraro *et al.,* 2006).

In heavily polluted waters, deformities in the foraminifera tests have proved to be good indicators of the environmental conditions (see fig. 2.5) and the presence of heavy metal pollutants (Elberling *et al.,* 2003). In this particular study of a Sphalerite (ZnS) and Galena (PbS) mine, heavy metal contamination from submarine tailings disposal in Affarlikassaa fjord, West Greenland produced a correlation of up to 0.790 with deformities found in foraminifera tests. Assemblage composition in proximal locations to tailings disposal sites also showed significant changes and even absence from the start of mining operations. These observed abnormalities have been classified into seven distinct groups (Frontalini and Coccioni, 2008): (1) reduced chamber size, (2) aberrant chamber shape, (3) distorted chamber arrangement or change in coiling, (4) Abnormal additional chambers, (6) Siamese twins, and (7) non-developed tests. Of the seven classification, it has been found that the first three are the most common deformities observed in foraminifera tests. Stouff *et al.,* (1990) noted that under

natural environmental conditions, not more than 1% of foraminifera test should exhibit abnormalities.

A consideration when conducting any ecotoxicological study is the non-linear response that might occur between the ecology and any environmental change. Another investigation into the presence of deformities within foraminifera test from three rivers in Brazil (Geslin *et al.,* 2001), found that the highest percentage of abnormalities where found in the two rivers (Rio Guarau. and Rio Una) that had not been affected by human activity. The findings showed that natural stresses within an estuarine environment can have similar effects to those brought about by anthropogenic pollution and may potentially mislead interpretations.

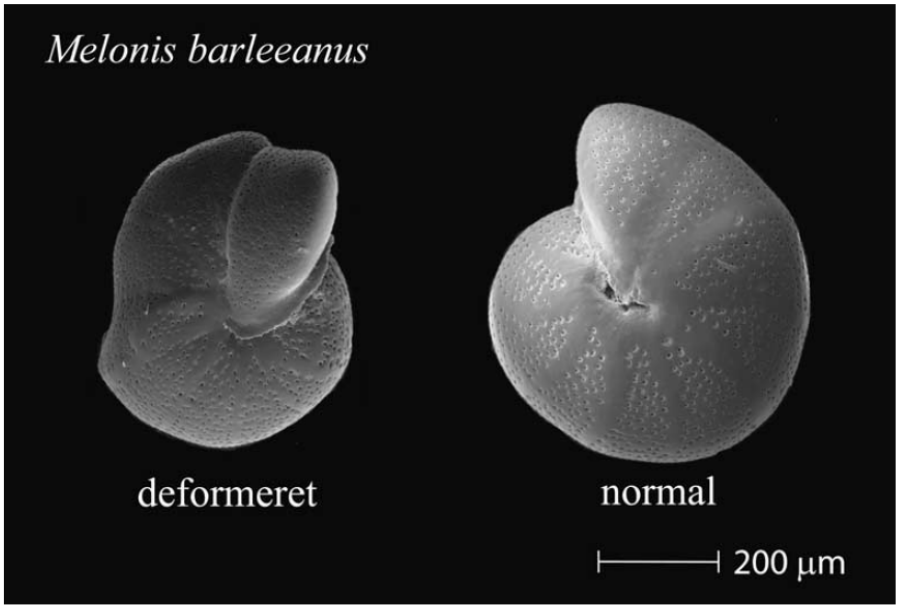

Figure 2.5. Normal and deformed *Melonis barleeanus* tests from Affarlikassaa fjord, West Greenland as a result of heavy metal contamination (Elberling *et al.,* 2003)

When conducting an ecotoxicological investigations using any type of foraminifera based investigation, it is imperative to understand the natural environmental regimes in operation and account for these when analysing the changes and trends observed (Langer and Lipps, 2003). A change in salinity could result in certain species disappearing or appearing within a population, with species existing at the very extreme of their environmental tolerance exhibiting deformities that could be mistaken for a pollution signature.

2.4 Hydrological and Marine Regimes

Hydrological and marine regimes in the PRE have the potential to account for much of the spatial and temporal distribution of heavy metal pollution across the region. As has already been discussed, the temporal distribution of heavy metals within estuarine sediment profiles are broadly encompassed within 3 depositional patterns that have been attributed to freshwater and marine interactions during deposition (Li *et al.,* 2000; Zhou *et al.,* 2004). There are certain key variables that need to be understood when assessing the PRE region; salinity, suspended sediment load, estuarine circulation, pollution sources and other anthropogenic activities such as land reclamation and dredging.

2.4.1 Estuarine Circulation

The main components of circulation in the PRE are river discharge, saltwater intrusion and tidal currents. The pattern of surface circulation is a freshwater dominated western boundary current from the discharge of three river outlets in the Northwest of the estuary, and saltwater intrusion via the eastern channel (Mao *et al.,* 2004). In addition to this, Coriolis deflection of discharging freshwater forces it through the western side of the estuary, which may have led to the increase concentrations of heavy metals found in this part of the estuary. The sediments of the eastern channel and shoal have a more marine geochemical signature (enrichment of CaO and Sr), from the sedimentation of biodetritus from marine processes (Zhou *et al.,* 2004). The intrusion of coastal shelf waters through the eastern channel leads to a change in circulation pattern from an estuarine circulation pattern in the north, to coastal circulation pattern in the middle of the PRE (Su, 2004). Alongshore current from east – west particularly during the dry season (Su, 2004), ensures that the anti-clockwise circulation in the estuary is maintained as shelf waters are deflect into the PRE through the eastern channel as a result of Ekman transport.

2.4.2 Salinity

Very little research into salinity changes in the PRE has been undertaken (see Larson *et al.,* 2005). Salinity changes can cause major changes in depositional regimes as they not only demonstrate a change in interaction between fresh and marine waters

but also cause changes in the rate of sedimentation. Changes in the salinity since the rapid development of the PRDEZ began, could potentially account for any variations in the benthic foraminifera assemblages. This notion was employed in a study of planktic and benthic diatom species across the estuary by Zong *et al.,* (2006). In this study modern diatom assemblages in different salinity zones were used as an analogue to account for the assemblage changes found through the mid-late Holocene from an estuarine core, and as a result a deduction of monsoon variability over this period was made.

In this articles, Zong *et al.,* (2006) used organic carbon isotopes ($\delta^{13}C$) and $C_{organic}/N_{Total}$ bulk ratios in addition to modern diatom assemblages to reconstruct this salinity variability, a technique that has been employed across a broad spectrum of estuarine and marine palaeoenvironmental reconstructions.

2.4.3 C/N Bulk Ratios

Changes in the bulk C_{org}/N_{Total} ratio within sediments have been widely used to support the results of organic carbon isotope ratios as a palaeoenvironmental proxy for the source of organic matter within sediments (Mackie *et al*., 2005; Liu *et al*., 2006; Mackie *et al*., 2007; Lamb *et al*., 2007). Terrestrial and freshwater organic materials tend to have higher C/N ratios (>12) than marine sourced, more nitrogen rich phytoplankton which have C/N ratios of 5-7 (Lamb *et al.,* 2007). The use of C/N ratios relies on our ability to distinguish and account for the varying sources of organic matter being transported into a mixed water system such as an estuary. The most significant sources of organic material being transported into the PRE are terrestrial and freshwater organic material by river flow, brackish and marine material produced *in situ* and marine material transported by tidal cycles into the estuary (Zong *et al.,* 2006). Fluctuations in this ratio over time will represent a shift in the sediment source at a given location in the estuary, and indirectly, will provide a proxy for salinity fluctuations. The ability to reconstruct the depositional palaeoenvironment in the estuary will allow for a more accurate interpretation of how heavy metal deposition in the estuary has been driven by natural factors. Whilst reconstruction of salinity changes without organic carbon isotope analysis is not possible (Liu *et al.,* 2006), the use of the C/N ratio will allow for a more accurate assessment of changes in the flux of

terrestrial (and freshwater) and marine material into the PRE. Used in conjunction with a conservative tracer element of surface weathering such as Fe (Schiff and Weisberg, 1999), the results should enable a more accurate appraisal of changes in the depositional environment caused by variability in sediment fluxes and circulatory regimes.

2.5 Global Perspective

One of the keys to understanding the spatial and temporal distribution of heavy metals within PRE sediments and their environmental significance, is to understand the results within a global context. Heavy metal pollutants in estuarine and coastal sediments is a problem for industrialised nations across the globe, and as such they have become the focus of a number of studies in recent years; with some key advances in our understanding (Rowlatt and Lovell, 1994; Selvaraj *et al.,* 2004; Lui *et al.,* 2006; Piper *et al.,* 2006; Maybeck *et al.,* 2007; Abrahim and Parker, 2008; Birch *et al.,* 2008 and Vaalgamaa and Conley, 2008).

In the UK, many estuaries have been the hub of of our industrial development and as such their sediments store a geochemical history of this development (Ridgeway and Shimmield, 2002).

Sediments of the Tyne and Tees estuaries and coastal zones in between are found to have some of the highest concentrations of Pb (110mg/Kg) and Zn (153mg/Kg) (Rowlatt and Lovell, 1994) and Cu (BGS, 2005; see fig. 2.6) in the UK. Based upon baseline Pb and Zn concentrations from a core taken 10miles from the Tyne estuary in the North Sea, Rowlatt and Lovell (1994) suggest that 80% of Pb and 49% of Zn in surface samples are the result of anthropogenic activities. The Tyne and Tees drain some of the largest metal sulphide (CuS, PbS and ZnS) ore deposits in the UK. Erosion of these deposits in their respective results in higher concentrations of Cu, Pb and Zn in estuarine and coastal sediments. Mining of Cu-Pb-Zn ores and development of heavy industry within the Tyne and Tees catchments since the industrial revolution has further enriched heavy metals concentrations (Ridgeway and Shimmield, 2002). The Humber and Thames river systems have also experienced a similar level of industrial development to that of the Tyne and Tees (Rowlatt and Lovell, 1994), yet

heavy metal concentrations in their associated estuarine and coastal sediments are much lower due to the lack of ore bearing deposits in their catchment and associated mining activities.

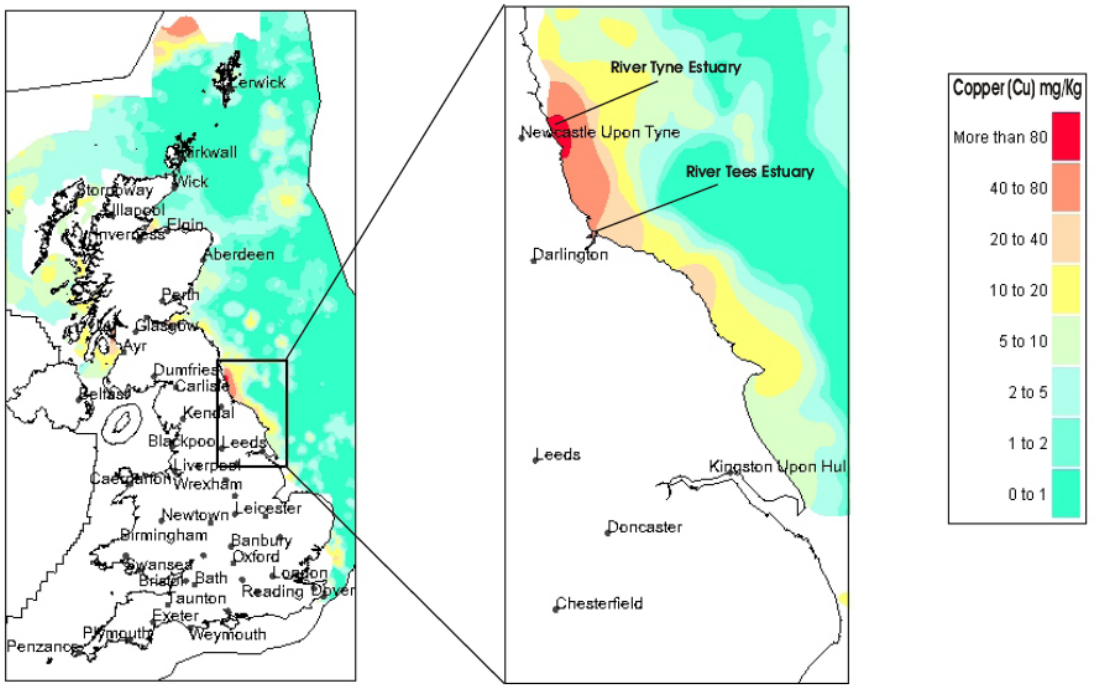

Figure 2.6. Distribution of Cu in coastal sediments around the UK. Enrichment in sediments adjacent to the Tyne and Tees estuaries is enlarged (adapted from BGS, 2005).

.

The Seine River, France has also been subjected to intense industrial development that has resulted in extreme levels of heavy metal pollutants entering its waters (Meybeck *et al.,* 2007). At the height of unrestricted industrial activity concentrations of Cr (150mg/Kg), Cu (275mg/Kg), Pb (1620mg/Kg), Ni (150mg/Kg) and Zn (370mg/Kg) where in the top 10% of all river systems in the world. De-industrialisation and major changes to the management of contaminated particles entering the Seine River system in the last 30 years has helped to drastically reduce the concentrations of Cr (150mg/Kg), Cu (99mg/Kg), Pb (108mg/Kg), Ni (31mg/Kg) and Zn (347mg/Kg) from their peak concentrations (Maybeck *et al.,* 2007).

The high concentrations of heavy metal pollutants in Tyne, Tees and Seine Rivers are a legacy of a long period of industrial development that has had similar effects to estuarine and coastal sediments all across Europe (Cundy *et al,* 2003; Howarth *et al.,* 2005). Concentrations of certain metals have been found to be

significantly higher in areas where mining activities (particularly of sulphide deposits) occur (Rowlatt and Lovell, 1994; Nieto *et al.,* 2007). The pattern of industrialisation that has been experienced in Western Europe is very different to that of nations that started their industrial development more recently (<30 years ago). These newly industrialising nations (NICs) should be benefiting from industrial process developments and waste management strategies to make their development significantly less polluting than that of western Europe.

The River Palar drains a catchment that has experienced intense industrial, urban and aquaculture development over the last 20 years into the Bay of Bengal 50km south of Madras, India. In addition to this, the Buckingham Canal accounts for another source of urban sewage, pesticides and fertilisers and waste from salt panning industry to the region (Selvaraj *et al.,* 2004). Results from geochemical analysis of the estuarine and coastal sediments highlighted enrichment of Cd, Pb and Zn that had averaged enrichment factors (EFs) of 6.7 and 5.4 respectively, compared with continental crust averages. Although enriched compared to continental crust, these results do not take into account the effect regional geology might have on the baseline geochemistry of sediments. Compared with other studies, the highest concentrations of Cd (0.31mg/Kg), Pb (28mg/Kg) and Zn (163mg/Kg) found within the River Palar estuary are relatively low.

The Haihe River in northern China drains an important economic area with a population of 126millon into the Bohai Bay. A transect of 10 sampling stations taken from just up-river of the Haihe estuary 50km upstream to Tianjin showed that sediments were were enriched in Cd, Cr, Cu and Pb, with Pb concentrations peaking at 80mg/Kg just above the Haihe estuary (Liu *et al.,* 2006).

The rivers discussed above have catchment characteristics that are found to a greater or lesser extent within the Pearl River catchment. Specifically, widespread metal sulphide deposits and intense agricultural and industrial development have driven different heavy metal sedimentation characteristics and will provide a benchmark to compare findings from the PRE.

2.6 Aims and Objectives

A review of the current literature on heavy metal pollution in the PRE has highlighted a number of areas that are still quite poorly understood. Many studies have ascertained the concentrations of heavy metals within PRE surface and sub-surface sediments, however, very few studies have attempted to understand heavy metal bioavailability other than by heavy metal speciation. Another issue is the spatial distribution of trace metal pollution. While many researchers have hinted at the possible causes of certain patterns of distribution, none have had enough sampling locations across the estuary to provide a statistically robust assessment. The natural effects of factors such as circulations patterns, sediment particle size and surface geology erosion also need to be accounted for, to determine the true anthropogenic signature.

Pollution and particularly heavy metal pollution is a serious problem in many parts of the world; whether they are the result of ongoing industrial development such as that in south China, or a relic signature of industrialisation in the west. If informed mitigation policies are to be proposed to deal with the potential future environmental impact of these 'stored' pollutants, it is imperative that we understand not only the concentrations present, but the actual effect they have on the ecology.

To achieve these outcomes, the follow research is proposed:

- Production of a high resolution assessment of the spatial and temporal heavy metal concentrations in sediments across the PRE and to identify where possible anthropogenic or natural sources.
- Complete an initial assessment of the feasibility of using presence of deformities within foraminifera tests to understand the biological availability of heavy metal pollutants within the estuary.
- Use the complementary techniques of ^{137}Cs and ^{210}Pb to more accurately date sediment cores from the PRE and therefore more accurately date the onset of environmental degradation and produce a pre-Industrial assessment of environmental conditions within the PRE.

3. Methodology

To achieve the goals of the research aims, it is imperative that carefully chosen sampling and analytical techniques are implemented to eliminate sampling errors and biases.

3.1 Surface Sampling

Surface sampling of sediments from the PRE was undertaken in the winter of 2005 at 89 locations using a van Veen grab sampler that captured the top 10cm of sediments. The sediment were immediately stored in sealed plastic containers and kept refrigerated. Water depth and salinity was also measured at each sample location. Salinity measurements were comparable with the monthly data published by the Environmental Protection Department, HK SAR Government and by the Water Resource Committee for the Pearl River in Guangzhou with a factory calibrated accuracy of ±1‰ for the salinity meter (R.M.S EcoScan Salt 6 Portable Salinity Meter). The 89 sampling points encompassed an area from tributaries to the north of the PRE, through the estuary and the adjacent continental shelf. Of the 89 surface samples taken, 77 were used in this study due to particle size data not being available for 12 of the sampling points. The 77 locations cover exactly the same area of the estuary as the 89 samples, but sampling density is slightly lower in the central parts of the estuary.

3.2 Sediment Cores

Four short sediment cores were taken along a transect across the estuary in January 2008. Cores were extracted using 40mm diameter PVC tubing using a gravity coring technique. With sediment coring taking place in water depths up to 4m, coring tubes were inserted and extracted vertically from the side of the boat. Keeping the cores vertical the bottom was immediately capped and supernatant water was slowly drained by gradually cutting the coring tube down from the top until the water sediment interface was reached so that the sedimentary profile of the core remained intact and undisturbed (see fig. 3.1). Top seals were placed on the core and before being wrapped in thick plastic bags. Water depths were measured at each coring

location. The transect from core 4 to core 3 via core 2 was chosen as it limits the amount of salinity variability at sampling locations (see fig. 3.2) whilst avoiding areas of dredging, land reclamation and localised pollution sources. The transect also crosses the western, middle and eastern shoals of the PRE, making sampling much easier due to water depths <5m.

Figure 3.1 Shows the various stages of processing after core extraction. Core remains in a vertical (*in situ*) orientation throughout.1) Draining supernatant water. 2) Water/Sediment interface remaining undisturbed throughout the draining of supernatant water. 3) Sealing and Packaging of core.

3.3 Particle Size

Particle size analysis was conducted on all cores at a minimum resolution of 6cm. Organic matter from each sample was digested using 40ml of 10% Hydrogen Peroxide(H_2O_2) solution in an 80°C water bath for 4-6 hours, then covered and left to stand over night. Samples were then topped up with 20ml of distilled water and centrifuged at 4000rpm for 4 minutes. The supernatant liquid was then decanted, 50ml of distilled water was re-added to the samples and centrifuging was repeated. The supernatant liquid was again decanted before a final 20ml of distilled water was added. Finally, 2ml of the dispersing agent Sodium Hexametaphosphate (NaP_2O_5) was added, and the samples were gently agitated for 1 minute before being left to stand for 24

hours. The samples were then sonicated for 30 seconds before being run through a Beckman-Coulter LS13 320 Laser Diffraction Particle Size Analyzer. Internal calibration of sensors was completed using the automated certification program (Beckman-Coulter, 2008). Calibrations was verified using the Coulter LS Control G15 standard (Mean=15.15+/-.184 µm, S.D. = 8.15 +/- 2.25 µm). Samples were run in pairs and results were only accepted when a <1% variation in the pair of results was obtained; the ascribed reproducibility of this particular laser granulometer. Detection errors were less than 5% (Beckman-Coulter, 2004). Classification of particle size was performed by the program GRADISTAT. Particle size analysis was conducted so the effect of particle size variations on heavy metal concentrations could be accounted for.

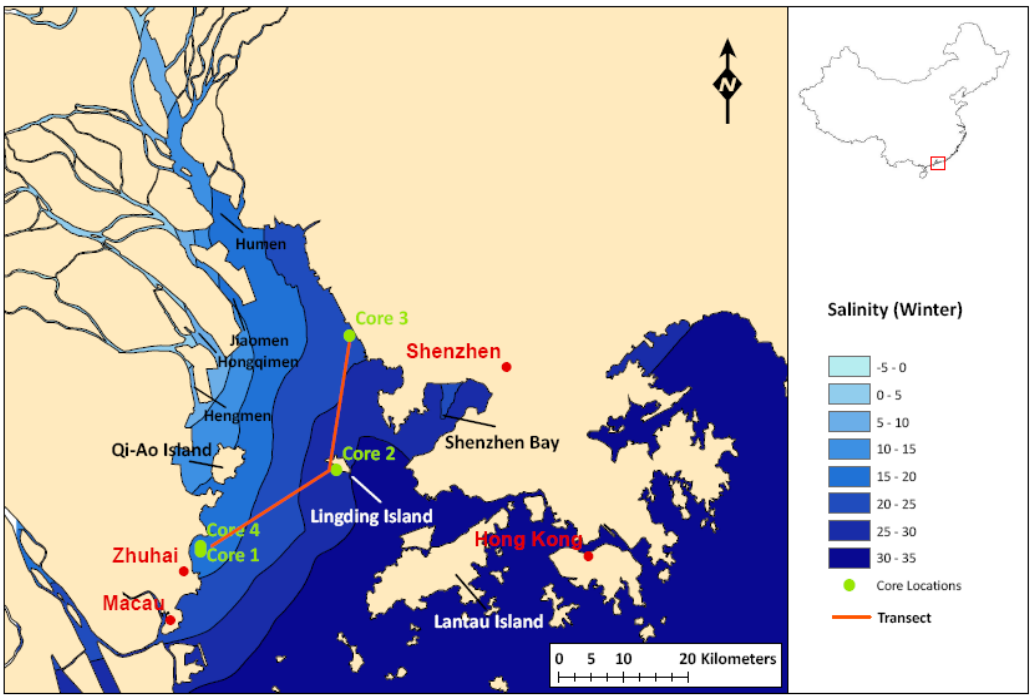

Figure 3.2. Transect to limit salinity variations at coring locations. Image produced by author of this thesis from Landsat ETM+ imagery (University of Maryland, 2008) and salinity data obtained from unpublished data from Zong *et al* (2006).

3.4 C/N Bulk Composition

Cores were sub-sampled at a varying resolution (2-8cm) for total organic carbon (TOC) and total nitrogen (TN). Samples were placed in a -80°C freezer for at least 24 hours before being freeze-dried for a further 24 hours and homogenised with an agate pestle and mortar. Samples were treated with 5% HCL solution for 10 minutes and

dried before being sealed in tin capsules for analysis. Carbon and nitrogen percentages were measured using a Carlo Erba elemental analyser, calibrated through an internal standard (Zong *et al.,* 2006). Samples were run in batches of 50, with Sulfanilamide and CHNSO B2152 soil standards, replicates and analytical blanks. Replicate analysis gave a precision of <2.51% for Carbon and <1.16% for Nitrogen. C/N ratio analysis was chosen so that changes in the dominant provenance of estuarine material could be identified and used to aid interpretations about changes in heavy metal concentrations: helping to distinguish the natural forcing factors.

3.5 ^{210}Pb and ^{137}Cs Dating

Both ^{210}Pb and ^{137}Cs are measured using gamma spectrometry. The emission of gamma radiation occurs due to dissipation of surplus excitation energy as a by-product of alpha or beta decay. Radioactive decay is random and each decay is independent. Gamma rays occupy the high-energy, short wavelength end of the electromagnetic spectrum with energies between 10 – 10,000 KeV. Radioisotopes have unique gamma ray energies:

^{210}Pb – 46.5 KeV

^{137}Cs – 661.66 KeV (stronger) and 32 KeV (weaker)

Sediments were sampled at either 7cm or 8cm intervals from the top of cores PRE 3 and PRE 4, freeze dried, ball milled and placed in sealed vials for 21 days. This allows ^{226}Ra and ^{214}Pb to be in equilibrium prior to gamma analysis, allowing the ^{214}Pb emissions from the sample record the supported decay caused by ^{226}Ra decay and not atmospheric fallout . Samples were then run for 3-4 days depending on activity using Ortec GWL p-type Series Germanium well detectors.

Age models for the two cores were calculated using the Simple (Robbins, 1978), Constant Initial Concentration (CIC) (Krishnaswami *et al.,* 1971) and Constant Rate Sedimentation (CRS) (Appleby and Oldfield, 1978) models to enable comparison between the models. ^{210}Pb and ^{137}Cs dating technique was chosen as it provides a method of producing a depth-age profile for sediment cores deposited over the last 150years. Based on the average sedimentation rates at the various core locations, it is

not expected that the bottom sections of any of the cores will be more than 104 years old (Zhou *et al.,* 2004).

3.6 Inductively Coupled Plasma Mass Spectrometry (ICP-MS)

Estuarine sediment samples for ICP-MS analysis were prepared using the following methodology (EPA, 1994). All chemicals used were trace analysis grade and all water is deionised (≥18.2 MΩ.cm).

Samples were placed in a -80ºC freezer for a minimum of 24hours, followed by freeze drying over 24 hours, then crushed and homogenised in a ball mill. After ball milling, samples were stored in a desiccator at 20ºC. A known mass (approximately 250mg) of the sample is weighed into a HF resistant microwave extraction vessel. The internal wall of the vessel was rinsed with 5ml of deionised water followed by the addition of 2ml of concentrated hydrogen peroxide (100 volumes = >30% w/v). A vented cap was placed on the vessel and it is left overnight to react. 9ml of HNO_3 was then carefully added to the sample so that no sample was lost due to efflorescence, then 3ml of Hydrochloric acid and 2ml of Hydrofluoric acid were added.

The vessels were capped and placed in a MARS pressurised microwave extraction system. An extraction program based on EPA 3052 (US EPA, 1996) method was used (reaching 180 ± 5 ºC in less than 5 minutes and remaining at 180 ± 5 ºC for 9.5 minutes). The samples were then allowed to cool to 40ºC before removing from the microwave. The samples were then filtered into Class A 100ml Plastic volumetric flasks through a pre-washed Whatman 542 filter paper and made up to the mark with deionised water. In order to bring the elements within a reasonable dilution range the analysis is split into 2 separate runs; one for high abundance metals (e.g. calcium), and one for low abundance metals (e.g. Bismuth).

The ICP-MS settings and internal standards are based on EPA 200.8 r5.4 methodology. A suite of internal standards were used. The internal standards were chosen to cover a range of masses and first ionisation potentials. The internal standards used give a final concentration of 50ppb in both standards and samples. Typical standards included the following: Sc_{45}, Ge_{72}, Rh_{103}, In_{115}, Tb_{159} , Re_{185}.

For low abundance elements, 5ml of digested sample solution was taken and made up to approximately 90ml with 2% v/v nitric acid in a 100ml plastic volumetric flask. 1ml of internal standard solution was added to the flask and then the solution is made up to the mark with 2% v/v nitric acid. Internal Standards were: Rh, In, Tb, Re

For high abundance elements, 1ml of the low abundance sample solution was taken and made up to approximately 90ml with 2% v/v nitric acid in a 100ml plastic volumetric flask. 1ml of internal standard solution was then added to the flask and then the solution is made up to the mark with 2% v/v nitric acid. Internal Standard: Sc. Sample batches were run with standards, analytical blanks and repeats using a Perkin Elmer Elan 6100 DRC.

ICP-MS was chosen to calculate heavy metal concentrations in sediments due to both its accuracy and superior detection limits for low abundance metals such as Cd. Cd abundances in nature are normally not much higher that 0.098mg/Kg (Taylor and McLennan, 1995) but ICP-MS detection limits for Cd are 0.05mg/Kg. In addition to this, the use of ICP-MS allows for stable Pb isotope analysis without the need for a second batch of samples to be produced and therefore more efficient use of limited sample volumes can be achieved.

3.7 Stable Pb Isotopes

The stable isotopic lead components (^{204}Pb ^{205}Pb ^{206} Pb^{207}Pb and ^{208}Pb) were calculated during the same runs as low and high abundance metal concentrations using ICP-MS, following the same methodology.

3.8 Foraminifera Analysis

Various surface samples were chosen for foraminifera analysis so that a spectrum of environmental conditions were included. Samples were prepared by wet sieving 5ml volume of sediment through 500µm and 63µm sieves, the fraction between 500µm and 63µm was then used for foraminiferal analysis. Where possible for each sample between 250 and 300 foraminifera were counted and observed for deformities to provide a statistically significant data set. Identification of deformed species followed the work of Frontalini and Coccioni (2008) based in the taxonomy

used by Wang (1985) and Yim and He (1988).

3.9 Geospatial Mapping and Statistics

Surface samples and core locations are mapped using ESRI ArcGIS 9.1. Interpolations of key metals and environmental variables is performed using a *kriging* function in the same software. The use kriging allows for an interactive investigation of the spatial behaviour of the variables being investigated unlike other interpolation techniques, making the interpolation more accurate (Childs, 2004). The use of a kriging function requires that the correct semivariogram for that data set used. The calculation of the semivariogram is done for each data points' separation to every other data point in the spatial set, and is calculated as the average squared difference in variable value (z) between data pairs with the same spatial separation (h). Kriging functions have been used to interpolate spatial data in the PRE previously, however, the use of this technique is not justified, and there is no mention of how the appropriate semivariogram was calculated to execute the kriging interpolation.

To calculate the most appropriate semivariogram, an adapted computation was run in MATLAB R2007b using the following ESRI equation:

$$\gamma(\boldsymbol{h}) = \frac{1}{2n}\sum_{i=1}^{n} \{Z(\boldsymbol{x}i) - Z(\boldsymbol{x}i+\boldsymbol{h})\}^2 \qquad \text{(ESRI, 2006)}$$

where *n* is the number of pairs of sample points separated by the distance *h*.

This equation was slightly adapted in the MATLAB computation due to the complexities of programming the software to attempt to calculate the semivariogram for every possible distance from a sample location. Instead the adapted programming ran this computation for every 100m with a buffer of 10m either side for every sampling location.

Statistical analysis of spatial data was conducted using SPSS 14 for Windows and Microsoft Excel 2003 and 2007 for Windows.

4. Spatial Distributions

In this chapter, the spatial distribution of heavy metals that may be enriched as a result of anthropogenic activity; Cadmium (Cd), Cobalt (Co), Chromium (Cr), Copper (Cu), Lead (Pb), Nickel (Ni), Titanium (Ti) and Zinc (Zn) and through natural weathering, erosion and transport of material from within the Pearl River catchment (Aluminium (Al) and Iron (Fe) will presented. In addition to this, environmental variables such as salinity and particle size distribution will also be presented so that a better assessment of the dominant factors causing the spatial distribution of these heavy metals can be conducted. The effects of particle-size affinity will also be accounted for later in this chapter, allowing for the 'true' spatial distribution of these metals that is not a result of this affinity process can be identified. Statistical analysis using Pearson's product-moment correlation coefficient and principal component analysis (PCA) will be used in conjunction with spatiality analysis to better ascertain which metals are enriched as a result of anthropogenic activities and which are the result of natural processes.

An initial ecotoxicological assessment of the biological availability of heavy metal pollutants will also be presented here. The results of this ecotoxicological study will endeavour to not only investigate whether there is a statistical correlation in the presence of foraminifera test deformities, relative the surface sediment heavy metal concentration (making particular reference to Pb and Zn concentrations) (Elberling *et al.,* 2003), but also if the use of foraminifera to conduct this assessment in the PRE is feasible.

The surface samples analysed from the PRE using ICP-MS and particle size analysis along with summer and winter surface water salinity values are here combined within an orthorectified GIS (see Fig. 4.1 for sampling distribution) of the region, compiled from a mosaic of landsat ETM+ images (University of Maryland 1997-2008). A kriging function using a spherical semivariogram was used to interpolate values for each variable across the PRE. The spherical semivariogram was found to be the most appropriate for the data set through analysis of the spatial structure of the data in a MATLAB R2007b computation (See Appendix A for coding and results).

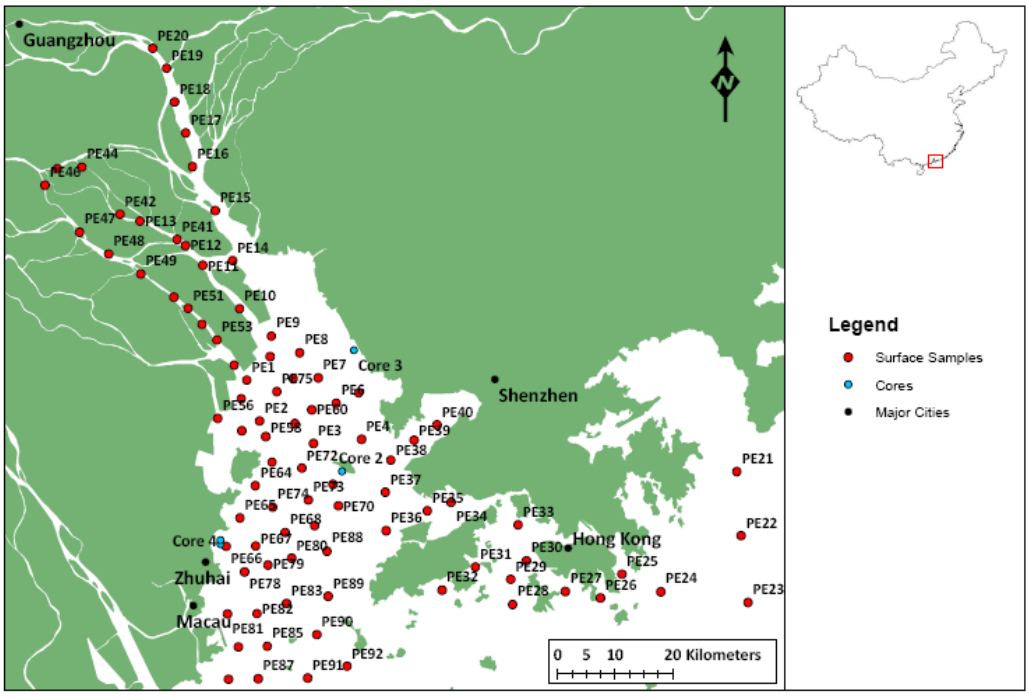

Figure 4.1. Locations of surface and short cores sampling points in the PRE.

4.1 Environmental Variables

Variables such as salinity and particle size have already been identified as possible forcing factors in the spatial distribution of heavy metal pollutants (Lee and Cundy, 2003). Salinity is important as it shows the way in which marine and freshwater bodies interact within the PRE. Particle size is also affected by this interaction, potentially driving clay deposition due to flocculation. The full raw data for all environmental variables measured can be found in appendix B, and is spatially presented in figures 4.2 and 4.3).

Summer and winter surface salinity measurement for surface sampling locations are shown in figure 4.2. It is clearly visible that there is increased freshwater discharge into the PRE in summer due to monsoon driven rainfall (An *et al.,* 2000) that results in lower salinity values in the south and west of the estuary, and to a lesser extent in the east. Relatively dry winter months see increased salinity along the Eastern shoal as marine water intrudes further into the estuary on flood tides. The salinity data also provides information about the circulation patterns that are present in the estuary. The dominant east-west along shore current outside the estuary (Su 2004) is deflected by Ekman transport into the estuary through deep water channels (Lantau and Lamma Channels, see fig. 1.1) either side of Hong Kong. This is characterised by higher salinity

values intruding into the east of the estuary. Freshwater flux results in low salinity along the western edge of the estuary and is the result of Coriolis deflection once the river water enters the estuary.

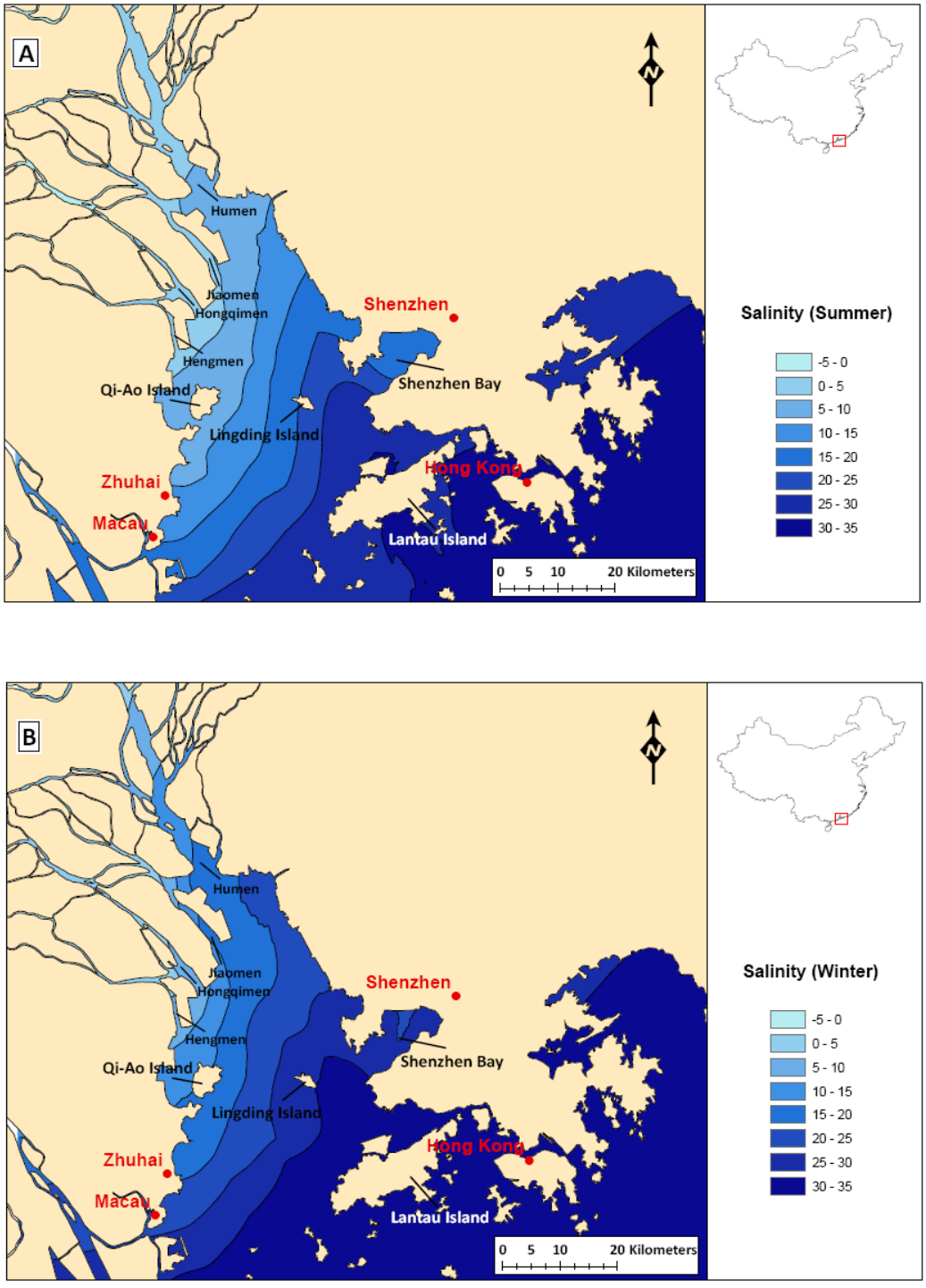

Figure 4.2. Summer (A) and Winter (B) surface salinity across the PRE.

The result of this, is an anticlockwise circulation of water in the estuary being driven by marine water intrusion along the East Channel and Shoal and freshwater

discharging along the Western Shoal. These results are concurrent with other

Sediment particle size was measured using a Beckman-Coulter LS13 320 Laser Diffraction Particle Size Analyzer for 0 – 2mm and classified using Folk and Ward (1957) (see chapter 3).

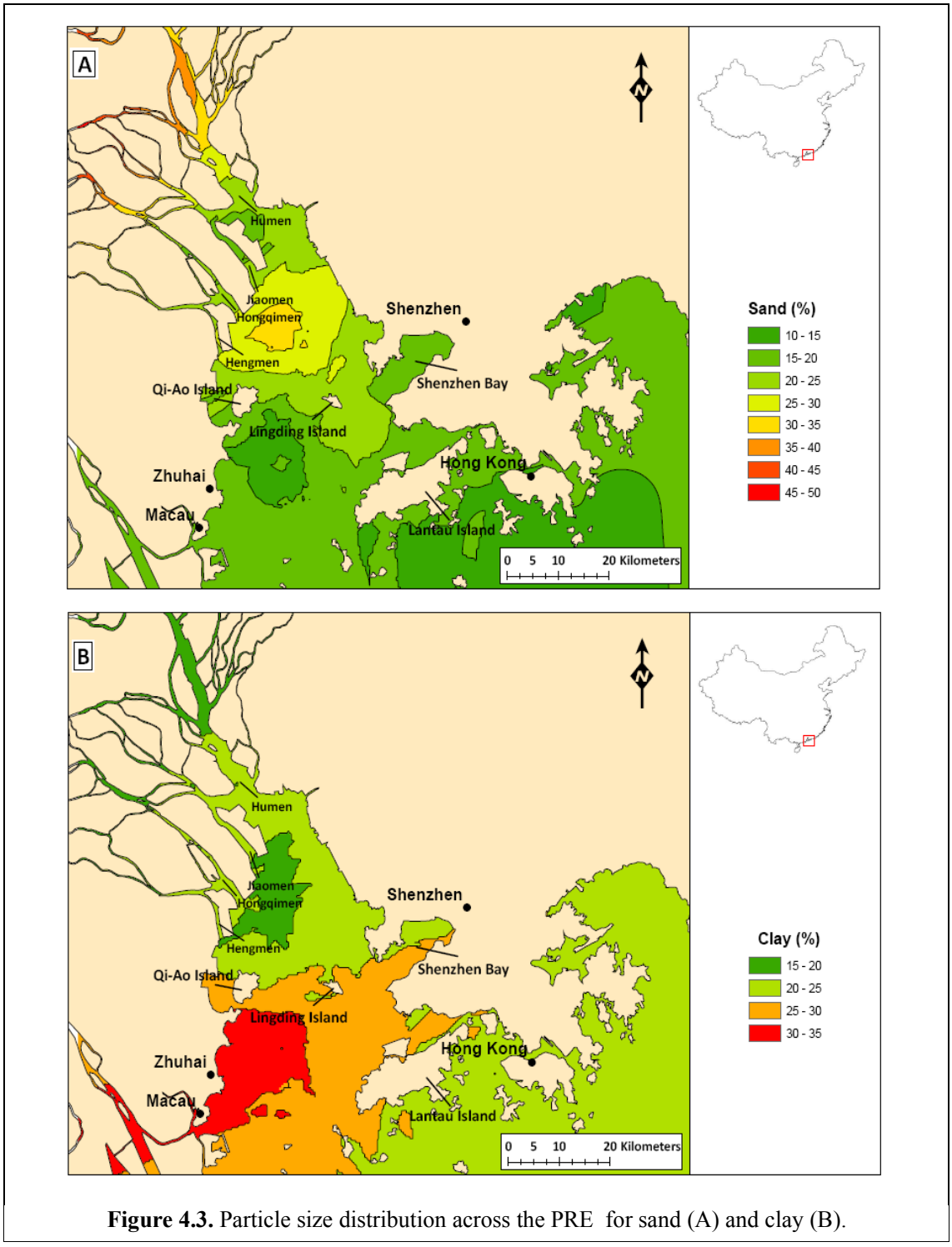

Figure 4.3. Particle size distribution across the PRE for sand (A) and clay (B).

Particle size has a very non-uniform distribution across the estuary, with maximum clay deposition occurring in the south west of the estuary near Zhuhai and

maximum sand deposition occurring in the central-north area of the estuary downstream of the *Humen, Jiaomen, Hongqimen* and *Hengmen* gates (see fig. 4.3).

This distribution is the result of the hydrological regime operating in the estuary. As the major dis-tributaries of the Pearl River enter the estuary, their velocity is greatly reduced and sand starts to be deposited straight away. The highest percentage of clay is found in a region where the salinity gradient is greatest and water velocity is the slowest, at just 0.07 m s^{-1} (Larson *et al.,* 2005). The salinity gradient is the result of the interaction between fresh- and marine water bodies that coupled with low water velocities (energy) results in flocculation and deposition of clay in this region: the turbidity maximum zone (Zhou *et al.,* 2004) (see fig. 4.3).

4.2 Heavy Metal Concentrations

Heavy metal concentrations for 25 low abundance and 8 high abundance metals were calculated using ICP-MS. Of these 33 metals, 7 low abundance (Cd, Co, Cr, Cu, Ni, Pb, Zn) and 3 high abundance metals (Al, Fe and Ti) were chosen for further analysis. The low abundance metals chosen are not only present within naturally weathered bedrock, but are highly associated with industrial and urban waste (Feng *et al.,* 2004). The three high abundance metals analysed are widely regarded as conservative tracer elements of natural weathering, erosions and transport process operating within a river catchment and are largely unaffected by human activities due to their high abundances in nature (Schiff and Weisberg, 1999; Ridgeway and Shimmield, 2002).

The geochemical composition of each surface sample can be found in appendix B (and will be referred to in the text hereafter) along with particle-size data, summer and winter surface salinity, and water column depth. A summary of the univariate statistics of data obtained for both metal abundances and environmental variables can be found in table 4.1.

The first spatial distribution maps show the raw concentrations detected from ICP-MS analysis and do not take into account any natural factors that may be helping to drive this distribution such as the effect of surface sediment particle size.

	Cr (mg/Kg)	Co (mg/Kg)	Cd (mg/Kg)	Ni (mg/Kg)	Cu (mg/Kg)	Zn (mg/Kg)	Ti (mg/Kg)	Fe (mg/Kg)	Al (mg/Kg)	Pb (mg/Kg)	Clay (%)	Water Depth (m)
Total Samples	77	77	77	77	77	77	77	77	77	77	77	77
Min	47.0	5.7	0.1	11.2	12.3	44.2	2074.0	14178.0	14784.0	16.9	7.3	1.8
Max	280.0	24.7	9.8	112.1	216.3	699.9	9713.0	56243.0	49253.0	168.0	38.3	35
Mean	120.5	15.0	2.5	40.2	50.5	163.2	5385.2	40796.6	28850.6	49.9	23.7	9.2
Std. error	3.6	0.6	0.2	1.7	3.5	10.0	144.7	1065.1	848.0	2.8	0.8	0.8
Stand. dev	31.6	4.9	1.9	15.0	30.3	87.5	1270.1	9346.6	7441.0	24.9	7.2	7.2
Median	118.97	15.76	1.93	37.31	46.57	148.81	5483	41472	27842	50.06	24.6	6.3
Skewness	1.6128	-0.08	1.42	1.602	2.292	3.1364	-0.1	-0.52	0.8248	1.4239	-0.44	1.4813
Kurtosis	7.1491	-0.96	2.57	5.572	9.802	16.16	1	-0.26	0.1787	4.7225	-0.54	1.914

Table 4.1. Univariate Statistics of key heavy metal and environmental data

4.3 Geospatial Analysis

Based on the distribution of individual heavy metal across the PRE illustrated in figures 4.4 – 4.7, their distributions can be grouped into four distinct distribution patterns. The patterns are North River enrichment, Western shoal enrichment, Zhuhai-Macau enrichment and Continental Shelf enrichment. These enrichment patterns are based on raw metal concentration data and the effects of natural variables and the marine and hydrological regimes operating within the PRE have not been accounted for. This initial geospatial analysis is important for understanding the actual distribution of various heavy metals across the PRE, but does not take into account what part of the distribution is driven by natural processes rather than human heavy metal pollution fluxes.

4.3.1 North River Enrichment

Cr, Cu Pb, Ni and Zn are all found to be enriched along the lower course of the North River between Guangzhou and *Humen* gate. In addition to this, Pb also shows enrichment below the *Humen* gate at the apex of the PRE. Cr and Pb also show enrichment along the western shoal between Zhuhai and Macau in the south-west of the Estuary. The highest values of Pb are found at PE20 (168 mg/Kg) and PE14 (105mg/Kg) (see fig. 4.1 and fig. 4.4b), with the values of 65-90mg/Kg in between from PE15-PE19. Zn enrichment gradually increased from the *Humen* gate along the North River towards Guangzhou, starting with concentrations of 145mg/Kg at PE14, rising to

295 mg/Kg at PE19 and peaking at 699 mg/Kg at PE20 (fig. 4.4c and fig. 4.5).

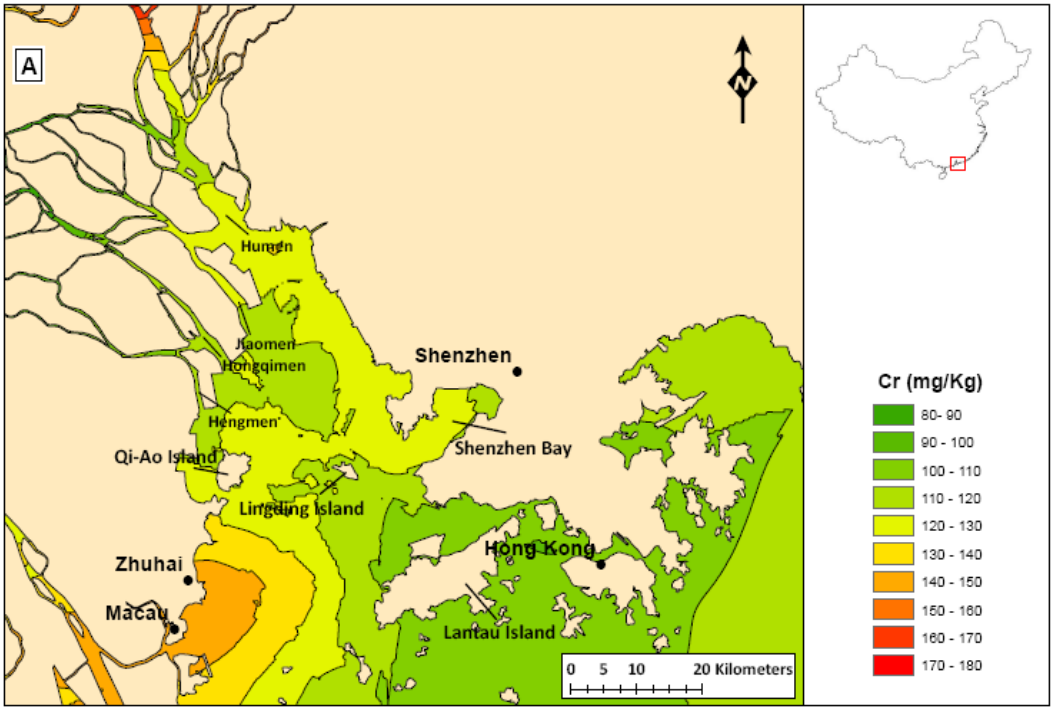

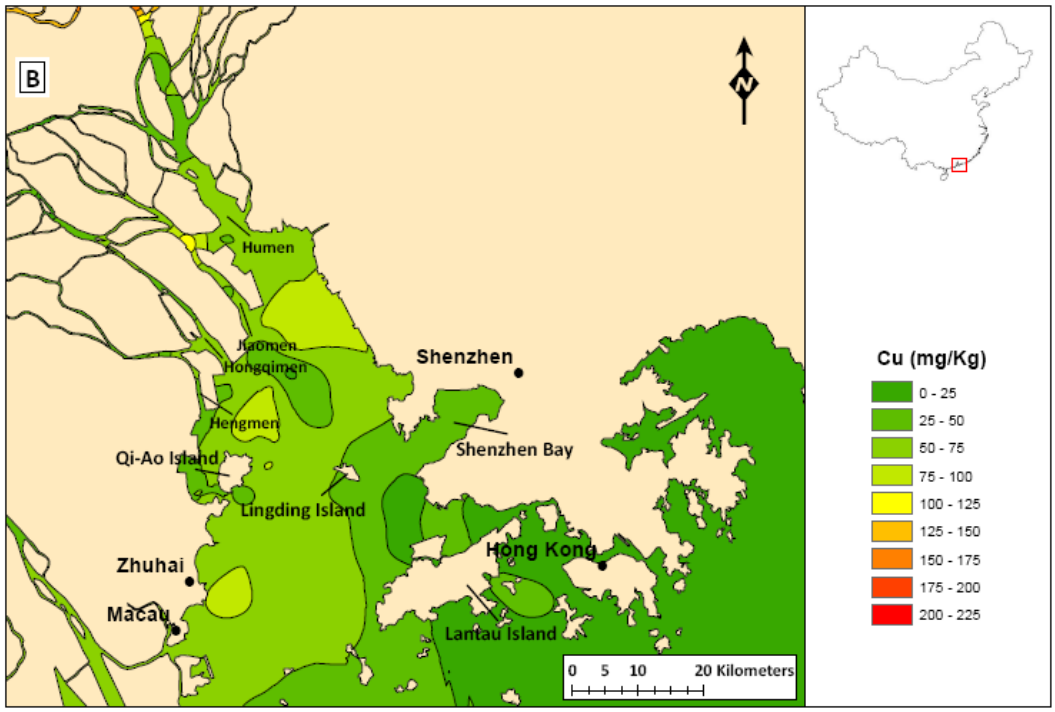

Figure 4.4a Heavy metals with North River enrichment: Cr (A) and Cu (B)

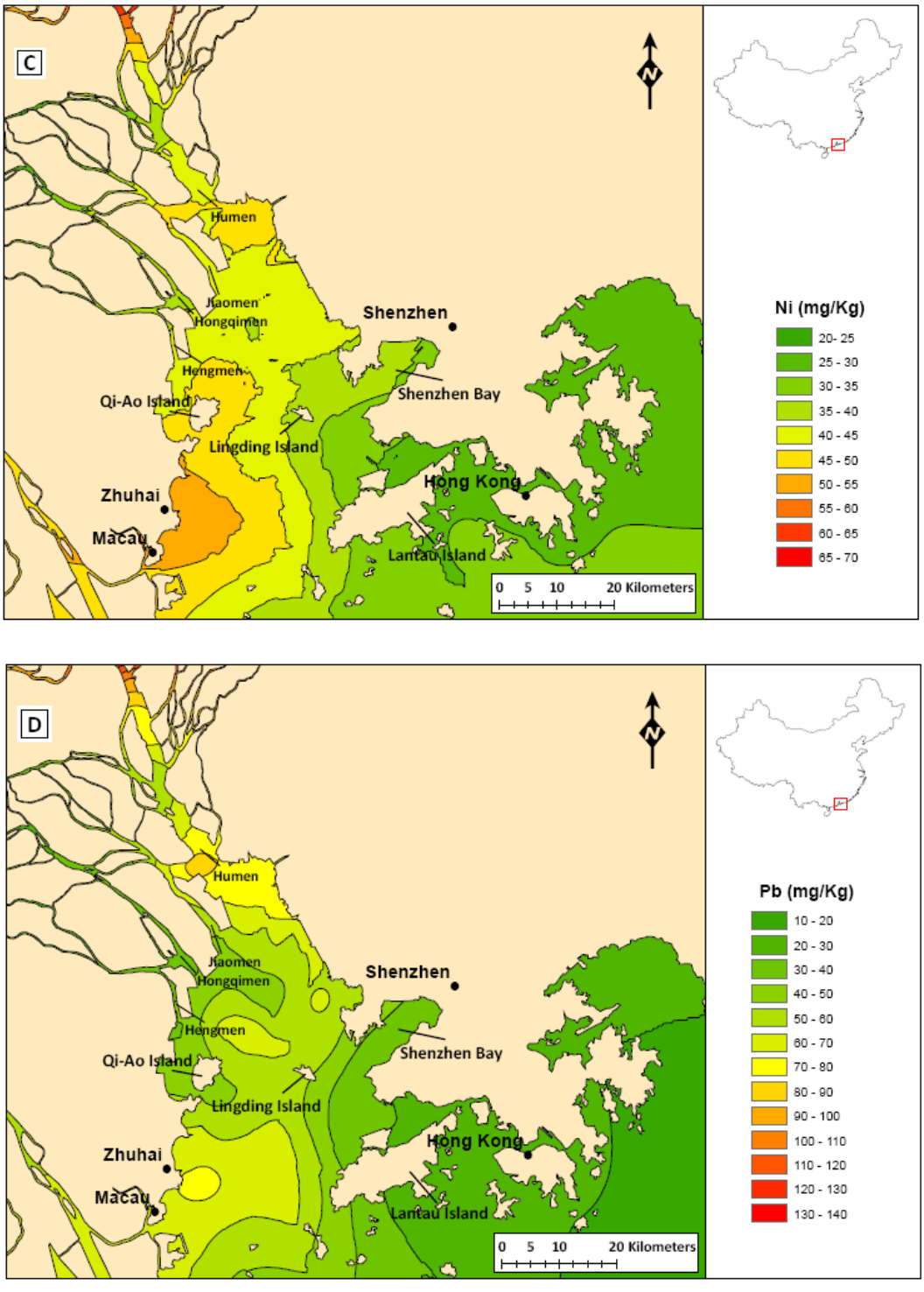

Figure 4.4b. Heavy metals with North River enrichment: Ni (C) and Pb (D)

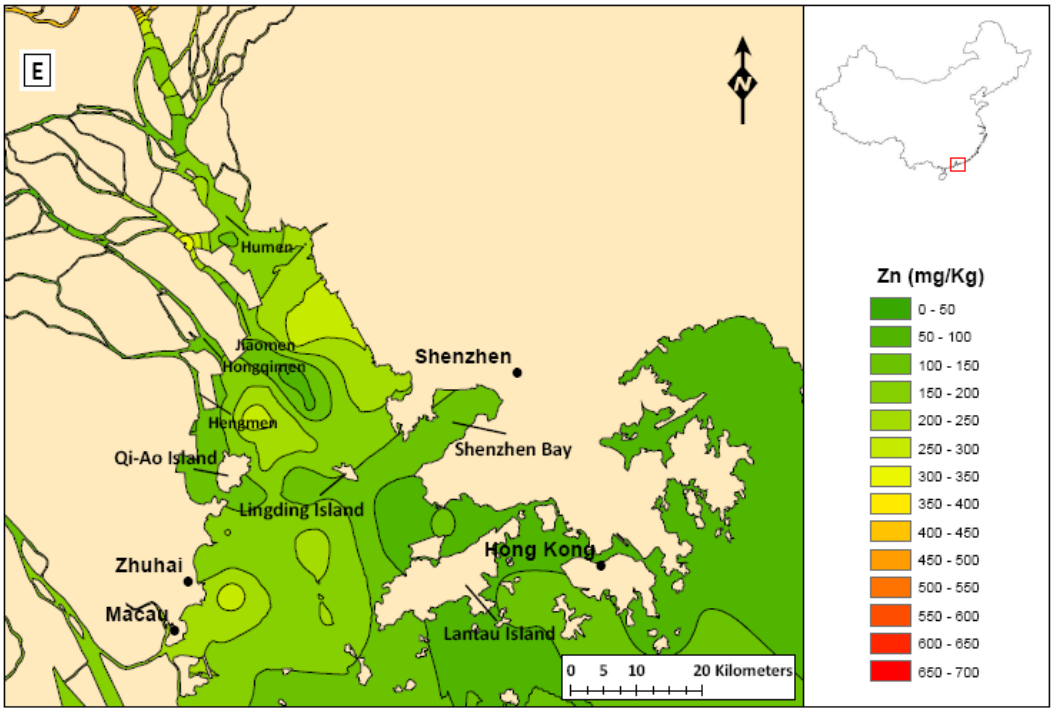

Figure 4.4c Heavy metals with North River enrichment: Zn (E)

Cr and Cu also displays a similar enrichment trend upriver of the *Humen* gate to Zn , with concentrations rising from 117mg/Kg to 144mg/Kg for Cr and from 47.48mg/Kg and 98.63mg/Kg for Cu from PE14-PE19 (see fig. 4.4a and fig. 4.5). Both metals peak in concentration at PE20 with values of 280mg/Kg for Cr and 216.32mg/Kg for Cu. Figure 4.5 illustrates the northward enrichment from the *Humen* gate towards Guangzhou. Sampling location PE20 was taken just down-river of the busy industrial harbour of Guangzhou, and as a result the very high heavy metal concentrations could be influenced by associated industrial activities and waste (Zhou *et al.,* 2004).

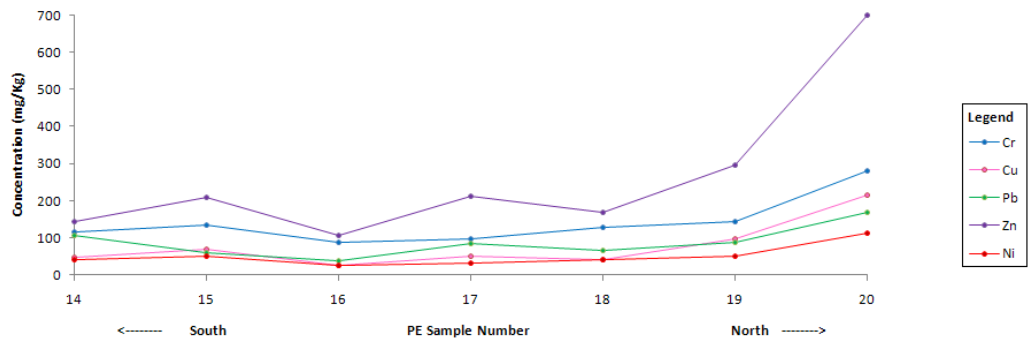

Figure 4.5. Long Profile of North River Enrichment (PE14 – PE20) for Cr, Cu, Ni, Pb and Zn.

4.3.2 Western Shoal Enrichment

This enrichment pattern is associated with Co, Fe and Ti. Fe concentrations are distributed relatively uniformly along the western shoal (see fig. 4.6a), with maximum concentrations of 45,000-50,000mg/Kg with a peaks of 56,243mg/Kg and 74,047mg/Kg at PE67 and PE75 respectively.

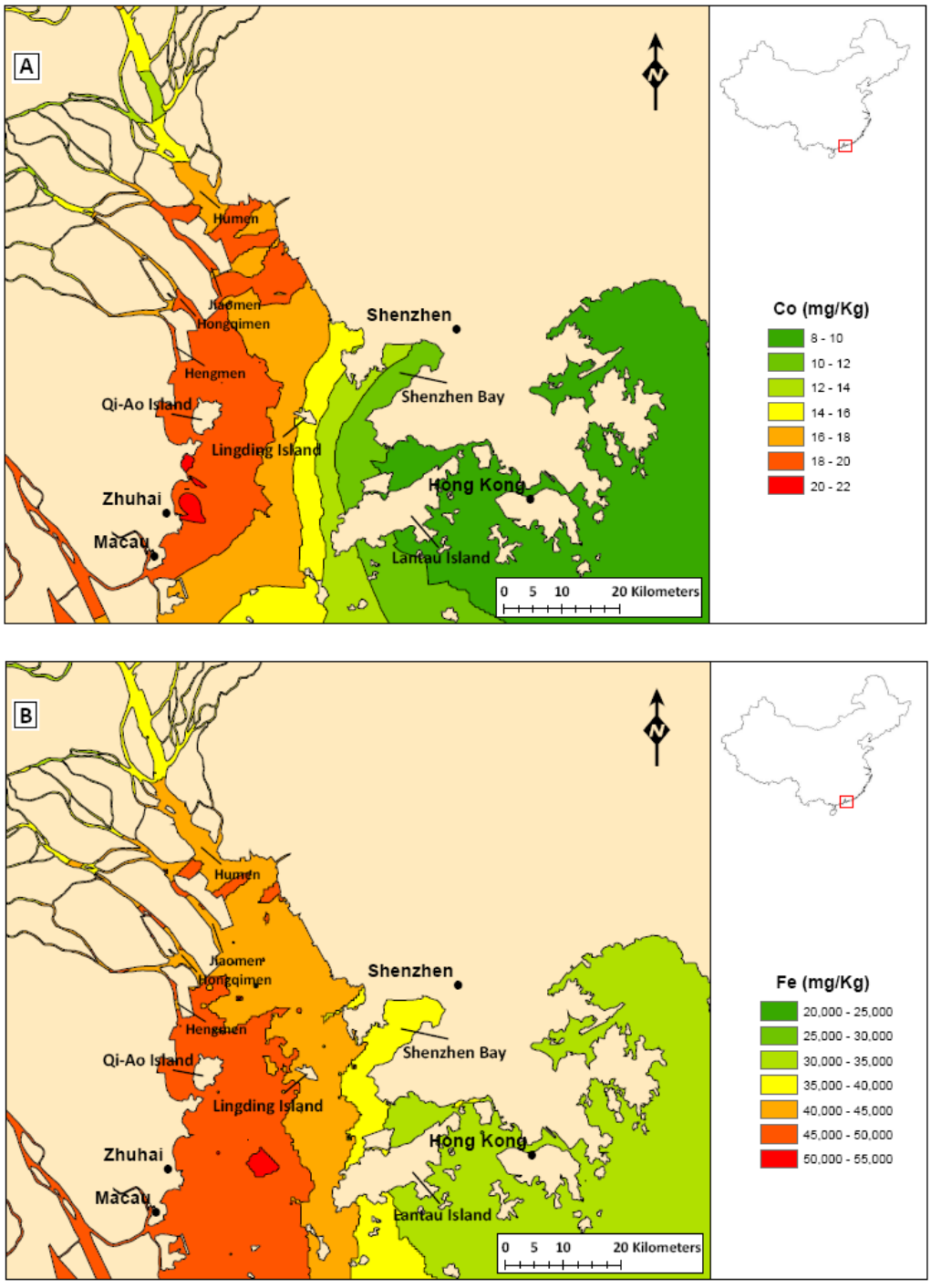

Figure 4.6a Heavy metals with Western Shoal enrichment: Co (A) and Fe (B).

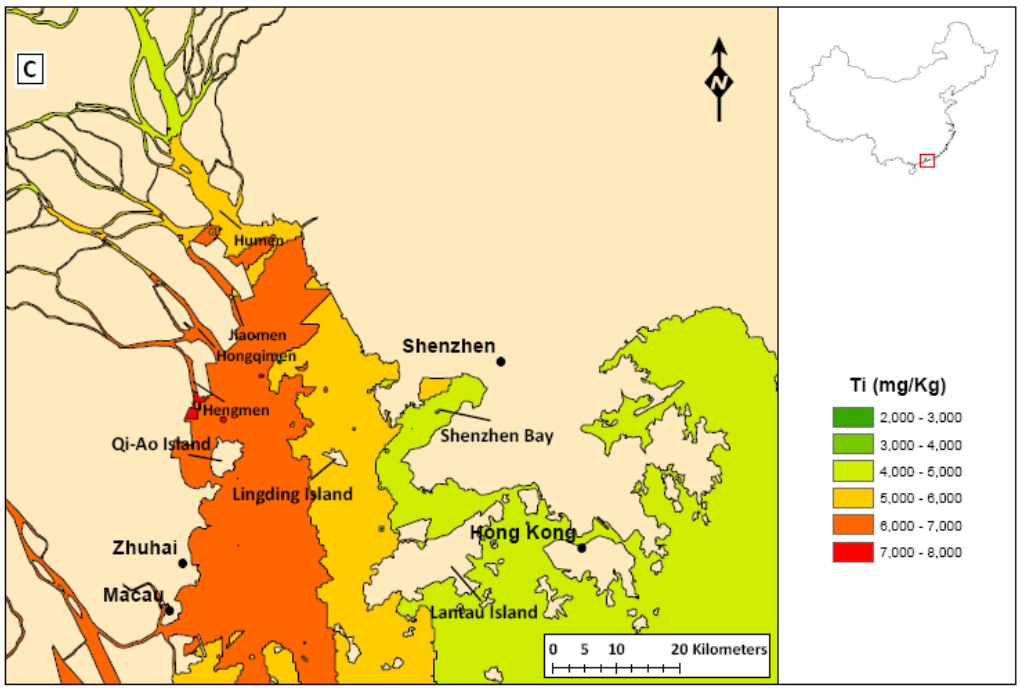

Figure 4.6b Heavy metals with Western Shoal enrichment: Ti (C).

Ti is most enriched in the area around and just north of Qi-Ao Island (see fig. 4.6b). The highest concentrations of Ti are found at PE54 (9713mg/Kg) where the Pearl River enters the PRE through the *Hongqimen* gate and at PE57 (8424mg/Kg) in the Maximum Turbidity Zone (Wai *et al.,* 2004). Co concentrations are highest in the area directly adjacent to Zhuhai, where maximum concentrations are found to be 28.11mg/Kg and 24.57mg/Kg at sites PE75 and PE78 (see fig. 4.6a).

4.3.3 Zhuhai-Macau Enrichment

This enrichment pattern is predominantly associated with Cd (see fig. 4.7a). Although occurring in very low concentrations (<10mg/Kg), Cd is spatially most enriched in sediments adjacent to Macau where concentrations are generally >4.5mg/Kg. The highest Cd concentration are found at locations PE20, PE78 and PE88 where concentrations are 6.16mg/Kg, 9.76mg/Kg and 8.99mg/Kg respectively. In addition to Cd, a component of the Cr distribution is *Zhuhai-Macau* enriched. Concentrations of >140mg/Kg are observed (see fig. 4.4a), with concentration peaks of 141.63mg/Kg at PE81 and 196.93mg/Kg at PE78.

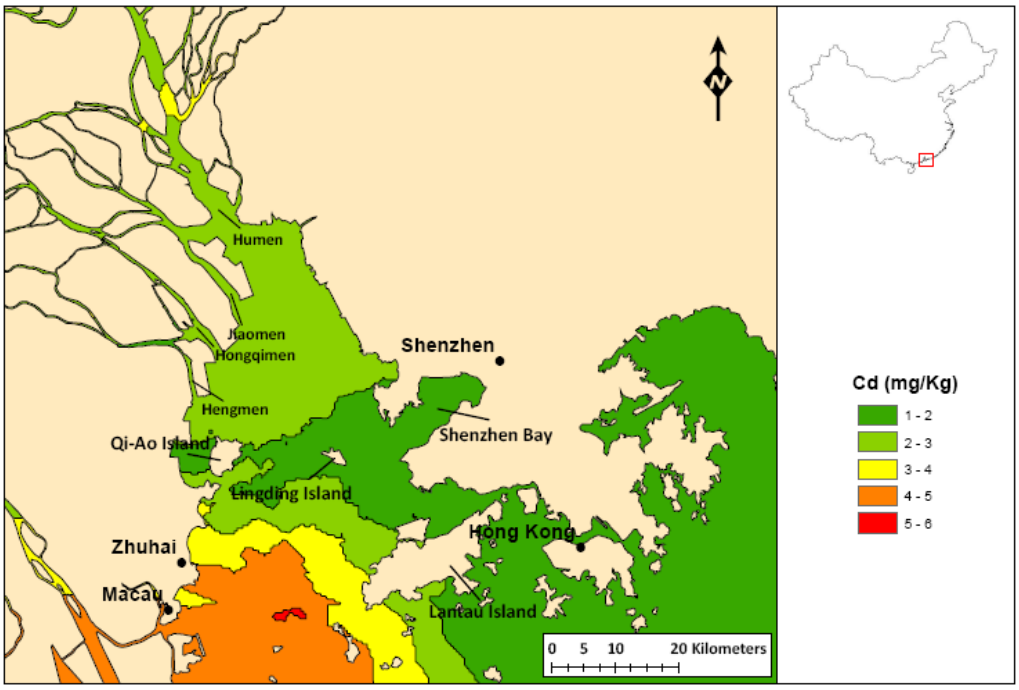

Figure 4.7a Heavy metals with *Zhuhai-Macau* enrichment: Cd

4.3.4 Coastal Water Enrichment

Al is most enriched within marine waters of the South China Sea outside the PRE and to a lesser extent in the south-central and mid-eastern parts of the estuary (see fig. 4.b).

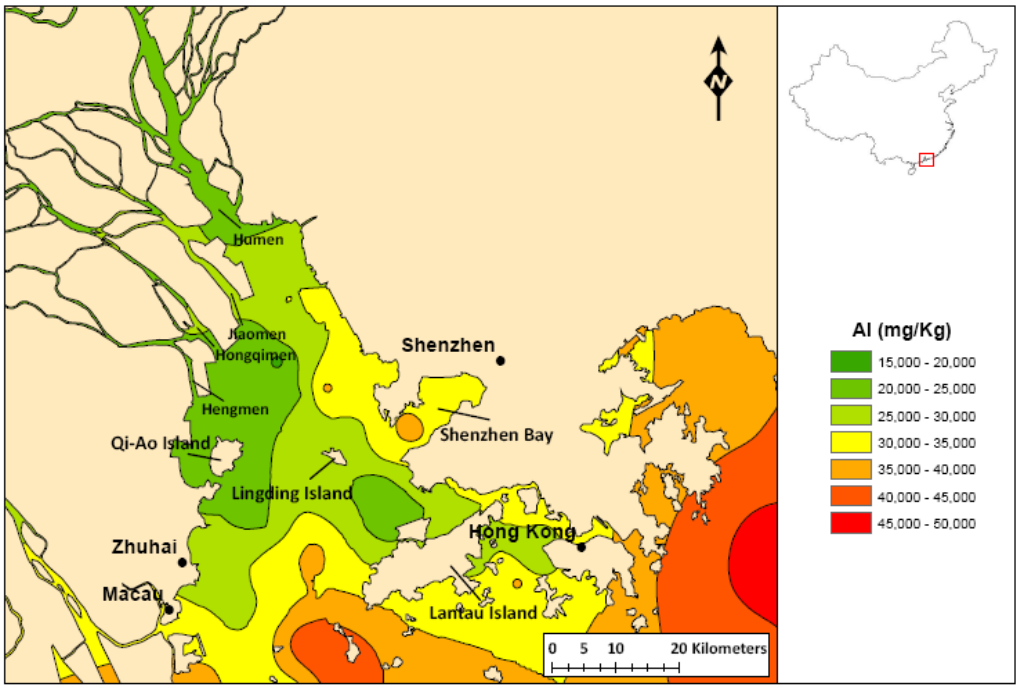

Figure 4.7b Heavy metals with Coastal Water enrichment: Al

Maximum Al concentrations of 49,024mg/Kg and 44,819mg/Kg found at PE22 and PE92 respectively.

4.4 Normalised Geospatial Analysis

Accounting for the effect of natural factors such as increased bedrock weathering or heavy metal particle size affinity may have in controlling the spatial distribution of heavy metals is key to understanding the sources, sinks and transport pathways of these pollutants. Various methods have been implemented to achieve this (see Schiff and Weisberg, 1999 for references) and in the PRE Al, Fe and Ti have been used (Li *et al.,* 2000; Zhou *et al.,* 2004). These elements were chosen for normalisation because they act as proxies for particle size and therefore any heavy metal particle size affinity, and they are conservative tracers of natural weathering and erosion rates within the Pearl River catchment. The problem with the use of conservative tracer elements such as Al, Fe and Ti is that they assume: the tracer element covaries in proportion to the naturally occurring concentrations of the metal of interest, that they are insensitive to anthropogenic enrichment and that they do not undergo diagenic chemical changes post-deposition (Schiff and Weisberg, 1999).

Based on the results from geospatial analysis (see fig. 4.3 and 4.7), enrichment of Al appears to be controlled by factors operating within the adjacent coastal waters and not solely due to weathering and erosion of bedrock within the Pearl River Catchment. This distribution highlights the problem of using Al as a conservative tracer of natural weathering and erosion variability within the PRE as suggested by Zhou *et al.,* (2004). For normalisation using Fe or Ti to work, they would need to act as a proxy for the affinity of heavy metals to bond with fine clay particles during deposition (Ridgway and Shimmield, 2002). With correlation coefficients of 0.22 for Fe and 0.05 for Ti with respect to clay content (see table 4.2), these elements also seem inappropriate for use in this study. For this reason, direct normalisation using particle size information was chosen.

A simple formula will be used to achieve this:

$$\text{Normalised Metal}_x = \text{Raw Metal}_x \times (1 - \text{Clay}_f)$$

where $Raw\ Metal_x$ is the concentration of given metal from ICP-MS (mg/Kg) and $Clay_f$

is the fraction of the particle size distribution that is clay (<4µm). This method means that samples with a higher percentage of clay carry a lower weighting and the effect of grain size affinity is accounted for (Ip *et al.,* 2004). It is important to note that the use of particle size is not without similar problems to those associated with Al and Fe (Daskalakis and O'Conner, 1995). In particular, the clay fraction can be affected by changes in suspended sediment load which is the result of human activities such as Dam building (reducing) and afforestation (increasing); activities that occur throughout the Pearl River catchment (Zhang *et al.,* 2008). Municipal wastewater inputs can also affect the proportion of fine particulates entering the river system (Schiff and Weisberg, 1999) and may bias the normalised data. With the high associated affinity of heavy metals to fine (clay) particulates, and the associated problems with using conservative tracer elements, particularly within this study area the use of particle size to normalise pollutants concentrations is justified.

Normalised concentrations for the same heavy metals as in sub-chapter 4.3 are presented below. The same kriging interpolation using a spherical semivariogram was used for consistency. Each of the metals analysed still exhibits the same overall pattern of distribution across the PRE (see fig 4.8 – 4.11) as before normalisation. Normalised metals are displayed in mg/Kg for easier visual interpretation, however, due to the normalisation technique this is an arbitrary value and no longer give a quantitative value for heavy metal concentration as the new value accounts for fine particle size affinity.

4.4.1 Normalised North River Enrichment

Cr, Cu, Ni, Pb, and Zn show the same distribution as before normalisation but their relative concentrations outside the areas of enrichment are much more uniform, particularly for Cr and Pb (see fig 4.4b and Fig 4.8b for comparison). A feature of all the metals with this North River enrichment pattern is a concentration minimum in the central-north region of the estuary. This feature although not as prominent in the non-normalised data is still evident (see fig. 4.4a,b,c) and falls in the same region where the highest sand particle size concentrations can be found (see fig 4.3).

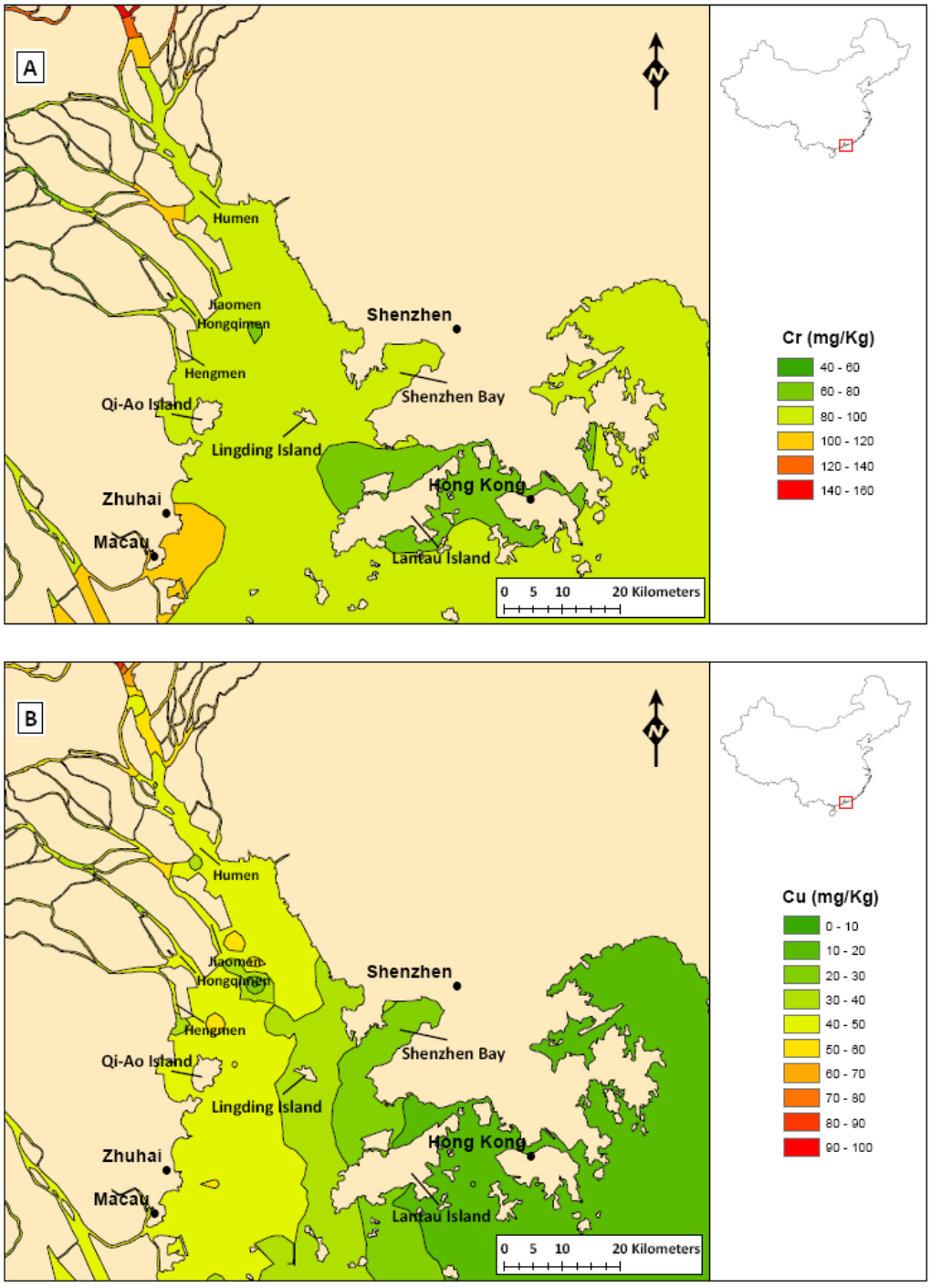

Figure 4.8a Normalised heavy metals with North River enrichment: Cr (A) and Cu (B)

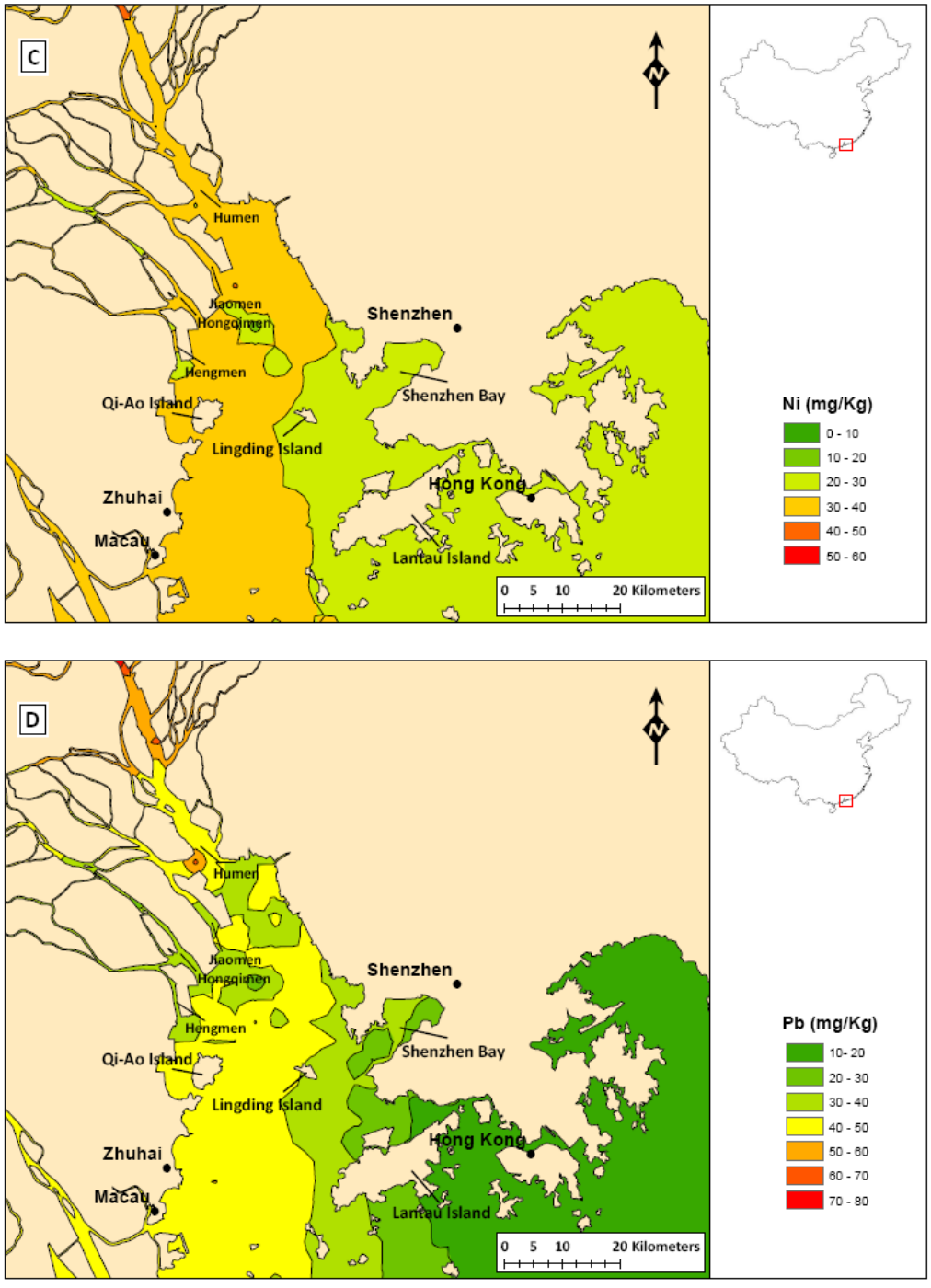

Figure 4.8b Normalised heavy metals with North River enrichment: Ni (C) and Pb (D)

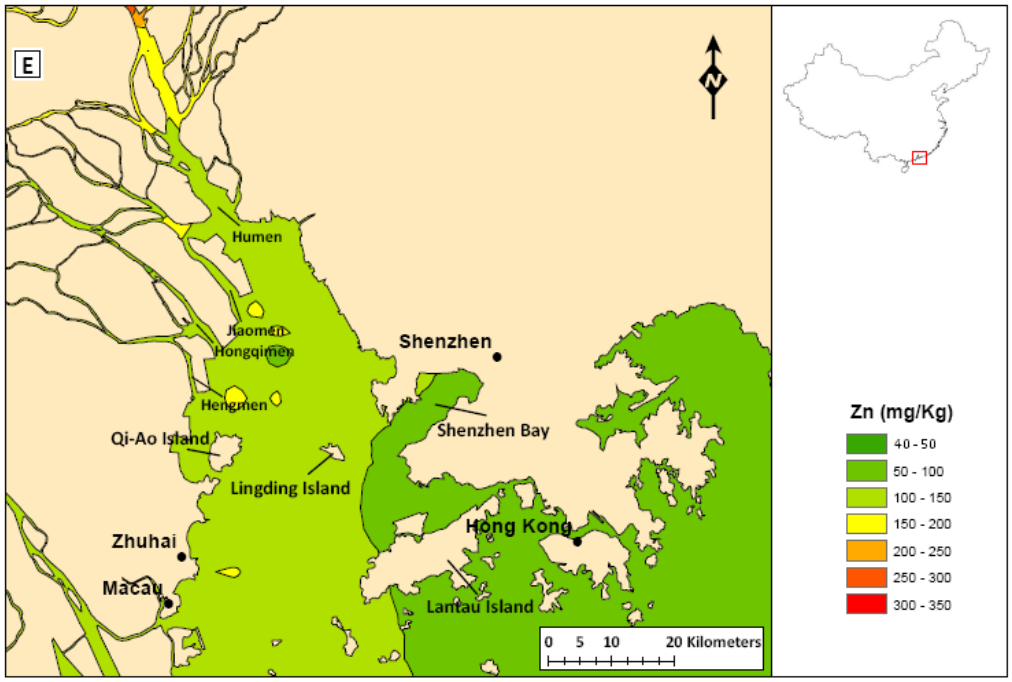

Figure 4.8c Normalised heavy metals with North River enrichment: Zn (E)

4.4.2 Normalised Western Shoal enrichment

Co, Fe and Ti still show Western Shoal enrichment (see fig. 4.9a,b) , but as with the North River enriched sediments, these metals are much more uniformly distributed along the western shoal. This further suggests that much of the variability in the raw data was due to localised areas of greater or lesser clay content.

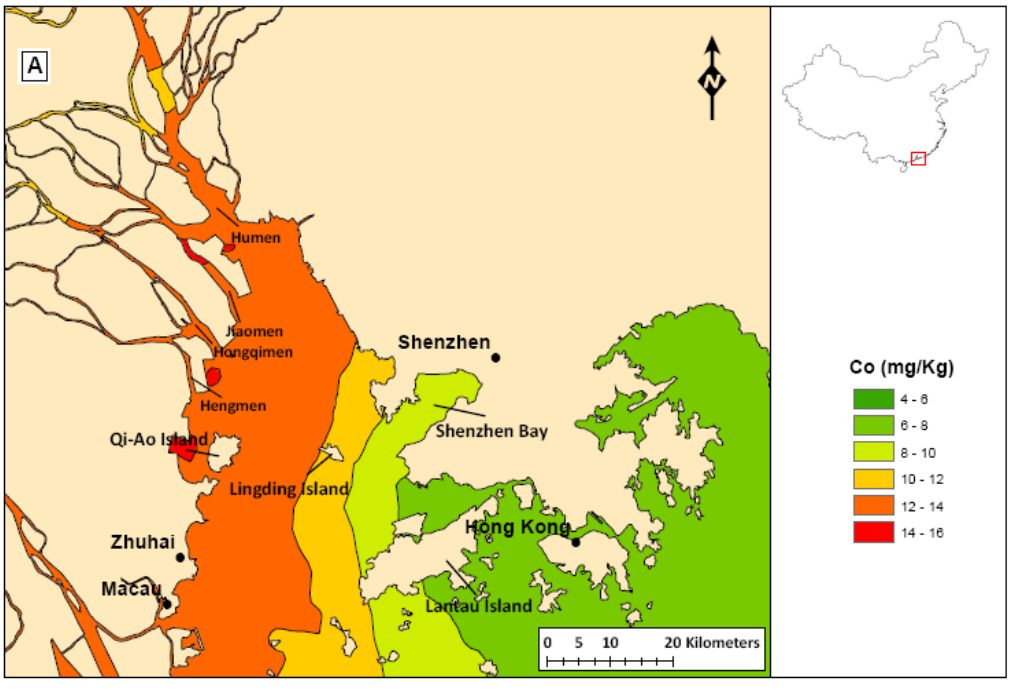

Figure 4.9a Normalised heavy metals with Western Shoal enrichment: Co (A)

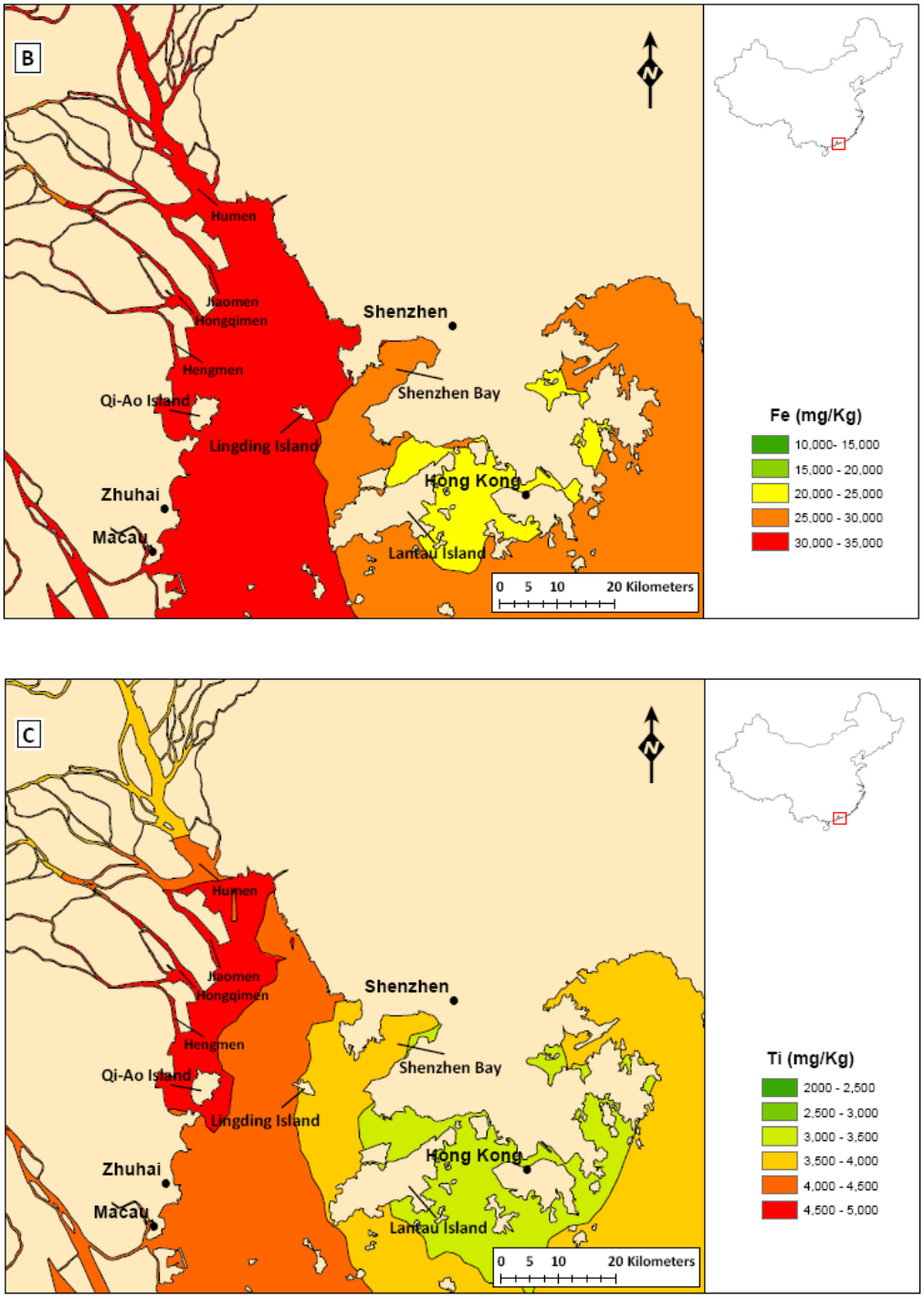

Figure 4.9b Normalised heavy metals with Western Shoal enrichment: Fe (B) and Ti (C)

4.4.3 Normalised Zhuhai-Macau and Coastal Water enrichment

Cd and Al still show Zhuhai-Macau and Coastal Water enrichment respectively. With the effect of grain size accounted for, it appears that both metals are more enriched outside the PRE. Cd displays some enrichment along the lower course of the *North River* before it exits through the *Humen* gate into the PRE. Interestingly, low concentrations are found extending from coastal waters, through Hong Kong and across the centre of the estuary to Qi-Ao Island (see fig. 4.10).

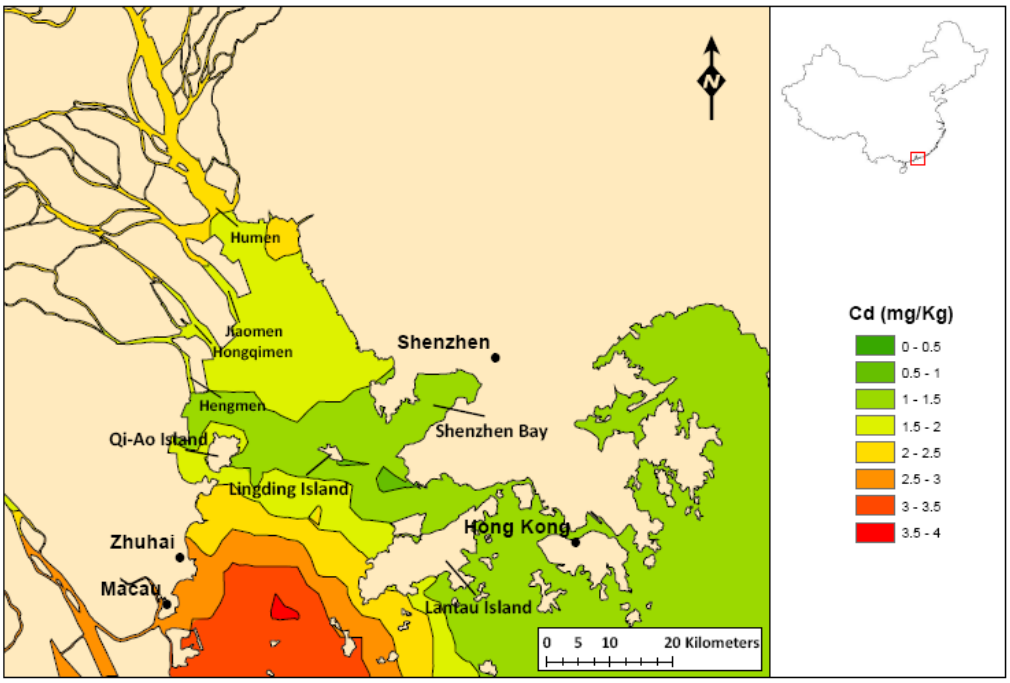

Figure 4.10 Normalised heavy metals with Zhuhai-Macau enrichment: Cd

Al enrichment is still highest outside the PRE in the adjacent coastal waters, and to a much lesser extent along the Eastern shoal and Shenzhen Bay and in the south-central areas of the PRE below Lantau Island (see fig. 4.11).

4.5 Statistical Analysis

Statistical analysis was performed on the raw ICP-MS heavy metal data from surface samples to assess the significance of distribution patterns observed in the geospatial analysis. Correlation coefficients for the normalised heavy metals studied and clay (%) were calculated by Pearson's Product-Moment method using SPSS 16 for windows and the results from this are shown in table 4.2, with all correlations being

significant at the 99% confidence limit (two-tailed). As expected, there are good correlations between metals with the same pattern of distribution in the PRE.

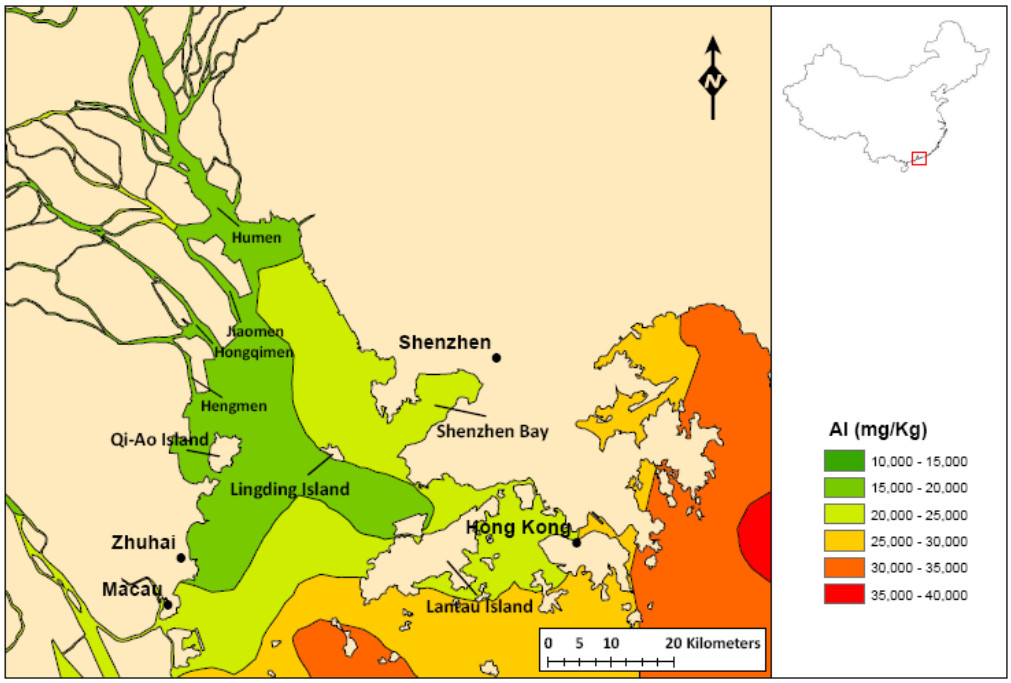

Figure 4.11 Normalised heavy metals with Coastal Water enrichment: Al

Values in red indicate correlations between North River enriched metals and green indicate Western Shoal enriched metals.

	Al	Cd	Co	Cr	Cu	Fe	Pb	Ni	Ti	Zn	Clay
Al	1.00	0.06	-0.27	0.03	-0.27	-0.01	-0.30	-0.14	0.03	-0.20	-0.08
Cd		1.00	0.39	0.53	0.48	0.43	0.46	0.53	0.35	0.48	0.05
Co			1.00	0.52	0.68	0.84	0.60	0.73	0.71	0.56	0.39
Cr				1.00	0.84	0.62	0.71	0.91	0.47	0.87	0.11
Cu					1.00	0.63	0.87	0.95	0.49	0.96	0.10
Fe						1.00	0.54	0.72	0.83	0.54	0.22
Pb							1.00	0.81	0.26	0.89	0.09
Ni								1.00	0.55	0.93	0.21
Ti									1.00	0.37	0.05
Zn										1.00	0.04
Clay											1.00

Table 4.2. Correlation coefficients of normalised heavy metals and clay.

Principal component analysis (PCA) reduced the 10 heavy metal variables mapped in the PRE to three principal components using a Varimax rotated method for comparability with the work of Zhou *et al.,* (2004). Factor 1 represents Cr, Cu, Fe, Pb, Ni

and Zn, factor 2 represents Co, Fe and Ti, and factor 3 represents Al. These three principal factors explained 86% of the total variance: factor 1 (46%) and factor 2 (28%) and factor 3 (12%).

The results from PCA illustrate the geochemical association of the selected metal elements. The grouping of elements within the first three factors is very similar to their geospatial association (see fig. 4.12). This identifies that each grouping of elements have either the same source, follow the same transport pathway, or are a combination of the two (Zhou *et al.,* 2004).

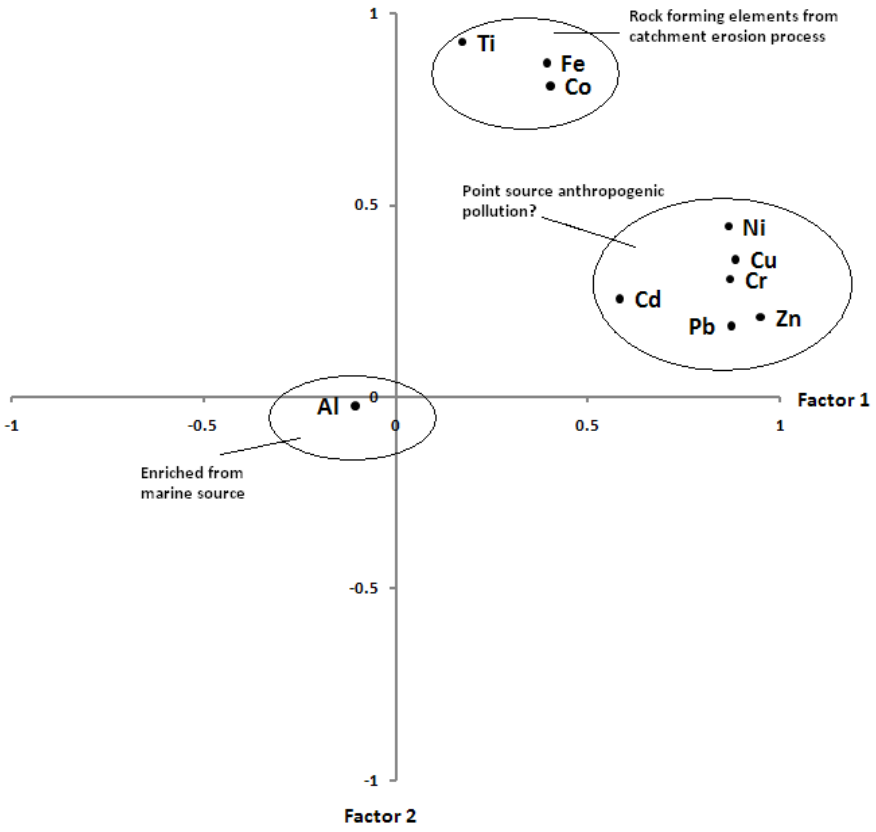

Figure 4.12. Principal component score plots for heavy metal elements in PRE sediments (n=77).

4.6 Interpreting the Spatial Data

Mapping of the raw and normalised data for Al, Cd, Co, Cr, Cu, Fe, Ni, Pb, Ti, Zn has shown that a number of different patterns of distribution occur within the PRE and that these are not simply driven by the affinity of heavy metal pollutants to fine particulates.

It is clearly visible that the distribution of various heavy metals within the PRE is

not simply the result of particle size affinity. Even when this natural variability is accounted for, four distinct patterns of distribution and enrichment remain. Heavy metal elements can be sourced from natural weathering and erosion and therefore should covary with tracer elements that are not affected by anthropogenic enrichment (Schiff and Weisberg, 1999). Enrichment above what can be accounted for by natural weathering and erosion must therefore come from point or diffuse anthropogenic sources. Point sources in the PRE are most likely to be the result of wastewater associated with mining (Zhang and Wang, 2001), industrial and urban activities (Ip *et al.,* 2004). Diffuse sources have been associated with the burning of fossil fuels from domestic and industrial sources resulting in atmospheric fallout that may be transported to the region over some distance (Wong *et al.,* 2003).

4.6.1 Marine Sourced Heavy Metals

Al distribution within the PRE shows strong enrichment in the marine waters outside the estuary to the south and east, where water depths exceed 15m and are generally greater that 20m. Surface sediments with higher Al concentrations are also found around Lantau Island, and extend along the eastern channel and shoal of the estuary as far north as Shenzhen Bay. This distribution is most likely driven by the association of Al with very fine clay particles (<0.002mm diameter) that are most abundant outside the estuary (Ip *et al.,* 2007) (see fig. 4.13) and are transported into the southern and east parts of the PRE on flood tides (Harrison *et al,* 2008). Particle size data from this study considers all particles <0.004mm in diameter as clay, but does not sub-divide the clays into fine, medium and course fractions. Ip *et al.,* (2007) conducted a study of the PRE and adjacent South China Sea (SCS) and looked at <0.002mm fraction. The results show higher concentrations of this fine clay fraction outside the estuary, that has a strong association with the highest concentrations of Al.

Winnowing driven by intrusion of shelf waters through the east channel during flood tides may drive result in the re-suspension and transport of very fine clays (Piper *et al.,* 2006) onto the eastern shoal causing higher concentrations of Al in this region of the estuary, but no research into the presence of winnowing is presented in this thesis. Another viable reason is simply the dilution of Al due to estuarine sedimentation.

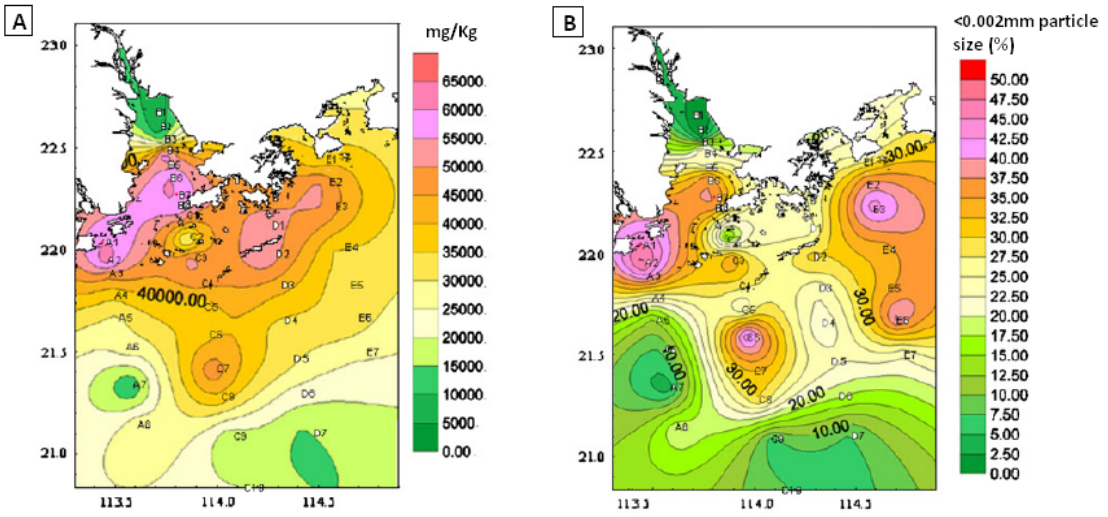

Figure 4.13. Concentrations of Al (A) and fine clay (B) on the continental shelf outside the PRE (Ip *et al.*, 2007)

4.6.2 Rock Forming Heavy Metals

Fe and Ti have been identified as elements that are present in PRE surface samples as a result of weathering and erosion of bedrock with the Pearl River catchment (Li *et al.,* 2000; Zhou *et al.,* 2004). This is verified by their very uniform enrichment along the Western shoal and North River (see fig. 4.9b), and their close association derived from PCA. This distribution is therefore the result of the flux of terrestrially derived sediment being discharged from the East, North and West Rivers into the estuary though the *Humen, Jiaomen, Hongqimen* and *Hengmen* gates. Subsequent to entering the PRE, circulatory patterns that have already been identified to operate in the PRE deflect the riverine freshwater along the western side of the estuary where it is deposited. Normalisation of Fe and Ti (fig 4.9b) shows that much of the variability in the raw data (fig. 4.6a,b) is the result of localised particle size variations.

Co distribution is highly correlated with Fe (0.84 correlation coefficient) and its distribution to an extent, must be attributed to either the same circulatory forcing, the same source or a combination of both. Other studies of the PRE have come to very different conclusions about the dominant source of Co in estuarine sediments. Zhou *et al., (*2004) concluded that Co in PRE surface sediments was the result of industrial drainage, whilst others suggest that the concentration ranges of Co in PRE sediments match those of the sub-surface geology and are therefore of lithogenic origin (Li *et al.,*

2000). Co exists within bulk continental crust in concentrations of approximately 29mg/Kg, ranging from 10mg/Kg – 35mg/Kg (see table 4.3) between the upper and lower crust respectively (Taylor and McLennan, 1995). With the maximum values of Co being <29mg/Kg in PRE sediments, its spatial distribution being relatively uniform in the areas that receive the bulk of freshwater input and terrestrial sediment flux, and its high correlation coefficient to other weathered rock forming elements (Fe and Ti), it is suggested here that its enrichment and distribution in PRE sediments is almost entirely the result of natural weathering, erosion and transportation processes. This conclusion will be further investigated in the next chapter when its temporal variability is analysed.

4.6.3 Heavy Metal Pollutants from Point Sources

This final group of heavy metals (Cd, Cr, Cu, Ni, Pb and Zn) have been identified through their spatial distribution that is very different from the rock forming elements in the PRE, high correlation coefficients, and similar factor loadings from PCA to be the result of point sources.

The enrichment of Cd occurs in the lower section of the western shoal between Zhuhai and Macau. Cd also has a much lower factor 1 loading based on results from PCA than the other metals that have been identified as coming from point sources. Cd is a rare element in nature and exists in concentrations <1mg/Kg in soil, <1µg/Kg in freshwater, <0.2µg/Kg in seawater (Hiatt and Huff, *1975*) and <1µg/Kg in bulk continental crust (Taylor and McLennan, 1995). Concentrations of Cd in nature that exceed 5mg/Kg are only found in a few organic rich sedimentary rocks such as shale where concentrations can reach 11mg/Kg. Within the Pearl River catchment, shale only accounts for a small percentage of the total area drained but accounts for about 30% of the *East River's* catchment (Zhang and Wang, *2001*). Cd is also highly associated within polymetallic complexes including Pb-Zn and Cu-Pb-Zn (Hiatt and Huff, *1975*). The slight enrichment of Cd along the North River between Guangzhou and the *Humen* gate is most likely the result of both the metals association with Cu, Pb and Zn which have elevated concentrations in this region, and the influx of Cd rich weather shale from the East River (see fig. 2.1) which is confluent with the North River in the same area.

Cd enrichment south of Zhuhai on the western shoal is however, is associated with elevated levels of Cu, Pb and Zn and therefore the concentrations of >4.5mg/Kg are the result of other forcing factors. Macau is widely acknowledged as an important manufacturing region and as a result is a localised source of Cd through production processes such as electroplating (galvanising), use of metallic alloys and the stabilisation of plastic compounds (Hiatt and Huff, *1975*). This region of the estuary also has the highest concentrations of organic carbon in surface sediments (Hu *et al.,* 2006) (see fig 4.14), which have a high Cd affinity (Hiatt and Huff, *1975*). The combination of hydrodynamic process that result in the deposition of organic matter combined with points sources of Cd from manufacturing are the most likely cause of Cd enrichment in the south-west of the PRE. It is further suggested here that the localised enrichment that does not extend into the centre-south of the PRE where the maximum organic carbon concentrations are (fig. 4.14) is due to estuarine circulation which is characterised in this region by a south-westerly flow direction.

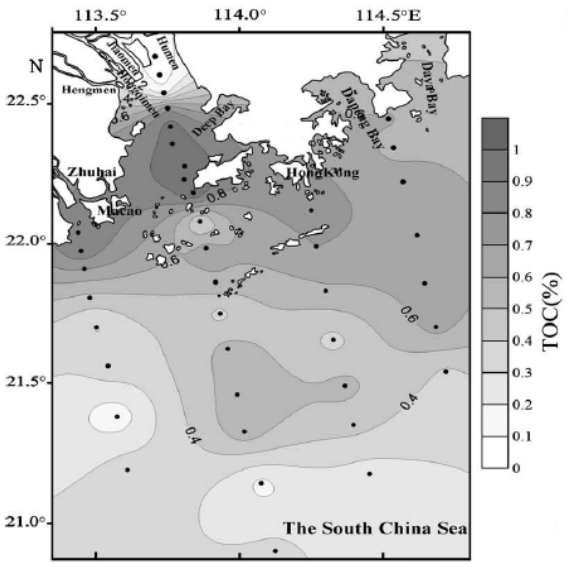

Figure 4.14. Spatial Distribution of TOC (%) in estuarine and shelf sediments of the Pearl River (Hu *et al.,* 2006)

The final metals to discuss are Cr, Cu, Pb, Ni and Zn which are all slightly enriched along the western shoal and highly enriched along the lower reaches of the North River near Guangzhou. Based on PCA, Pb and Zn have slightly lower factor 2 loadings which suggests that their enrichment is less a result of natural weathering and erosion as for Cr, Cu and Ni (see fig.4.12). These metals are all highly correlated, with

coefficients ranging from 0.71 (Cr Vs Pb) to 0.96 (Cu-Zn) and make up the first principal component from PCA. This is significant in itself, as other studies from the PRE have show no or very little correlation between Pb and other heavy metals (Li *et al., 2000*; Zhou *et al.,* 2004). Compared to upper continental crust concentrations (Taylor and McLennan, 1995) and agricultural soils in the PRD (Wong *et al.,* 2002), the concentrations of the North River enriched sediments are significantly higher for Pb and Zn, and less obviously for Cr, Cu and Ni (see table 4.3). Due to these metal belonging to a separate component group to the rock forming metals Co, Fe and Ti determined by PCA, their spatial distribution and enrichment must be partly due to anthropogenic inputs.

Group (mean values)	Cr (mg/Kg)	Cu (mg/Kg)	Pb (mg/Kg)	Ni (mg/Kg)	Zn (mg/Kg)
Estuarine Sediments (n=77)	120.5	50.5	49.9	40.2	163.2
Agricultural Soils (n=38)	71.4	33.0	40.0	21.2	84.7
Bulk Continental Crust (Upper Crust – Lower Crust)	185 (35-235)	75 (25-90)	8 (20-4)	105 (20-135)	80 (71-83)

Table 4.3. Concentrations of heavy metals as a background reference for estuarine sediments.

Pb and Zn are highly correlated in the surface samples (0.89), and both show the same pattern of increasing enrichment from PE14 – PE20 (see fig. 4.5), with both having maximum concentration values at PE20. Much of the literature associates anthropogenic enrichment of Pb in the PRD to non-point sources such as atmospheric deposition and wastewater discharge (Li *et al.,* 2000; Wong *et* al., 2003; Liu *et al.,* 2003; Zhou *et al.,* 2004; Lee *et al.,* 2007). The strong correlation between these two metals, their greatly enriched concentrations along the North River compared to background (naturally occurring) values, and their low factor two loadings from PCA suggests that a component of their enrichment is not the result of natural processes. In fact, their enrichment as a result of anthropogenic forcing could result in as much as 25% and 90% of Pb and Zn respectively[2] within the most enriched sediments, based on table 4.2. Pb and Zn aerosols are emitted as the result of coal burning (Okudo *et al.,* 2008). Pb and Zn are also closely associated through mining as their parents ores Galena (PbS) and Sphalerite (ZnS) which occur together (Sonke *et al.,* 2008) and are mined at

2 Percentage enrichment values are based on the concentration of Pb and Zn (mg/Kg appendix B) compared with concentrations in upper continental crust (table 4.3).

Lechang and Fankau then smelted at Shaoguan approximately 200km north of the *Humen* gate along the *North River (*Zhang and Wang, 2001; Shu *et al.,* 2002). Zhang and Wang, (2001) found that sediments of the North River we highly enriched in Pb, with concentrations peaking at 234.6mg/Kg immediately down-river of the Shaoguan smeltery and Pb concentrations were only slightly reduced 100km north of the *Humen* gate at Qingyuan. This is just one example of a number of Pb/Zn and Cu mining operations that are exploiting carbonate bearing metal sulphide deposits in Guangdong, Guizhou and other provinces that are directly linked to the PRE through the Pearl River drainage system (Zhang *et al.,* 2004; Liu *et al.,* 2005; Zhou *et al.,* 2007).

With severe enrichment of Cu, Pb and Zn of mining wastewater and tailings, mobilisation of metals through acidification (Shu *et al.,* 2001) and carbonate solubility (Zhang *et al.,* 2004) and connectivity to the PRE through the Pearl River drainage basin, the highly enriched values of Pb, Zn and to a lesser extent Cu in the North River are most likely the result of anthropogenic enrichment from mining activity, atmospheric deposition and some direct input from urban wastewater. The peak in concentrations north of the *Humen* gate are likely to be caused by extra point source enrichment associated with urban drainage and waste (Zhou *et al.,* 2004), however, the overall elevated concentrations observed, particularly along the western shoal (due to estuarine circulatory regimes) are most likely the result of numerous mining activities, and atmospheric deposition within the Pearl River catchment; hence the strong association between Pb and Zn.

While there is little information regarding the sources of Cr and Ni within the Pearl River system, their close correlation to Cu, Pb and Zn suggests that their moderate enrichment within PRE sediments is the result of similar transport pathways to Cu, Pb and Zn. Their sources are most likely from industrial and urban waste from population centres along the low course of the Pearl River and tributaries (Zhou *et al.,* 2004) and from coal burning which has proven an important source of Cr and Ni in studies from Canada (Goodarzi *et al.,* 2008). This is deduced again by the lack of correlation of Cr and Ni with the rock forming elements Fe and Ti, and by their high factor 1 loadings from PCA, suggesting that their respective enrichment is more likely to be anthropogenic.

An interesting characteristic of all the heavy metals spatial analysed with the

exception of Al, is their low concentrations found in the waters in and around Hong Kong. Hong Kong has been identified as a point source of pollution due to wastewater and other effluents being discharged into its surrounding waters as the result of domestic and industrial activities (Yin and Harrison, 2007). This pattern is further verification of the forcing effect the estuarine circulation plays in controlling the distribution of these pollutants within the estuary. The 'flushing' of shelf waters through the Lantau and East Lamma Channel (see fig 1.1) is likely to account for these low concentrations. Once in Hong Kong waters, wastewater and its associated dissolved and particulate pollutants are transported into the PRE along the East Channel during flood tides before being circulated around to the western side of the estuary and drained back out into the SCS.

4.7 Ecotoxicological Assessment

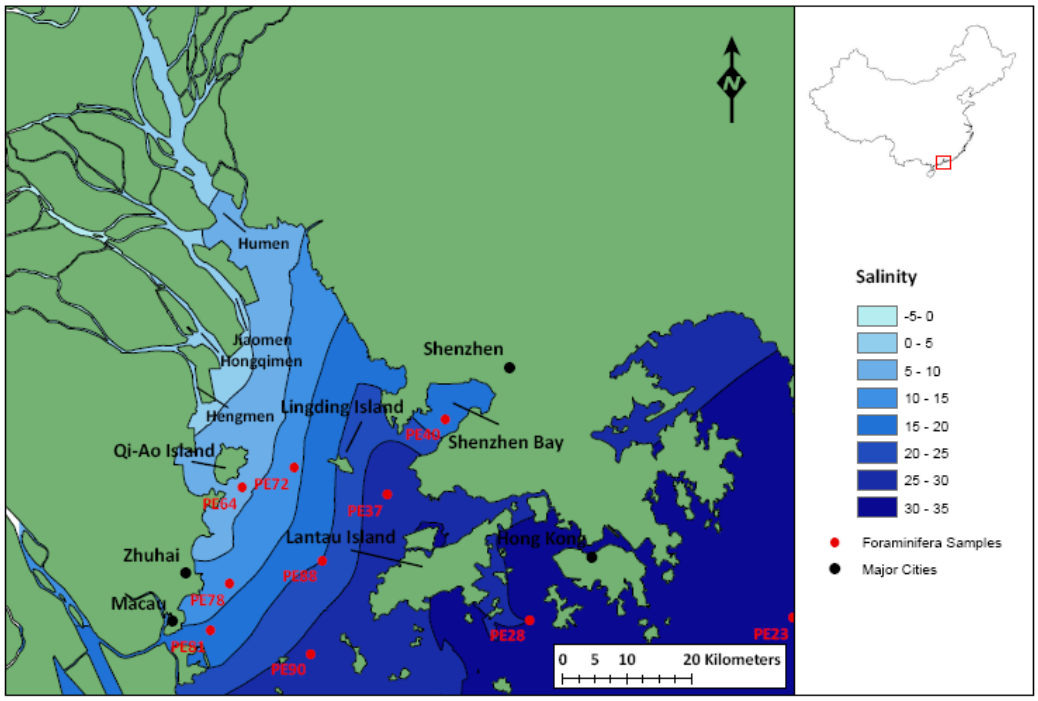

Figure 4.15 PRE surface samples analysed for foraminifera test deformities

An initial assessment of the ecological significance of heavy metal pollution in the PRE is presented below using a simple method which distinguishes foraminifera test with deformities from those without within surface samples. Identification of various deformities followed the protocol of Frontalini and Coccioni, (2008). The

results from the 10 surface sampling sites are shown below in table 4.4.

Zones for each of the sampling sites were assigned so that locations outside the PRE (zone 1), eastern shoal adjacent to urban centres (zone 2), central shoal (zone 3), mid-western shoal (zone 4) and Zhuhai-Macau (zone 5) were sampled (see fig. 4.15). The samples therefore follow a roughly east-west orientated transect across the PRE. The transect should therefore sample benthic environments from the least polluted areas to areas receiving the largest pollution fluxes.

The application of this technique is not widely used, as significant correlation coefficients between heavy metal concentrations and foraminifera test deformities have not been easily established. Pb has proved to be a heavy metal that in high enough concentrations, produces significant correlations within ecotoxicological assessments from Greenland (*Elberling et .,* 2003).

Sample ID	Zone	Total Tests	Total Tests (Deformed)	Percentage Deformed	Types of Deformities Present
PE23	1	231	3	1.30	1x Non-developed test 3x Aberrant chamber shape
PE28	1	264	4	1.51	2x Reduced chamber size 2x Distorted Chamber Arrangement
PE37	2	243	3	1.28	2x Reduced chamber size 1x Abnormal additional chamber
PE40	2	246	4	1.63	3x Aberrant chamber shape 1x Distorted chamber arrangement
PE64	4	85	1	1.18	1x Aberrant chamber size
PE72	3	204	3	1.47	2x Reduced chamber size 1x Distorted chamber arrangement
PE78	4	75	0	0	
PE81	5	93	2	2.15	2x Aberrant chamber size
PE88	3	76	1	1.32	1x Abnormal additional chamber
PE90	5	233	2	0.86	1x Non-developed test 1x Distorted chamber arrangement

Table 4.4 Deformities in foraminifera from PRE surface samples.

Based on the results illustrated in figure 4.16, it would be very difficult to make any interpretation of the applicability of using benthic foraminifera test deformities to assess the ecological significance and biological availability of heavy metal pollution in the PRE.

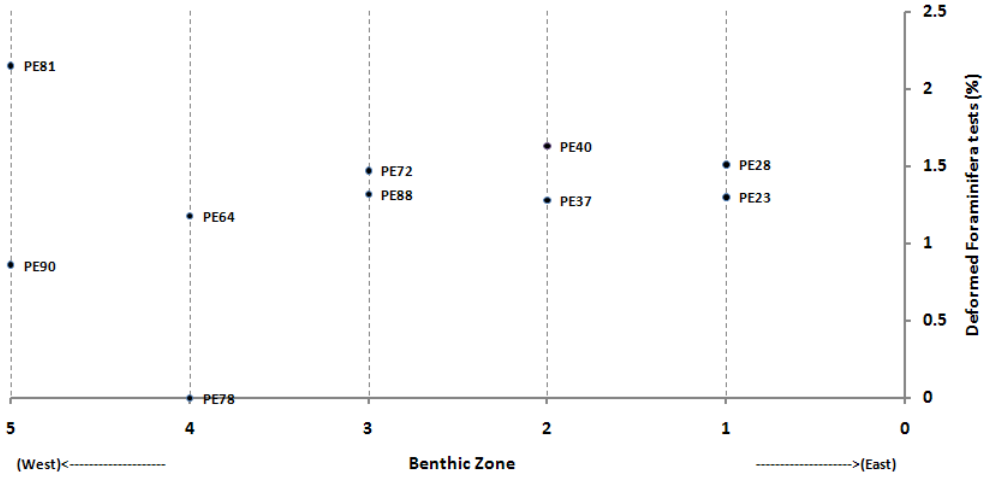

Figure 4.16. Percentage of deformities in foraminifera tests from an East-West transect across the the lower PRE and adjacent coastal waters.

The main problem is the changes in salinity resulting in different foraminifera assemblages. In the lower salinity waters, agglutinated foraminifera dominate, but in lower numbers. The preservation of agglutinated species can sometimes be poor and identifying deformities on tests of species such as *Jadammina macrescens* which often exhibit collapsed and broken chambers post deposition can be problematic. Another issue is that of stresses caused by food abundances, whereby a lack or over-abundance result in test deformities (Murray, 2006). A similar effect causing test deformities has also been noted due to changes in dissolved oxygen concentrations (Murray, 2006).

Compared to implementation of this technique by Elberling *et al.,* 2003 where concentrations of Pb as a result of mining tailing exceeded 200mg/Kg, the levels found in the south and west PRE are much lower (averaging 50mg/Kg). This is the caveat of using foraminifera, as they are not present in low salinity and freshwater environments, where in the case of the PRE the highest concentrations of Pb occur. In addition to this, Elberling *et al.,* (2003) also acknowledged that the presence of high accompanying Zn concentrations inhinited the effects of high Pb concentration by detoxification. In the PRE, Zn exists in high concentrations with Pb. In that particular study, Elberling *et al.,* (2003) had Zn/Pb ratios ranging from 1.4 to 2.1. In the PRE Zn/Pb ratios range from 1.36 (PE14) to 5.87 (PE29) and therefore the affect of Pb along with other toxic heavy metals is likely to be greatly reduced.

Based upon the spatial distribution of Zn/Pb ratios within the PRE illustrated in fig. 4.17, it is likely that the south-central, mid-central and Humen gate regions of the

PRE are the areas where the least Zn detoxification of Pb occurs. This is particularly important for the North River, where Pb concentrations are the highest yet Zn detoxification might be relatively low.

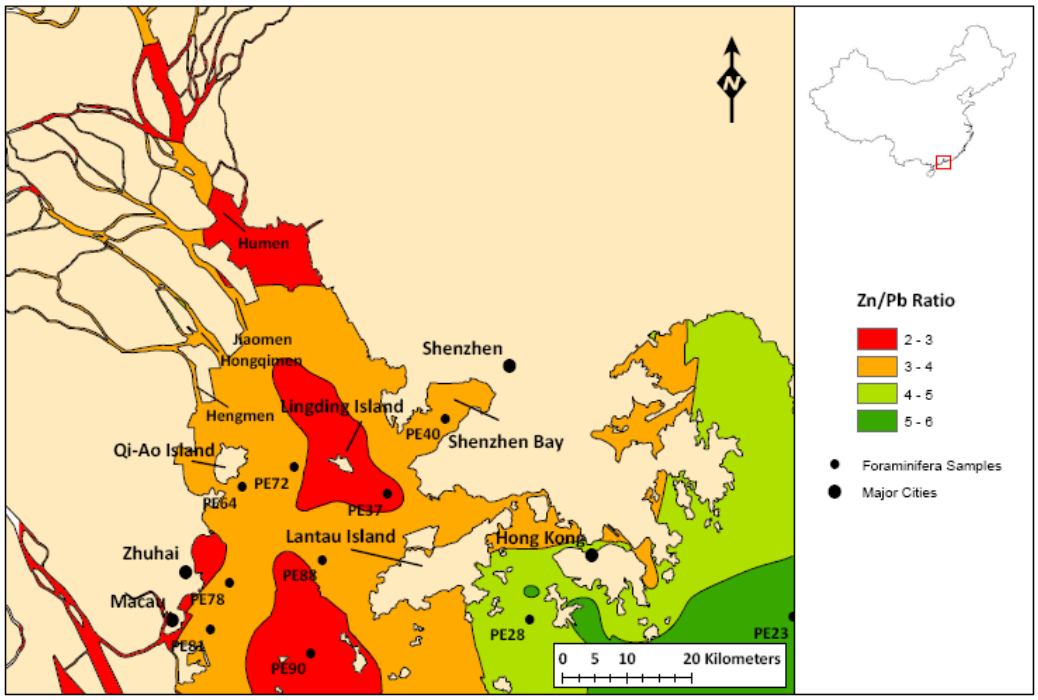

Figure 4.17 Spatial distribution of Zn/Pb ratios across the PRE. Lower values (red) indicate areas where Zn detoxification of Pb is likely to be lowest.

4.8 Summary

Statistical and geospatial analysis of various heavy metal elements in the sediments of the PRE and its major tributaries has highlighted a number of enrichment distributions that are the result of both natural and human forcing factors. Conclusions about the source and transport pathways of the anthropogenically sourced heavy metals have been analysed based on the available data and presented. An initial appraisal of using the presence of foraminifera deformities has been made and the results of which indicate that this particular technique which has proved very informative in extremely polluted benthic environments is not very approporiate for use within the PRE.

5. Temporal Distributions

In January 2008 four short cores were extracted from the PRE (see fig. 5.1), of which cores 2, 3 and 4 were sub-sampled and analysed for particles size, heavy metal concentrations, stable Pb isotope ratios, C/N ratios and ^{210}Pb and ^{137}Cs dating (appendix C).

Figure 5.2 shows the sampling resolution for the various analytical techniques with respect to each core. Sub-sampling and analysing the cores in this way means that a chronological history of natural and anthropogenic change can be deduced from each core and across the whole estuary.

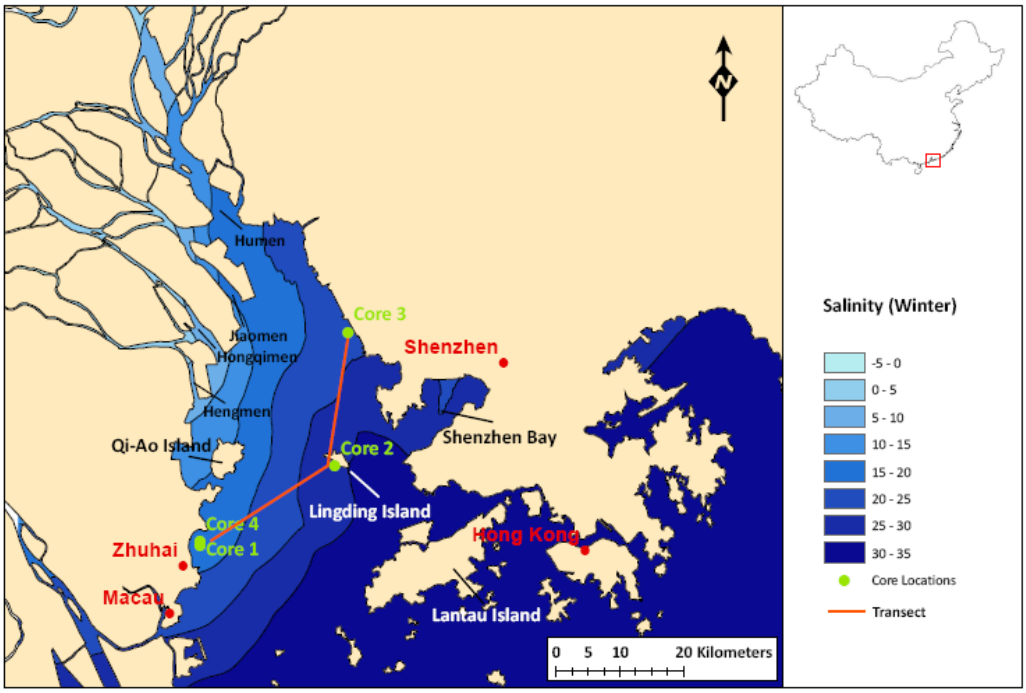

Figure 5.1. Transect showing coring locations.

Core 4 was extracted 2km north of Zhuhai harbour on the western shoal south of Qi-Ao island. This location, being up-estuary of Zhuhai harbour was chosen so that any localised pollution sources associated with harbour activities would not influence the geochemical profile of the core. Sedimentation rates for this area of the estuary were estimated at 1.5 – 3 cm/yr based on Zhou *et al.,* (2004) and indicate that the age of sediments at the base of the core should lie between approximately 56 and 28 yr BP.

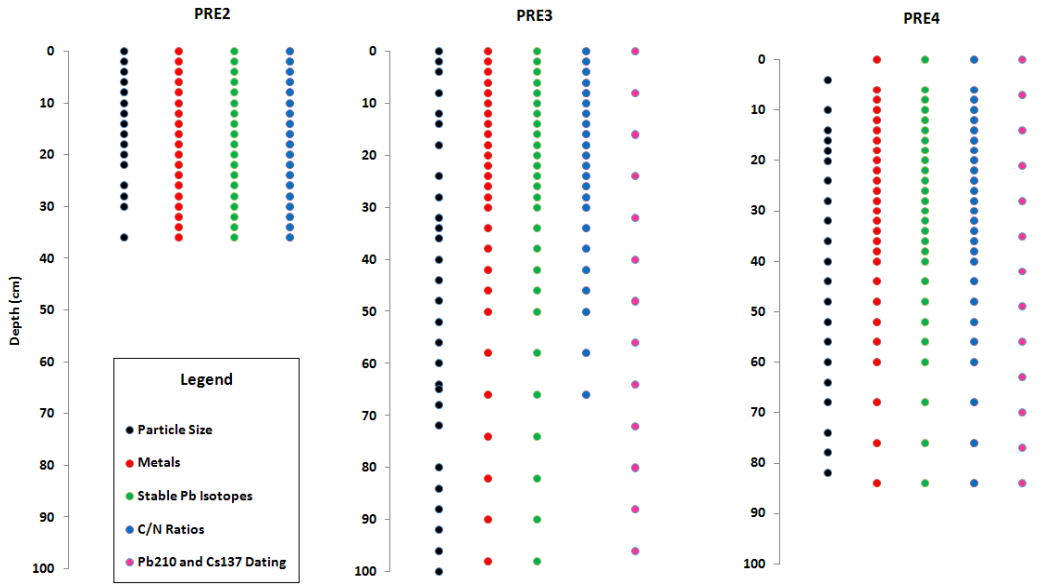

Figure 5.2. Sub-sampling of cores 2, 3 and 4 for geochemical analysis

Core 3 was taken off the coast of Shenzhen 2km south of sea defences built around Shenzhen's *Boa'an* International Airport and 4km north of the entrance to the Port of Shenzhen. This site was chosen so that an anthropogenically undisturbed core could be taken. The site is at least 1km away from any dredging operations or sites of land reclamation that could cause disturbances to sediments during deposition and accumulation. Sedimentation rates along the eastern shoal are variable, but rates of 1 - 2 cm/yr are expected (Zhou *et al.,* 2004) giving an approximate age of 104 – 52 yr BP at the base of the core.

Core 2 is the shortest of the cores taken from the PRE. Due to water depths >5m in the the east and west channels, this core had to be taken on the central shoal close to Lingding Island and as a result the corer stopped in sand after just 38cm, making the extraction of a deeper core impossible. As a result, core 2 was not sub-sampled to produce a ^{210}Pb and ^{137}Cs dated chronology, but was still used for geochemical analysis. Sedimentation rates of >2cm/yr were calculated for the central shoal (Zhou *et al.,* 2004) indicating an approximate maximum core age of 18 yr BP at the bottom, which lies well within the time of anthropogenic influence in the region.

Core 1 was not analysed due to sampling errors. During the extraction of the core, the boat shifted position in the current and wake from other vessels, resulting in

a sub-vertical extraction and possible stratigraphic disturbance, particularly to the base of the core.

5.1 Particle Size Analysis

Figure 5.3 shows the particle size-depth distribution for cores 2, 3 and 4. Particle sizes were classified into 4 groups: Gravel (>2mm), Sand (2 – 0.063mm), Silt (0.063 – 0.004mm) and Clay (<0.004mm) based on Folk and Ward (1957). Core 2 has a very variable particle size distribution, particularly within the sand fraction towards the top of the core. Cores 3 and 4 have much more stable particle size profiles. The silt fraction accounts for 70 – 80% of the particle size throughout all the cores, with the only major exception being two sand dominated layers (0-2cm and 10cm depth) in core 2. These sand laminations are likely to be the result of storm surges in the absence of evidence of a change of sedimentation regime. Core 4 also records a sand lamination at a depth of 18cm that may be from the same storm surge as found at 10cm in core 2. Core 3 exhibits much higher variability in sand content, ranging from 0 – 19% with an average of 4%. Core 3 is located on the eastern shoal, a higher energy environment that results from incoming flood tides into the estuary through the eastern channel. A number of visible fine sand laminations are also present at depths of 14, 24 and 36cm and may be the result of storm surges as a result of typhoon (hurricane) activity transporting sand into the estuary (Cantwell *et al.,* 2007).

Apart from one sand lamination at a depth of 18cm (9%) core 4 is completely devoid of a sand fraction, the result of the low-energy depositional environment that exists along most of the western shoal, resulting in the majority of coarse sediment flux being deposited north of Qi-Ao Island where the *North* and *West Rivers* discharge into the PRE through the *Jiaomen, Hongqimen* and *Hengmen* gates (see fig 4.3).

It has already been noted in earlier chapters that particle size distribution can have a profound effect on the deposition of heavy metal pollutants within estuarine sediments. Large percentage changes in the clay fraction between sample may account for much of the variance in the heavy metal concentrations within the same sub-sample. Therefore, throughout this chapter, the potential effect that changes in the clay fraction proportion might have on the metal concentrations will be noted. This will

be particularly important for core 2 and 3 where the clay variations are sometimes quite large and very sharp.

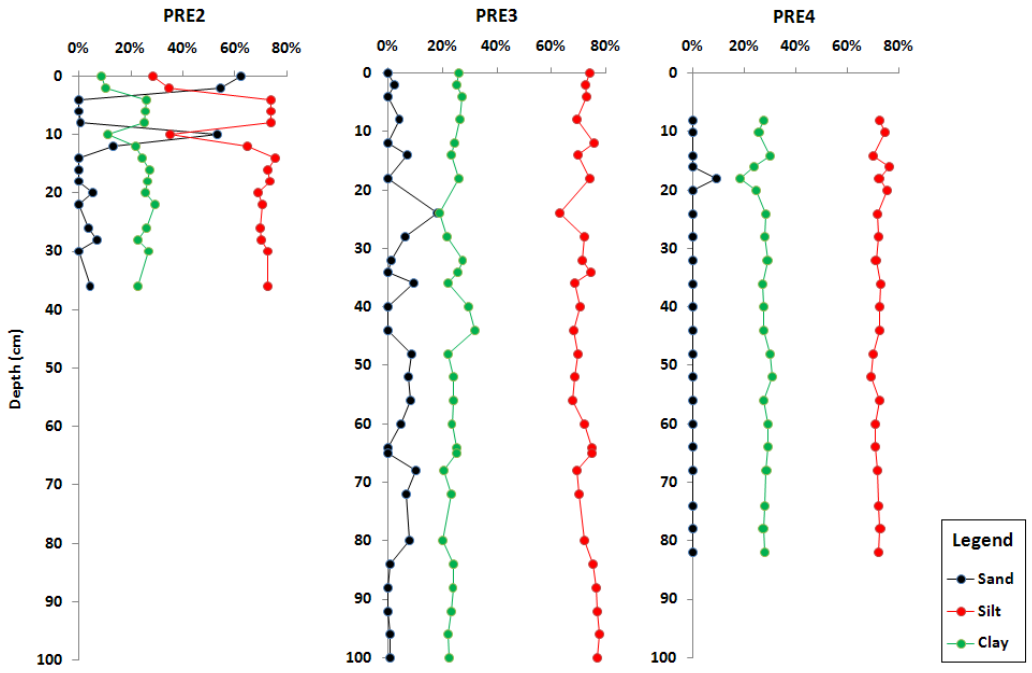

Figure 5.3. Depth profiles of sand, silt and clay (%) from cores 2, 3 and 4.

5.2 Chronostratigraphy

Cores 3 and 4 were sub-sampled for gamma-ray spectrometry at 8cm and 7cm resolution respectively. A chronological profile for the cores was produced using the vertical distribution of unsupported ^{210}Pb ($^{210}Pb_{xs}$) and ^{137}Cs (see fig. 5.4). Under conditions of constant ^{210}Pb supply and uniform sediment deposition, the vertical distribution of unsupported ^{210}Pb should be a good approximation to an exponential radioactive decay curve (Lee and Cundy, 2001). There is no unsupported ^{210}Pb in core 3 below a depth of 10cm. Because of this, a depth-age profile can not be calculated using any of the available models (Vaalgamaa, 2004). The lack of a unsupported ^{210}Pb with depth indicates that either significant mixing and resuspension of sediments has occurred during deposition, or that the sediments below 10cm are outside the range of this technique (>130years) (Lee and Cundy, 2001). The significant variability in the sand, silt and clay composition of core 3 (see fig. 5.3) may also be another influential factor, as like many other geochemical variables, ^{210}Pb and ^{137}Cs are preferentially

deposited with fine-grained organic-rich sediments (Álvarez-Iglesias *et al.,* 2007). The eastern shoal has already been identified as a much higher energy depositional environment; coupled with the presence of dredging activities in the neighbouring East channel and the effects of particle-size affinity, these factors are the most likely cause of the observed $^{210}Pb_{xs}$ distribution profile. Based on the presence of ^{137}Cs throughout the core (although some in extremely low activities), the sediments must have accumulated more recently that 1954 when above ground nuclear weapons testing began (Álvarez-Iglesias *et al.,* 2007). This gives a minimum sediment accumulation rate of 1.81cm/yr.

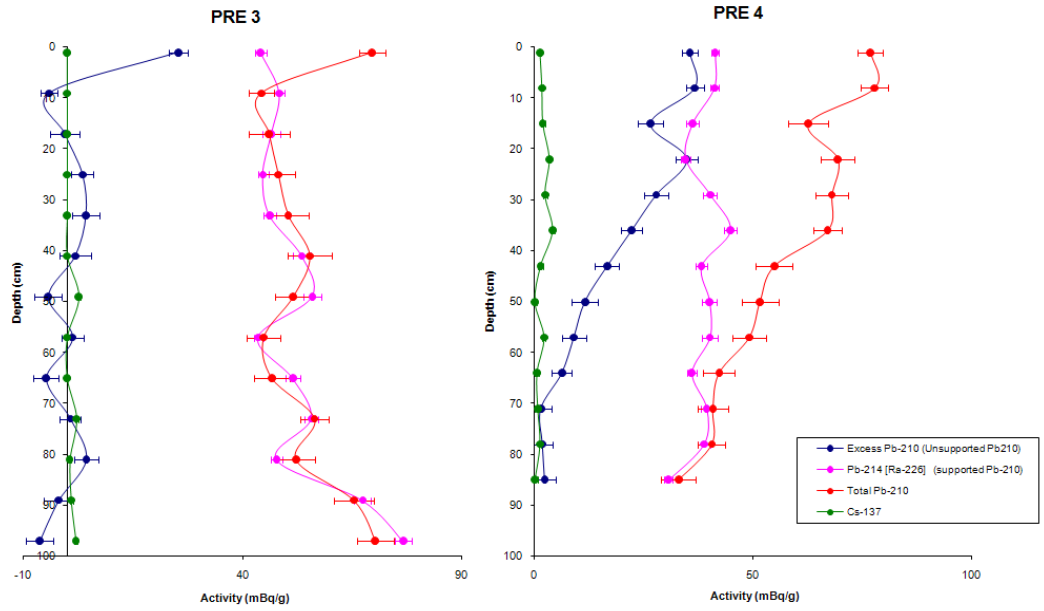

Figure 5.4. Total ^{210}Pb, supported ^{210}Pb, $^{210}Pb_{xs}$ and ^{137}Cs activity profiles for cores 3 and 4.

Core 4, deposited in a much lower energy environment to core 3 shows a good exponential decay curve for unsupported ^{210}Pb. The results from the Constant Rate Sedimentation (CRS), Constant Initial Concentration (CIC) and Simple Model age calibrations for the unsupported ^{210}Pb profile are presented in figure 5.5 for comparison.

The sudden drop in age relative to depth (based on cumulative dry mass) for the CRS model at 13 g/cm^2 is a result of ^{210}Pb activity dropping to 'supported' background values (^{226}Ra) below a depth of 64cm. This means that the model can not be used to directly calculate the age-depth profile below 64cm.

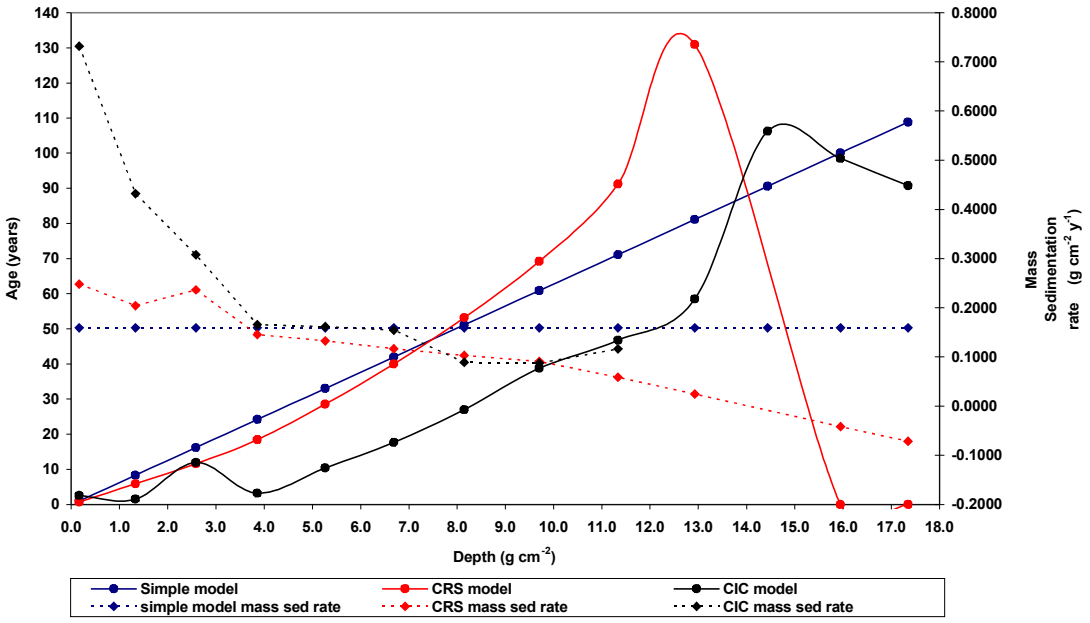

Figure 5.5. Age-cumulative dry mass profiles and dry mass sedimentation rates based on calculations using the simple, CRS and CIC models for core 4.

The simple, CRS and CIC models give maximum ages of 109±17 yr BP (depth=85cm), 130±24 yr BP (depth=64cm) and 106 yr BP (depth=71cm) respectively. The depth model produced by the CIC model can however, be immediately rejected as samples taken from a depth of 15cm (11.54 yr BP) are calculated as older than samples from 22cm (3.21 yr BP) and 29cm (10.39 yr BP). Using the CRS model allows for the presence of variable sedimentation rates during the deposition of the core by using changes in the wet and dry bulk densities (Vaalgamaa, 2004). With an estuarine system being very dynamic, it is highly unlikely that sedimentation rates would remain constant over long periods of time. For this reason, the CRS model will be utilised. The problem of producing a age-depth profile beyond 64cm has already been discussed. To achieve this, a linear interpolation from the gradient of the last calculated age-depth sample will be calculation to continue the age profile to the bottom on the core.

As with core 3, ^{137}Cs activity for core 4 is relatively low along the whole core profile. For this reason, the use of the ^{137}Cs technique to provide reliable chronostratigraphic index points can not be made, especially when compared to the ^{137}Cs activities needed for verification of this technique in other studies (Anderson et al., 2000). Maximum activity of 4.15mBq/g at a depth of 36cm, dropping to 1.36mBq/g at 43cm and 0.03mBq/g at 50cm (see fig. 5.6). Below 50cm, the ^{137}Cs activity increases

again to 2.17mBq/g at 57cm before return to a value of 0.03mBq/g at 85cm. The problem that lies herein is that the age-depth profiles calibrated by the ^{210}Pb exponential decay curve, do not correlate with the ^{137}Cs profile, as this anthropogenic radiogenic isotope should not be present before 1954 (Lee and Cundy, 2001).

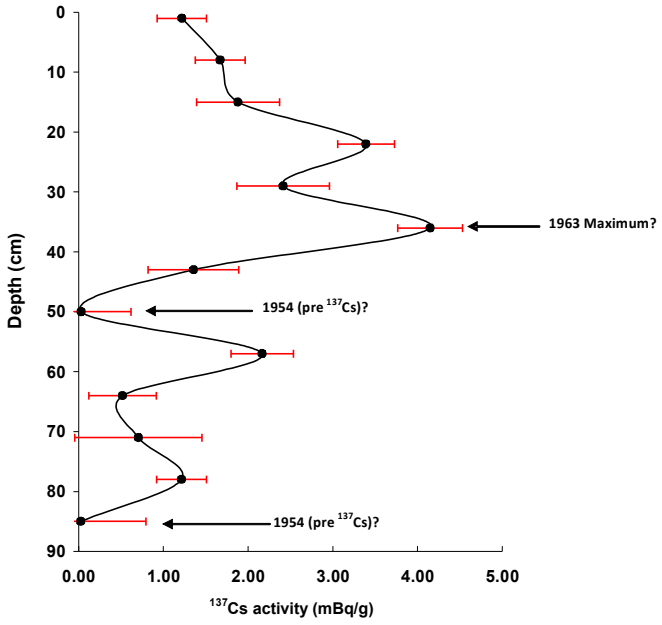

Figure 5.6 ^{137}Cs activity profiles for core 4.

If the ^{137}Cs peak at 36cm depth is taken to be correct (the 1963 maximum), the corresponding ages from the simple and CRS models of 1967 and 1968 respectively are in quite good agreement. Moreover if the falling ^{137}Cs activities below the 36cm (1963) peak, to almost zero values (0.03mBg/g) at 50cm show the transition to the very start of ^{137}Cs production through atmospheric weapons testing in 1954, then the corresponding simple (1948) and CRS (1939) model derived ages appear slightly too old. Below this depth, ^{137}Cs activity increases again suggesting that the activity low of 50cm is actually post 1954. If this is the case, then the final fall to almost zero (0.03mBq/g) at 85cm must indicate a deposition date ≈1954. A depth-age that is contradictory to the ages of 1900 and pre-1878 from the simple and CRS models respectively.

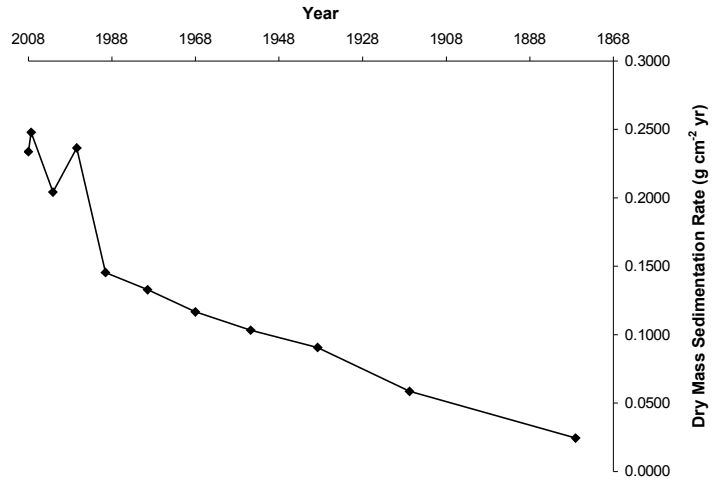

Figure 5.7 Changes in sedimentation rate during the deposition of core 4

Figure 5.7 shows the calculated changes in dry mass sedimentation rate during the deposition of the core. Calculations show there has been a linear increase in sedimentation rates from pre-1878 to 1988, and significantly increase from 1988 to the present day. Overall, the calculated average sedimentation rate for the core is very low. The bottom 15cm of core 4 are outside the dating range of the ^{210}Pb technique ($T_{1/2}$ (^{210}Pb) = 22.26yr). Based on sediment accumulation rates for the top of the core, the average sedimentation rate is 0.5±0.12cm/yr, much lower than values calculated by Zhou *et al.,* (2004) but similar to Ip *et al.,* (2004) who calculated an average sedimentation rate of 0.41cm/yr using the CRS model for a core taken 18km south of core 4, near Macau.

5.3 C/N Bulk Ratios

C_{org}/N_{Total} profiles for cores 2, 3 and 4 are presented in figure 5.8. Error bars are not included as the associated detection error is <±2% (see appendix B). As expected due to its central position within the estuary, core PRE2 exhibits a C/N ratio profile characteristic of a mixed environment whereby organic material deposited comes from both terrestrial and freshwater/marine sources (Lamb *et al.,* 2006). This also verified from a diatom study in the PRE, which found that the site of core 2 falls within the mesohalobous (brackish water) diatom group (Zong *et al.,* 2006).

Core 2 also exhibits a trend towards more freshwater/marine dominated organic material towards the top of the core, with one terrestrial excursion at a depth of 14cm. This trend of lessening terrestrial influence is significant, as it suggests that

either tidal forcing has increased or freshwater and suspended sediment flux to this part of the estuary has decreased over time.

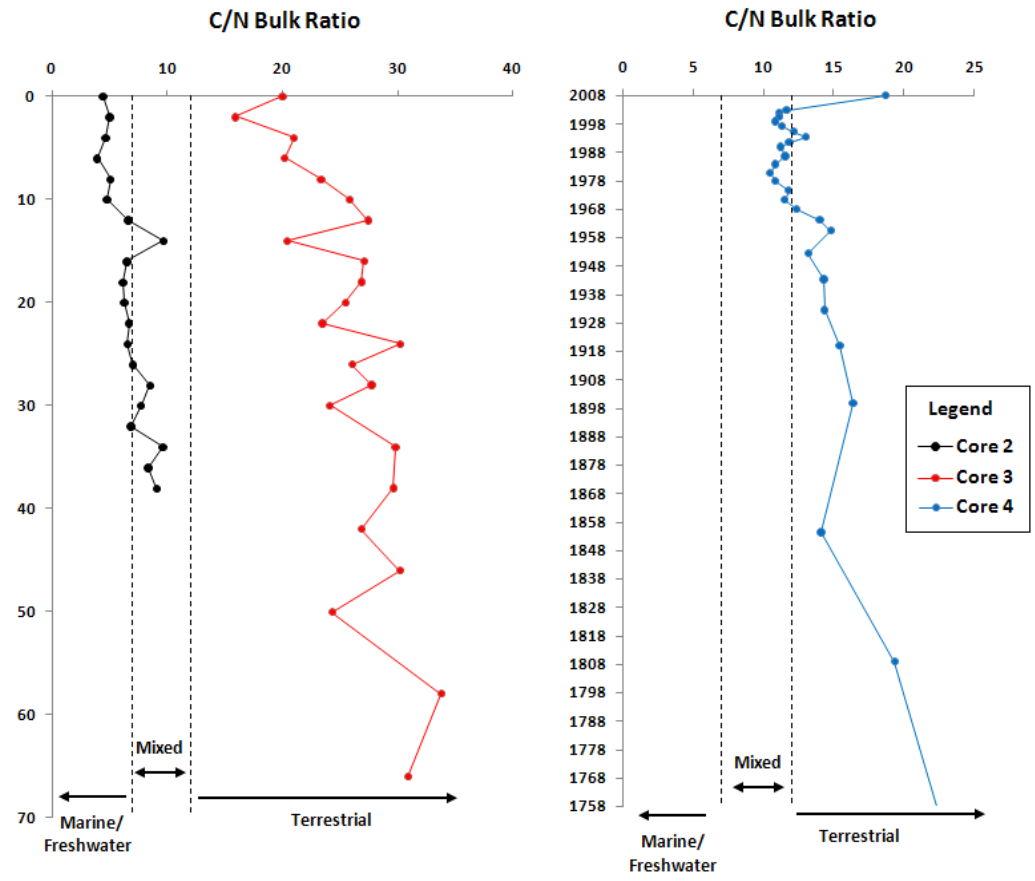

Figure 5.8 C/N ratio profiles of cores 2, 3 and 4 with upper marine ratio and lower terrestrial ratio boundaries (Lamb *et al.*,2007) shown.

Research into long-term changes in discharge along the *North* and *West River's* have proven not to be significant at the 0.05% confidence limit and is likely to be the result of precipitation variations (Zhang, *et al.,* 2008). Suspended sediment load has however, decreased significantly along these rivers since the 1950's (Lu *et al.,* 2007). This decrease in terrestrially derived material as a result of sand mining and dam building (Lu *et al.,* 2007), is the most likely reason for the decreasing trend in terrestrially derived organic material deposited in core 2.

Core 3 has a very variable C/N ratio with generally high values (<20) suggesting strong influence of terrestrially derived material in the region. This variable profile profile is likely the result of the dynamic sedimentation and sediment resuspension regimes that operates in this part of the estuary based on the ^{210}Pb profile of the core.

Another interesting aspect of the profile is the presence of high C/N ratios in a region where marine influence due to tidal currents is expected to be relatively high. No explanation for these high C/N ratios can be given at this time, however, freshwater and terrestrial material entering the region from the Shenzhen River through Shenzhen Bay might have an influence. Freshwater water and suspended sediment entering the PRE through Shenzhen Bay would be deflected northwards along the Eastern shoal by tidal currents and may provide carbon rich organic material to the region. Another possible reason for this high C/N ratio might be explained by unpublished diatom data (Zong *pers. Comm*). This data shows that while the highest concentrations of benthic freshwater diatom species are found in the north-west of the estuary, the highest concentrations of freshwater planktonic species are found along the northern parts of the Eastern shoal. This suggests that a component of freshwater entering the estuary through the *Humen* gate discharges through this regions, maybe during ebb and neap tides, and deposits carbon rich terrestrially derived organic material as a result. In addition to this , input from water sources along the east of the estuary may also be a contributing factor.

Core 4 has been identified as containing an undisturbed record of sediment accumulation based on its $^{210}Pb_{xs}$ profile. The C/N ratio displays a decreasing trend at the site of core 4 since the 1750s which is accelerated the late 1950s. Zhang *et al.,* (2008) also suggest that it is in the 1950's when a decreasing trend in sediment load being transported through the Pearl River system began. By 1979, the C/N ratio becomes relatively stable (mean 11.4), with gentle increasing trend in organic carbon content that peaks significantly in the early 1990s (=13) before returning to pre-1990 values until 2006. From 2006 to present day there is a second significant increase in the C/N ratio. Based on the individual changed in total organic carbon (TOC) and total nitrogen (TN) (fig. 5.9), it appears that while both have increased, the increase in total nitrogen has been an ongoing process since the 1750s that has significantly increased since the mid-late 1960s. The amount of organic carbon being accreted ion the other hand remained quite stable until the mid-late 1960s, where it started to increase and then dramatically increased between 2006 and 2008. Without the addition stable carbon isotope analysis, it is hard to draw conclusion about what is driving these changes (Mackie *et al.,* 2007). Based on the individual trends of TOC and TN it seems

that the an increase in freshwater productivity, marine influence or both has been the dominant driving factor in changes in the C/N profile of core 4.

5.4 Environmental Summary

Sections 5.1-5.3 have provided an assessment of the environmental forcing that plays a significant part during the deposition of sediments at the locations of cores 2, 3 and 4. The $^{210}Pb_{xs}$ profiles suggest that core 3 is unlikely to possess an undisturbed chronology of deposition and therefore will be of limited use for the assessment of temporal variations in heavy metal concentrations. Core 2 was not sub-sampled for ^{210}Pb ($^{210}Pb_{xs}$) and ^{137}Cs due to constraints on the number of samples that could be analysed for this study and its relatively short length. As a result, no chronology of deposition can be produced or evaluated. Based on the low variability between neighbouring C/N bulk ratio samples and the its position away away from erosive tidal currents and human activity, the core is taken to show a relatively undisturbed depositional profile.

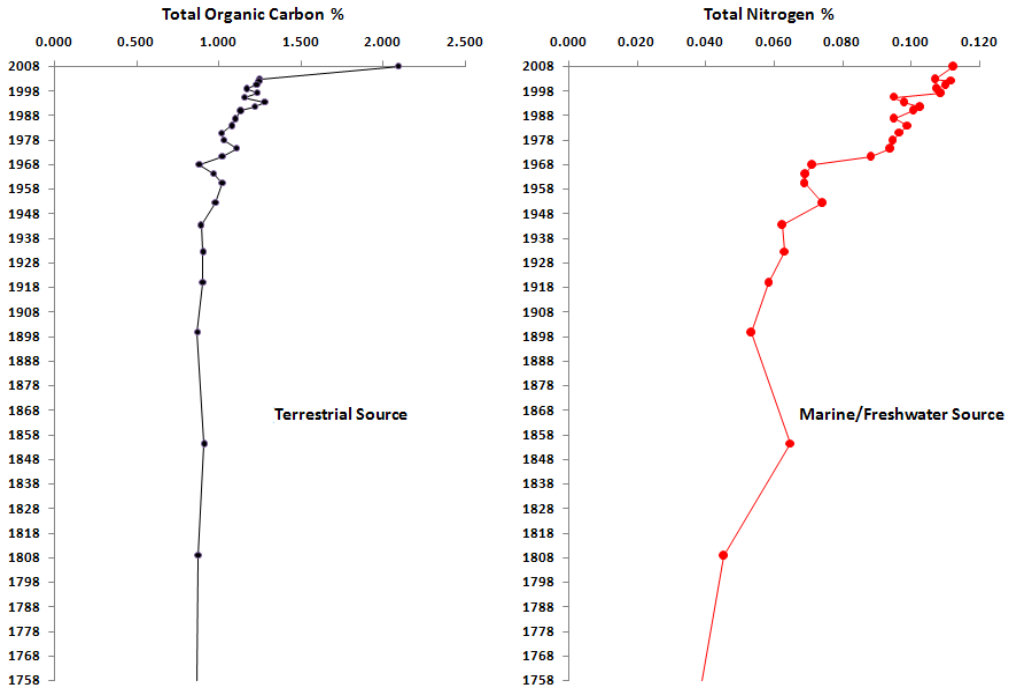

Figure 5.9 Total organic carbon (%TOC) and total nitrogen (%TN) profiles of core 4.

Based on the $^{210}Pb_{xs}$ profile core 4 is assumed to contain an undisturbed history of sedimentation dating back to 1758. In addition to providing an undisturbed profile

of sedimentation, the bottom section of this core will also allow for the pre-industrial (background) levels of the various heavy metals to be assessed and used to calculate their anthropogenic *enrichment factor* (EF) (Ridgeway and Shimmield, 2002; Abrahim and Parker, 2008; Wang *et al.,* 2008). This technique calculates the level of enrichment of a sub-samples relative to its natural background concentration. The comparison is done using a conservative tracer element to account for concentration variability as a result of changes in bedrock weathering and erosion rates and not through anthropogenic sources. For this study based upon the results of geospatial and PCA in chapter 4, Co, Fe and Ti have been identified as the most appropriate conservative tracer elements. In this study Fe is used as it has already been successfully implemented in a number of other studies (Schiff and Weisberg, 1999; Ip *et al.,* 2004) , has been statistically proven to be the most appropriate in the PRE (Zhou *et al.,* 2004), and has strong relationships with other conservative elements of erosion (Ti) in chapter 4, this study. In addition to the work of Zhou *et al.,* (2004) the concentrations of Fe in PRE sediments is generally greater than 30,000 mg/kg (or 3%) of the total sediment and therefore variability driven by seasonally estuarine oxygenation changes (causing Fe redox reactions) (Dashkalakis and O'Conner, 1995) is likely to be less than the accuracy of elemental detection by ICP-MS.

5.5 Heavy Metal and Pb Isotope Distribution

Heavy metal and stable Pb isotope profiles for cores 2, 3 and 4 are presented in the following sections for the analysis of temporal variations in the their concentrations.

5.5.1 Sedimentary record for Core 2

Figure 5.10 illustrates the variability of the trace heavy metals Cr, Co, Cu, Pb, Ni and Zn with depth for the core 2. Core 2 displays a relatively uniform distribution of low abundance heavy metals with respect to depth. All trace metal elements concentrations display concentration lows at depths of 20cm (except Co), 10cm and 0cm. These low concentrations occur at the same depths sand becomes a dominant particle size fraction and clay content is reduced. The uniform distribution along the whole core suggest very little variability in heavy metal fluxes during sediment

deposition, and little evidence of anthropogenic enrichment. Based on the work of Zhou *et al.,*(2004), the bottom of this core is expected to have a minimum age of roughly 18 years and should therefore display a depositional record spanning a period of intense industrialisation and maximum enrichment of certain heavy metals.Fe which has already been identified as a good natural tracer element of weathering in sediments of the PRE (Zhou *et al.,* 2004), and Ti has also been shown to be derived from natural weathering and erosion of bedrock based on PCA and geospatial analysis in chapter 4. Fe and Ti profiles suggest that there has been only a slight reduction in the flux of weathered material being transported to this region of the PRE during the deposition of this core. This is in agreement with the results from C/N bulk ratio profiles which also suggest a reduction in the flux of terrestrially derived organic material over time (see fig 5.8). Although displaying some variability in concentrations along its profile, overall there is no overall trend in Al concentrations. This implies that long term changes in Fe and Ti concentrations are either a result of reduced erosion of bedrock within the catchment or a reduction in suspended sediment flux into this region of the PRE. Based on other research, it is most likely to be the result of reduced sediment flux due to the construction of dams along the main tributaries of the Pearl River (Lu *et al.,* 2007; Zhang *et al.,* 2008). In chapter 4 it has been found that Al enrichment occurs outside the PRE where the percent abundance of the <2µm particle size fraction is the highest. Its presence within the estuary appears to be driven by tidal movements into the estuary. The fact that there is no overall change in Al concentrations in core 2, suggest that marine water intrusion into this region of the estuary has not intensified during the period that suspended sediment flux has reduced. This further implies that although sediment flux has been reduced, overall river discharge has remained relatively constant, results that are concurrent with the findings of Lu *et al.,* (2007) and Zhang *et al.,* (2008).

Stable $^{208}Pb/^{207}Pb$ and $^{206}Pb/^{207}Pb$ isotope ratios have been used in a number of studies to investigate the relative sources (natural or anthropogenic) of Pb within soils and sediments (Munksgaard *et al.,* 1998; Wong *et al.,* 2003, Aggarwal *et al.,* 2008).

To assess the presence of an anthropogenic signature in the isotopic composition of Pb, it is imperative that background isotopic ratios of bedrock (Zhu, 1995) and uncontaminated soils (Zhu *et al.,* 2001) are known.

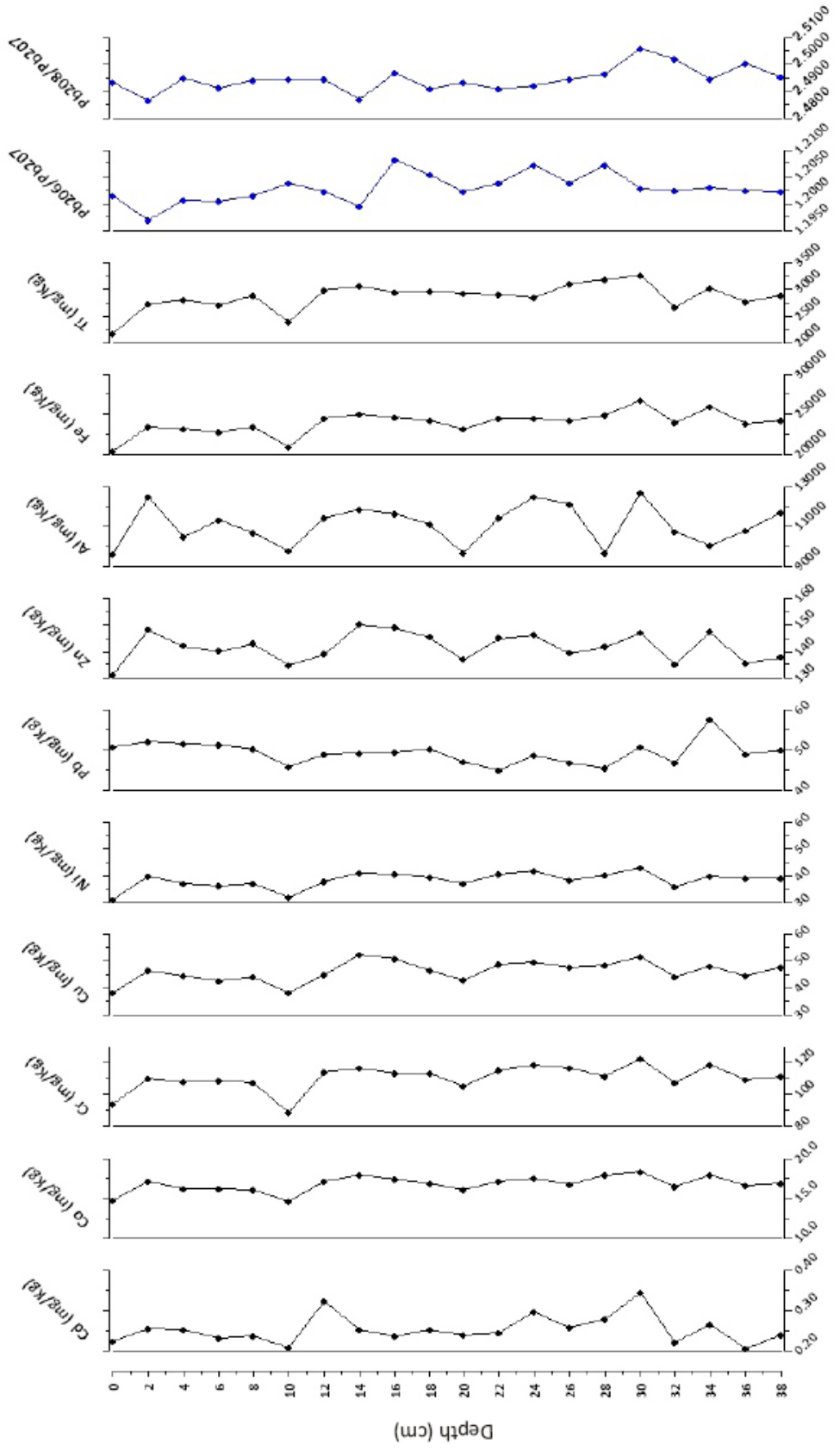

Figure 5.10. Core 2 depth profiles of heavy metals and stable Pb isotope analyses ($^{208}Pb/^{207}Pb$ and $^{206}Pb/^{207}Pb$) from ICP-MS analysis.

Core 2 is unlikely to show a profile of deposition that extends into pre-industrial times and therefore standard values for Pb isotopes will have to be used to assess Pb sources (see table 5.1).

Source (Natural)	$^{208}Pb/^{207}Pb$	$^{206}Pb/^{207}Pb$
East Cathaysia Granite	1.1834	2.4680
Pearl River Delta Granite	1.1843	2.4824
Foshan Volcanics	1.1993	2.4965
Uncontaminated Soils	1.1952	2.4815
Mean	**1.1906**	**2.4821**
Source (Anthropogenic)		
Fankou Pb-Zn deposits	1.1716	2.4725
Car Exhaust	1.1604	2.4228
Mean	**1.1660**	**2.4477**

Table 5.1. Stable Pb isotope ratios for some natural and anthropogenic sources of Pb in the Pearl River Catchment (adapted from Zhu, 1995; Zhu *et al.,*2001 and Wong *et al.,* 2003)

The mean isotope ratios obtained for natural and anthropogenically sources of Pb from table 5.1 are slightly lower than the ratios presented by Ip *et al.,* (2004), who found pre-industrial sediment ratios of $^{208}Pb/^{207}Pb$ and $^{206}Pb/^{207}Pb$ to be >1.20 and >2.49 respectively. Core 2 shows a slight falling trend in both $^{208}Pb/^{207}Pb$ and $^{206}Pb/^{207}Pb$ ratios (see fig.5.8), with mean values of 2.4918 and 1.2008 respectively for the top 14cm of the core. These isotope ratios are at the boundary between natural and anthropogenic sources of Pb (Ip *et al.,* 2004) and are within the natural ratios based on table 5.1, further suggesting that the anthropogenic influence of heavy metals in this region of the PRE is relatively low.

5.5.2 Sedimentary record for Core 3

Profiles of heavy metals and stable Pb isotopes for core 3 are shown in figure 5. 11. Heavy metal profiles of core 3 show a similar distribution from 0-58cm to that of core 2 except for concentration peaks at 22cm in all metals, 12cm and 4cm in Cr and Zn, and a pattern of increasing enrichment in Pb from 6-0cm. Between 58cm and 98cm, Cr, Cu, Ni and Zn show large concentration fluctuations that in the case of Cu and Zn are as large as 474% and 143% respectively compared to concentrations in sub-samples immediately above and below.

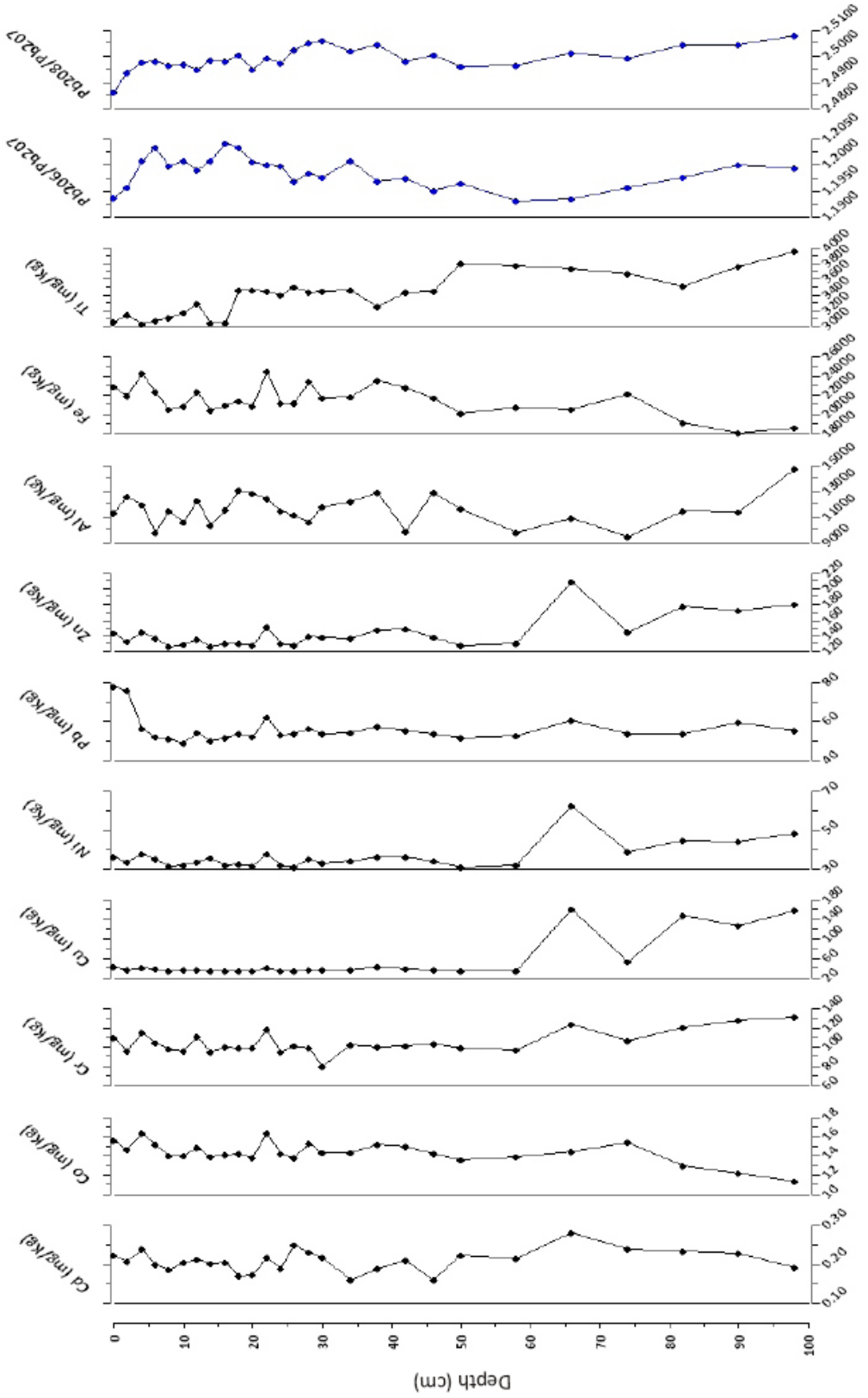

Figure 5.11. Core 3 depth profiles of heavy metals and stable Pb isotope analyses ($^{208}Pb/^{207}Pb$ and $^{206}Pb/^{207}Pb$) from ICP-MS analysis.

A depositional chronology of core 3 could not be established using either ^{210}Pb ($^{210}Pb_{xs}$) or ^{137}Cs due to erosion/resuspension of sediments after initial deposition. The significant variability in the heavy metal profiles is also likely to be a result of this dynamic sedimentary environment (Ip *et al.,* 2004; Zhou *et al.,* 2004). Stable Pb isotope ratios normally co-vary with each other to produce a positive linear regression between $^{208}Pb/^{207}Pb$ and $^{206}Pb/^{207}Pb$ (Ip *et al.,* 2004). The results from core 3 however, show very different trends between 58cm and 4cm for the two isotope ratios: the $^{206}Pb/^{207}Pb$ ratio shows an increasing trend and therefore a reduction in anthropogenically sourced Pb, the $^{208}Pb/^{207}Pb$ ratio shows an initial rising trend (58-30cm) and then a decreasing trend to the top of the core.

The disturbed depositional history recorded in core 3 means that no further analysis of temporal trends in heavy metal concentrations will be conducted. Resuspension and erosion of sediments after deposition means that older pre-industrial sediments are reworked into younger ones, masking any anthropogenic signature.

5.5.3 Sedimentary record for Core 4

The depositional environment of core 4 is of much lower energy that core 3 and is also not susceptible to erosion as the result of tidal currents. Moreover, core 4 is much further away from any harbours, sea defences or dredging activities compared to core 3 and with the use of ^{210}Pb ($^{210}Pb_{xs}$) dating technique, has been identified as providing a chronological and undisturbed history of heavy metal deposition spanning a period from 1758 until the present day (see fig. 5.12).

Cd and Co appear very uniform from 1758 until the 1950s in core 4. Between the 1950s and 2008 they display much more variability, particularity for Cd which shows a slight reduction in concentrations between from 2002-2008 (0.41-0.33mg/Kg) after an increase between 1993 and 1997 (0.35-0.41mg/Kg). Co also shows a reduction in concentrations that occurs in two stages. The first stage is a gradual reduction in concentration between the mid-1940s and late 1960's (22.15-20.26mg/Kg) after which concentrations remain relatively constant until 1990. It is here that a very sudden drop in concentrations occur between 1990 and 1992 (20.49-18.79mg/Kg) and then Co concentrations remain relatively stable until the present day. Cr concentrations appear

relatively stable along the whole profile of the core, just exhibiting a little more variability since 1990.

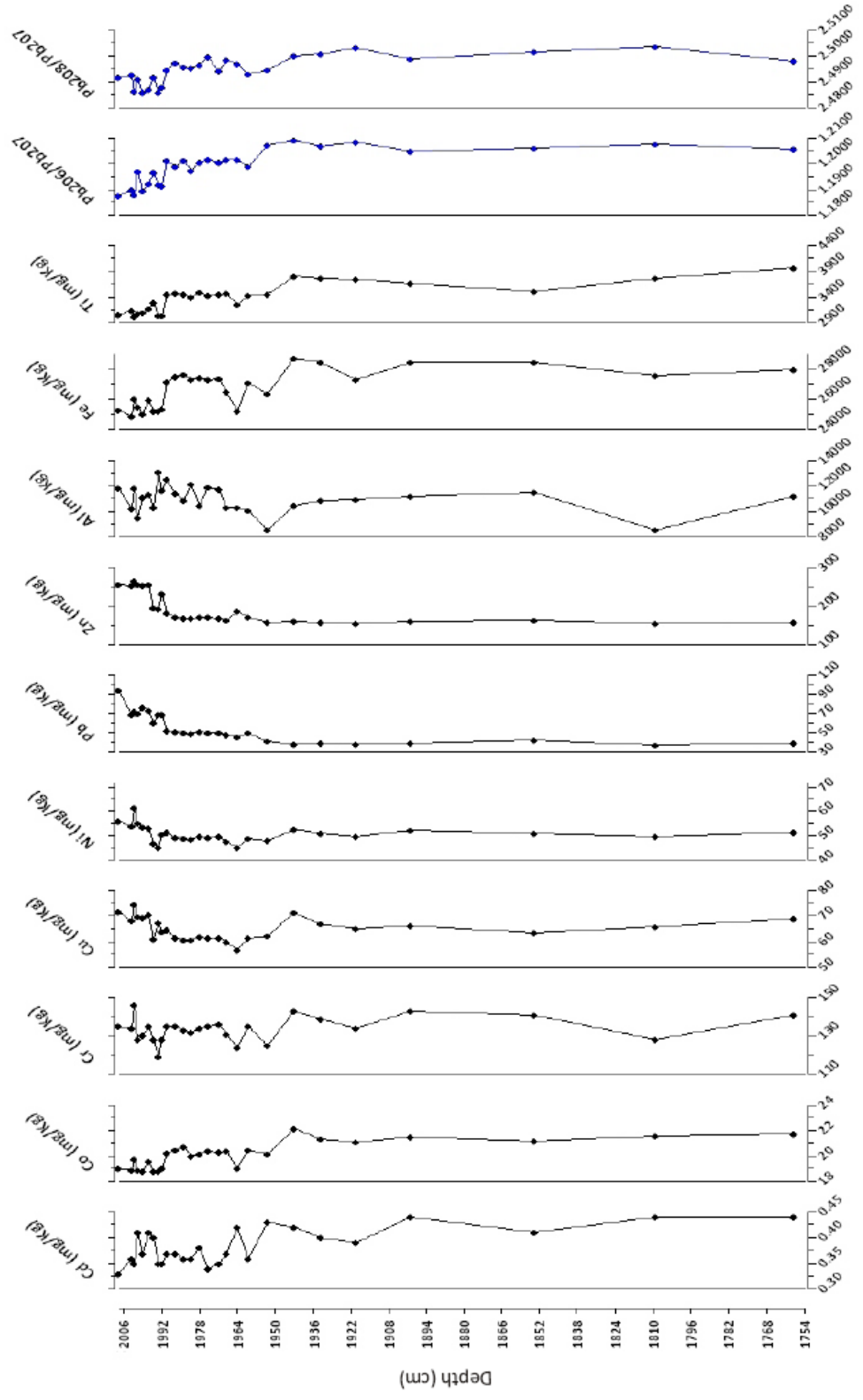

Figure 5.12. Core 4 depth profiles of heavy metals and stable Pb isotope analyses ($^{208}Pb/^{207}Pb$ and $^{206}Pb/^{207}Pb$) from ICP-MS analysis.

Cu and Ni profiles show a decreasing trend in concentrations between the early 1940s and 1964, dropping from 71.16-56.71mg/Kg in the case of Cu, and 52.71-45.02mg/Kg for Ni. From 1964, Cu, Ni, Pb and Zn all display and increasing trend in concentrations. Cu and Ni concentrations increase quite uniformly from 1964 until 2008, where they are 71.62 and 56.02 mg/Kg respectively. Values that are very similar to pre-1940 abundances. Pb and Zn profiles are very uniform from 1758 until 1964. Between 1964 and 1992 both metals an initial increasing trend from concentrations of 45.44 from Pb and 188 mg/Kg for Zn to 68.66 and 231 mg/Kg respectively. Between 1992 and 2008 Pb and Zn undergo a second, more intense phase of enrichment, where concentrations reach maximum values 93.72mg/Kg for Pb and 256mg/Kg for Zn in 2008. These phases of enrichment are coincident with changes in the isotopic composition of Pb at the same depth intervals. The mean isotopic ratio values for $^{206}Pb/^{207}Pb$ and $^{208}Pb/^{207}Pb$ for 1758-1964 were 1.2069 and 2.5009, rising to a mean of 1.2006 and 2.4965 respectively for the period 1964- 1990. The period 1990-present sees a further significant drop in isotope ratios again to mean values of 1.1915 and 2.4888 for $^{206}Pb/^{207}Pb$ and $^{208}Pb/^{207}Pb$ respectively. The fact that the decreases in $^{206}Pb/^{207}Pb$ and $^{208}Pb/^{207}Pb$ isotopic ratios are coincident with accelerated phases of Pb and Zn enrichment, suggested that the sources of these extra metal fluxes is very likely to be anthropogenic.

In chapter 4, Zn and Pb were highlighted through their spatial distribution, surface concentrations and PCA to be the most enriched heavy metals in the PRE and the most affected by anthropogenic sources. The temporal distribution of these two elements suggests that their enrichment has occurred in two stages. The first starting in the 1960s and the second starting in roughly 1990 (see fig. 5.13).

Particle size variability is very low for core 4 and therefore no clay fraction normalisation is necessary. Conservative trace element profiles show that the flux of Fe and Ti to this region of the PRE was very stable from 1758 until 1943. With mean concentrations over this period being 28090 and 3747mg/Kg respectively. After 1943 both metals show a decreasing trends in concentration, reaching values of 25181mg/Kg for Fe and 3247mg/Kg for Ti in 1964. After 1964 the concentrations of both metals immediately rise and plateau from 1971-1990, with mean concentrations

of 27355mg/Kg of Fe and 3450mg/Kg for Ti.

The concentrations of both metals fall steeply again from 1990-1992, where although displaying some variability, show no changing trends through to 2008. Averages values over this period 1992-2008 are 25364mg/Kg and 3105mg/Kg for Fe and Ti respectively (see appendix C and fig. 5.12). These stages drops in concentrations are also mirrored exactly by Co, further verifying its presence the estuary being solely the result of natural sources.

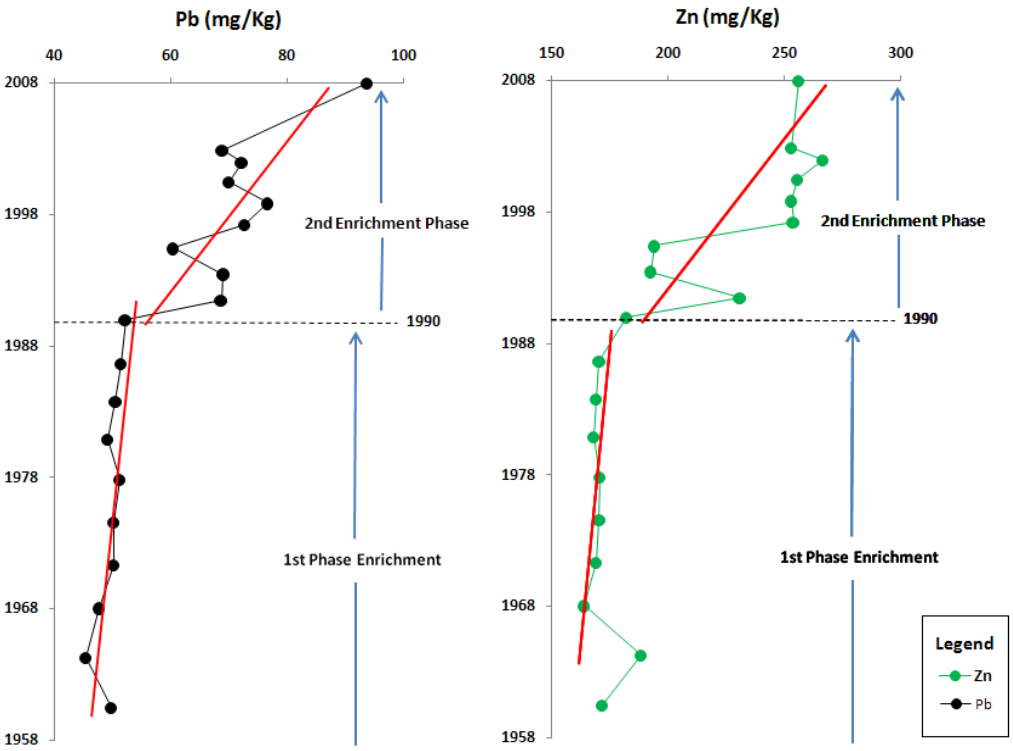

Figure 5.13. Phased enrichment of Pb and Zn in since 1964 in core 4.

This two stages decrease in the rock forming minerals Fe and Ti being deposited in the PRE is significant for two reasons. The first is that the timing of these stages of decreasing concentrations coincide with the enrichment of Pb and Zn. This suggests that in addition to increased pollution entering the PRE, economic and industrial development is having a much wider impact on the transportation of weathered and eroded material through the catchment. In addition to the wider implications of this development, the decrease in weathered material coincident with increases in Pb and Zn concentrations suggests that the enrichment of these metals is more significant than initial analysis of the metal profiles suggests. For Pb and Zn, based on the ratio of

their respective means concentrations from pre-1950 and post-1990, Pb and Zn have shown concentration increases of 183% and 151% respectively in this region of the Western shoal. When it is considered that this increase has occurred at the same time as the flux of naturally weathered material has decreased suggest that much of this increase in the result of anthropogenic sources of these metals.

5.6 Heavy Metal Enrichment Factors (EFs)

By comparing enriched and background concentrations of various heavy metals relative to a conservative tracer of natural weathering and erosion, it is possible to calculate a particular heavy metal's anthropogenic enrichment factor (EF) (Ridgeway and Shimmield, 2002; Abrahim and Parker, 2008; Wang *et al.,* 2008). Based on the findings of section 5.5.3, enrichment of Pb and Zn has come at a time when the flux of these metals from natural sources has decreased. This suggests their anthropogenic enrichment is even greater than the 183% and 151% for Pb and Zn respectively, based simply on the difference in their concentrations between pre-1950 and post-1990 abundances. Co, Fe and Ti have already be identified as elements with distributions and enrichments that are directly related to natural weathering, erosion and transportation processes in the Pearl River basin. Due to the very high concentrations of Fe, this element's concentrations will be the comparatively less affected by any anthropogenic sources (Schiff and Weisberg, 1999; Abrahim and Parker, 2008). Heavy metal EFs at a given depth are calculated using the following equation:

$$EF = (Metal_x/Metal_{Fe})_{sub\text{-}sample}/(Metal_x/Metal_{Fe})_{background}$$

where $(metal_x/metal_{Fe})_{sub\text{-}sample}$ is the concentration ratio of heavy $metal_x$ to normalising $metal_{fe}$ for a given sub-sample and $(Metal_x/Metal_{Fe})_{background}$ is the concentration ratio of $metal_x$ to normalising $metal_{fe}$ for background (pre-anthropogenic) sub-samples (based on Ridgeway and Shimmield, 2002). By normalising to Fe, the fluctuations of the metal concentrations due to changes in the natural flux of heavy metal bearing weathered material is accounted for, and the true anthropogenic enrichment can be identified.

Background concentration values for EF calculations will be based on the mean concentration of each metal from 1900-1758, where any anthropogenic sources of

heavy metal pollutants should be minimal. Based on the work of Zhang and Lui (2002) and Wang *et al.,* (2008), an EF<1 indicates depletion of that particular metal relative to background concentrations; EF=1 indicate natural (background) concentrations, EF>1 indicates enrichment but not necessarily from anthropogenic sources; EF>1.5 indicates an important portion of enrichment is coming from non-natural sources and EF>2 indicates significant anthropogenic enrichment.

All EF values calculated for metal can be found in appendix C and displayed in figure 5.14. From figure 5.14 it is clearly visible that only Pb and Zn are enriched or significantly enriched from anthropogenic sources. Maximum EFs for both Pb and Zn are found between 2006 and 2008, with values of 2.6 and 1.8 respectively. Cd displays slight depletion along most of the top 48cm of the core. Co shows no enrichment and further confirms its natural origins. Cr, Cu and Ni show no enrichment in during the first phase of Pb and Zn enrichment, but do show some enrichment during second phase enrichment of Pb and Zn (1990-2008).

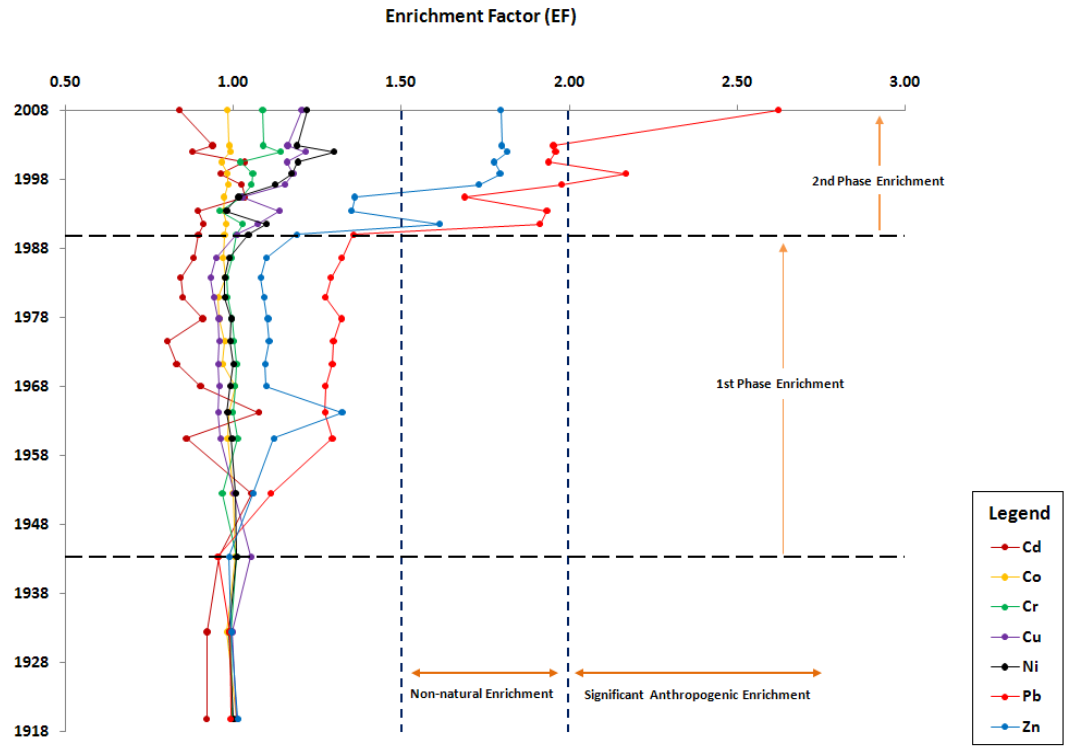

Figure 5.14. Enrichment Factor (EF) profiles for Cd, Co, Cr, Cu, Ni, Pb and Zn using Fe as a conservative tracer for the top 48cm of core 4.

The maximum EF values obtain are all <1.2 except Ni which reaches a maximum of 1.3 in 2002. Although this enrichment is not significant enough based on the work

Zhang and Lui (2002) to be attributed to anthropogenic sources on its own, with the knowledge that there has been an obvious decrease in naturally derived metal bearing sediment to the region since 1990, it is suggested that this slight enrichment is the result of anthropogenic sources. Anthropogenically significant EFs for Pb and Zn (EF>1.5) are present in core 4 from 1990 to 2008.

In another study using EFs in the 'west-four' region of the PRE, where the 70% of the *West River* discharges directly into the South China Sea through the *Jitimen*, *Hutlaomen* and *Modaomen* gates (see fig. 1.1), Pb and Zn where also found to be highly enriched (Wang *et al.,*2008). Maximum EFs of 2.23 for Pb and 2.14 for Zn were calculated. Wang *et al.,* (2008) attributes this enrichment to local point source contamination. With similar EFs for Pb and Zn being found in the PRE, which although geographically separated from the 'west-four' region is hydrologically connected through distributaries of the West River which drain through the *Jiaomen, Hongqimen* and *Hengmen* gates, it appears likely that the sources of this pollution are coming from further up the river catchment. Much of which is likely the result of mining of metal sulphide bearing carbonates within the Pear River catchment.

5.7 Interpreting the Temporal Distribution

Geochemical and geochronological techniques have been used to assess the temporal trends in heavy metal concentrations in three locations spanning the Western, Central and Eastern shoals of the PRE.

Core 3 has proven to display an unreliable depositional chronology and as such has not been analysed in any great detail. The core does however, highlight the dynamic depositional environment along the Eastern shoal that is affected by erosion, sediment re-suspension and human activities including dredging (Zhou *et al.,* 2004).

Core 2, a relatively short core although not sub-sampled for ^{210}Pb and ^{137}Cs is assumed to span a period of approximately 20 years based on previous research (Zhou *et al.,* 2004). Evidence from C/N ratio analysis suggests that there has been a gradual decrease in the transport of terrestrially derived organic matter to this part of the estuary, although over what time-scale is hard to say definitively. Heavy metals show no enrichment trends and suggest that anthropogenic influence in this region of the estuary is either very low, or has remained unchanged during the time in which this

core has been deposited. This is most likely due to the anti-clockwise circulation that exists in the estuary, with the majority of suspended sediment load being discharged along the Western shoal of the PRE away from the centre of the estuary. These findings are in agreement with hydrological and suspended sediment load studies of the main tributaries of the Pearl River (Zhang *et al.,* 2007; Lu *et al.,* 2008).

Core 4 presents the most useful and undisturbed chronology of deposition spanning back to 1758. Particle size variability is extremely low making analysis of the raw data much more reliable as particle-size normalisation is not necessary. Bulk C/N ratios show that the flux of terrestrial organic matter being sedimented has decreased over time, which is confirmed by the gradual fall in Fe concentrations indicating reduced input of weathered terrestrial material. Cr, Cu and Ni show some enrichment, especially since 1990. EFs of <1.3 were calculated for these metals which although not significantly high are taken to be the result of anthropogenic sources. Pb and Zn do however, display significant anthropogenic enrichment which is mirrored in another study from the 'west-four' region of the PRE (Wang *et al.,* 2008).

In this study, Wang *et al.,* (2008) attributes the significant enrichment of Pb and Zn in this region of the PRE to a localised point source of contamination. The fact that this pattern of significant Pb and Zn enrichment also exists in sediments from the western shoal of the main estuary, suggests that this may not be the case, or at least an oversimplification. Analysis from the spatial distribution of Pb and Zn identified that both metals were significantly enriched immediately down-river of Guangzhou, and along the western shoal. Based on the results from chapter 4 (this study), enrichment of these two metals is considered to be attributable to Pb-Zn mining of carbonate bearing ores in the Pearl River basin to, and potentially from atmospheric deposition from fossil fuel burning and urban/industrial waste that result from activities such as electroplating and ship painting. Hydrologically, these two geographically separated regions of the PRE are connected due the brief confluence of the *North* and *West Rivers* to the west of Guangzhou (see fig. 1.1) and because 30% of the *West River* discharges through the *Humen, Jiaomen, Hongqimen* and *Hengmen* gates north of Qi-Ao Island in the main estuary (Li *et al.,* 2001). The other 70% is discharged through the *Jitimen*, *Hutlaomen* and *Modaomen* gates in the 'west-four' region (Wang *et al.,* 2008) (see fig. 5.15).

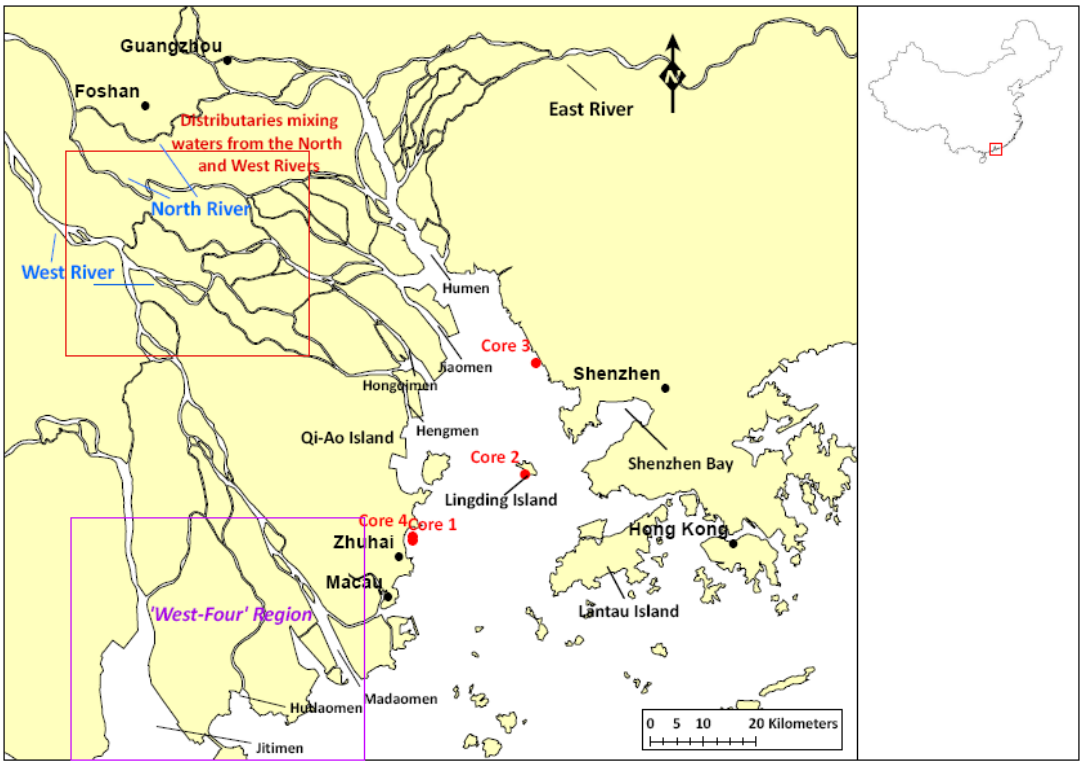

Figure 5.15. Map showing connectivity between 'west-four' and main PRE. Mixing of West and North River waters occurs in the region south of Foshan City.

The distributaries that discharge through the main and 'west-four' regions of the PRE have been shown to interact and mix much further upsteam, to the west of Guangzhou. It is suggested here that anthropogenically significant EFs associated with Pb and Zn along the Western shoal of the main estuary, and 'west-four' estuary are not primarily the result of the point sources suggested by Wang *et al.,* (2008). Instead it is much more likely that Pb-Zn mining operations within the Pearl River basin account for a large amount of their enrichment. The slightly higher EFs associated with Pb compared with Zn indicates there must be a second source of anthropogenic Pb that is not the result of waste from metal sulphide mining. This second source is likely to come from atmospheric deposition from the burning of fossil fuels in industrial process, power generation (Li *et al.,* 2000; Ip *et al.,* 2004; Zhou *et al.,* 2004) and until the 1990's, the combustion of leaded fuels (Zhu *et al.,* 2001). This is however a supposition, and although much research has been presented on atmospheric deposition of heavy metals in the PRE, and no further analysis of the samples examined in this study have been conducted to verify this.

Stable Pb isotope ratios have proven useful in verifying changes in Pb

concentrations as they have been coincident with falls in both $^{206}Pb/^{207}Pb$ and $^{208}Pb/^{207}Pb$ ratios at the same depths within the cores. This has proven especially useful in core 4. The values for $^{206}Pb/^{207}Pb$ and $^{208}Pb/^{207}Pb$ ratios are however, much higher compared to their isotopic ratios in other studies (see fig. 5.16). This is especially true for the composition of atmospherically deposited Pb (Wong *et al.,* 2003).

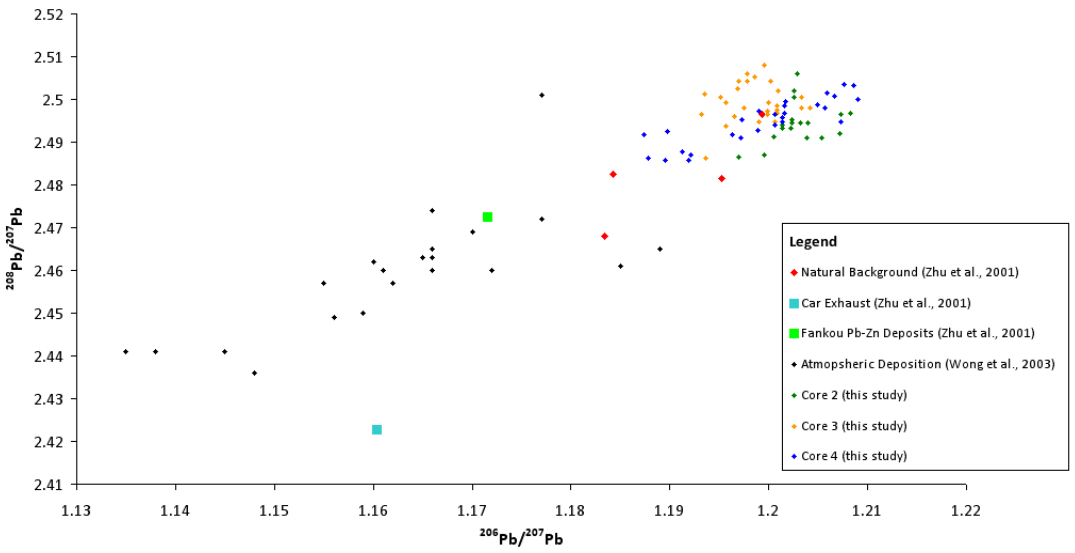

Figure 5.16. Correlation of stable Pb isotope ratios from this study and a number of others conducted in the PRD

Most of the isotopic ratios found in this study reside within known natural background values obtained from bedrock and uncontaminated soils (Zhu *et al.,* 2001). This is most likely due to the dilution effects that the large suspended sediment load and discharge from the North, East and West Rivers. This will result in the anthropogenic signature being masked by the large volume of naturally weathered and eroded material being transported within the Pearl River system.

6. Summary and Conclusions

A spatial and temporal investigation of the concentrations of Al, Cd, Co, Cr, Cu, Fe, Ni, Pb, Ti, and Zn existing within sediments of the PRE has been conducted. The raw data has been presented and analysed with conclusions being put forward to explain the various spatial and temporal distribution patterns observed.

6.1 Spatial Distribution

Four patterns of distribution within the estuary have been identified through raw and normalised geospatial analysis that based on PCA, have been attributed to being the results of three very different heavy metal sources.

Cd, Cr, Cu, Ni, Pb and Zn are all found to be enriched along the lower course of the North River between Guangzhou and the Humen gate, particularly Pb and Zn (see fig. 4.4a,b,c). Cu, Ni, Pb and Zn are also found in higher concentrations from the *Humen* gate, along the whole Western shoal to Macau. This pattern is suggested as being the result of higher background values that are the result of the weathering and erosion of metal sulphide bearing ores in the Pearl River catchment, enriched through mining activities and point sources from industrial and urban waste. Outside the North River, Cd and Cr are only enriched along the Western shoal in the region of Zhuhai-Macau. This enrichment is thought to be due to these metals having similar sources from metal alloy processing industry that is prevalent in this region.

Fe and Ti enrichment along the western shoal is due to suspended sediment eroded within the Pearl River catchment being discharged into the PRE. The uniform enrichment along the lower course of the North River and all along the Western shoal is a result of estuarine circulation patterns which deflect the North and West River water through this side of the PRE. Co has proved to be highly associated with the rock forming elements Fe and Ti, displaying an almost identical pattern of distribution and is therefore considered to be distributed in the PRE entirely as a result of natural weather within the catchment and circulatory forcing. These findings also suggest that the use of Fe as a conservative tracer element of weathering (Schiff and Weisberg, 1999) is much more applicable for studies of the PRE.

Al is most enriched outside the estuary, in the adjacent coastal waters of the

South China Sea. This may be due to its affinity to very fine clays (<0.002mm) found in these waters (Ip *et al.,* 2007) but no evidence for this is presented here. Often used as a conservative tracer elements of natural weathering and erosion (Dashkalakis and O'Conner, 1995) and implemented in previous studies of the PRE (Zhou *et al.,* 2004). This study finds that in the PRE, the dominant source of Al appears not to be from weathered bedrock. The uncertainties about its origins and the high abundance of Fe throughout the PRE mean it has not been used in this case.

The use of benthic foraminifera to assess the ecotoxicological significance of heavy metal concentrations have proved inconclusive. The application of this technique has proved particularly problematic due to foraminifera not living in the very low-salinity/freshwater benthic environment of the North River where heavy metal concentrations are highest. The other caveat of using foraminifera species is that they display the same deformities as a result of environmental stresses (such as salinity tolerances and competition for food) as they do for significant heavy metal pollution.

Development in the estuary over the last 30 years is widely considered to have had a significant impact on the aquatic environment (Li *et al.,* 2000; Ip *et al.,* 2004), however, the findings of this study are slightly contradictory. It is acknowledged that Pb and Zn are significantly enriched along the lower course of the North River, and to a lesser extend along the Western shoal. This is most likely the result of waste from significant metal sulphide mining operations within the Pearl River catchment, point source urban waste from population centres such as Guangzhou, and atmospheric deposition from fossil fuel burning. Further enrichment along the North River as a result of point source waste from population centres is also identified in the distribution of Cd, Cr, Cu and Ni, and between Zhuhai and Macau for Cd and Cr as a result of waste from metal processing industries.

Based on these results, the majority of the PRE appears relatively unaffected by anthropogenic pollution. Much of the elevated heavy metal concentrations found along the Western shoal are likely to be the result of natural process including estuarine circulation patterns, increased deposition due flocculation in the turbidity maximum zone and the relatively slow movement of water that result in much of the water and suspended sediment entering the PRE being discharged along the Western

shoal were conditions enhance deposition in this region.. This is verified by the distribution of clay, Fe and measured surface salinity which support this interpretation. Outside this area of the PRE, higher energy environments, tidal flushing and some dredging activity in the East and central regions of the estuary help prevent the enrichment of heavy metals. This is particularly true for Hong Kong, where low heavy metal concentrations are found in what is widely regarded as a polluted aquatic system (Yin and Harrison, 2007).

When compared to other industrialised estuaries from Western Europe, the highest concentrations of heavy metals, particularly Pb and Zn are very similar to those of the Tyne and Tees Rivers in the UK but higher than those of the River Humber (Rowlatt and Lovell, 1994; Ridgeway and Shimmield, 2002). This is likely the result of similarly exploited metal sulphide bearing ores in the North-east of the UK with the waste from these operations entering the Tees and Tyne Rivers. Compared to the River Seine, PRE sediments are significantly less enriched in Cd, Cr, Cu, Ni, Pb and Zn (Meybeck *et al.,* 2007). The estuarine sediments of the Humber, Seine, Tees, Tyne and many other rivers in Western Europe display a legacy of industrial development that spans a time period back to the industrial revolution when many industrial processes where much more polluting and less efficient (Cundy *et al,* 2003; Howarth *et al.,* 2005). In comparison with heavy metal concentrations found in sediments of the Palar River draining the rapidly industrialising region of Madras, India. Maximum heavy metal concentrations are found to be similar for Cd and Cu, but lower for Pb and Zn than those of the PRE (Selvaraj *et al.,* 2004). Again, this is likely due to pollution associated with metal sulphide mining in the Pearl River Catchment.

6.2 Temporal Distribution

Three cores extracted from the Western, Central and Eastern shoals of the PRE were analysed to assess the temporal changes in circulatory regimes, freshwater influx, weathering and erosion rates and heavy metal concentrations.

Based on ^{210}Pb and ^{137}Cs dating techniques, C/N bulk ratios, particle size analysis, stable Pb isotope ratios and heavy metal concentrations, core 3 extracted from the Eastern shoal could not be used to assess temporal variations as contained

sedimentary sequence that showed the signatures of erosion and resuspension of sediments post-deposition. Core 2 was not dated using ^{210}Pb and ^{137}Cs techniques but was taken to show a relatively undisturbed chronology of deposition. C/N bulk ratio analysis shows an increasing dominance from nitrogen rich marine/freshwater organic matter towards the top of the core that is interpreted as being the result of decreased terrestrially derived suspended sediment load being transported into the estuary. The likely reason for this is activities such as dam building and water abstraction. The activities will reduce the suspended sediment load and the carry capacity of the river, resulting in less water and sediment discharge into the PRE (Zhang *et al.,* 2007; Lu *et al.,* 2008). The heavy metal profiles are uniform along the whole length of the core and suggest that their supply has remained relatively constant throughout the cores deposition. Stable Pb isotope ratio do show a drop in both the $^{208}Pb/^{207}Pb$ and $^{206}Pb/^{207}Pb$ ratios which is indicative of changes in the source of Pb from natural to anthropogenic. Whilst this change is evident, the values for $^{208}Pb/^{207}Pb$ and $^{206}Pb/^{207}Pb$ at still slightly >2.49 and >1.20 at the top of the core. Based on the work of Ip *et al.,* (2000), this demonstrates that they are derived primarily from natural sources, although especially for the $^{206}Pb/^{207}Pb$, ratio values are close to this natural-anthropogenic threshold.

Core 4 shows a undisturbed chronology of deposition spanning back to 1758 based on calibration of $^{210}Pb_{xs}$ data using the CRS model and linear interpolation of the age-depth profile from 64cm to the base of the core. Results from C/N bulk ratios suggest that there is also a slight decrease in the dominance of terrestrially derived organic material towards the top of the core until a depth of 6cm, after which it is a terrestrially dominated signature. Values obtained from raw ICP-MS derived heavy metal concentrations show a two stepped stages of enrichment of Pb and Zn first starting in the 1950's and then accelerating in at the beginning of the 1990's. This stepped two-stage enrichment is also evident in the stable Pb isotope ratios at the same time, and also in the decreasing trends of Fe and Ti concentrations over the same period. $^{208}Pb/^{207}Pb$ and $^{206}Pb/^{207}Pb$ ratio drop below the natural-anthropogenic ratio threshold (Ip *et al.,* 2004) in the very early and late 1990's respectively.

Calculation of enrichment factor profiles for core 4, normalised to the

conservative weathering tracer element Fe show that Cr, Cu and Ni show some enrichment starting in the early 1990's, the maximum EFs <1.3 are interpreted as enrichment resultant from anthropogenic sources because of the reduced flux of naturally weathered material over this time. Co shows the most uniform EF profile (=1) further verifying its concentrations are the result of natural weathering and erosion as it covaries with Fe. Pb and Zn are significantly enriched from anthropogenic sources with maximum EFs of 2.6 and 1.8 respectively at the top of the core.

6.3 Conclusions

Investigation of the spatial and temporal distribution of heavy metals in the PRE based on 77 surface samples and 3 cores has been completed. From the results it has been found that there are four patterns of distribution for the heavy metals Al, Cd, Co, Cr, Cu, Fe, Ni, Pb, Ti and Zn that are the result of three different heavy metal sources.

Environmental variables such as estuarine circulation and the interaction of fresh- and marine-water account for a large proportion of the distribution of these metals spatially, especially along the Western shoal. This environmental forcing also accounts for the low heavy metal concentrations in what are considered polluted waters around Hong Kong. Tidal 'flushing' transports much of the pollution north into the PRE, where it circulates to the Western side of the estuary.

Pb and Zn have proved to be the only significantly enriched heavy metals in the estuary which is hear attributed to metal sulphide mining within the Pearl River catchment. These catchment wide mining activities cause enrichment along the whole Pearl River catchment, particularly along the North River. Through the PRD, discharge from the North and West Rivers is mixed within the network of distributaries that enter the PRE. This mixing further accounts for the high levels of Pb and Zn that are also found in the 'west-four' section of the estuary as opposed to it being the result of point pollution sources (Wang *et al.,* 2008). Additional fluxes come from atmospheric deposition of heavy metals, particularly Pb from fossil fuel burning and some point sources from population centres such as Guangzhou. Their enrichment has seen a 2 stage increase, the first beginning in the 1950's and the second in the early 1990's.

Co concentrations have been identified as being entirely the result of natural

sources and not anthropogenic as has been previously suggested. Al has also been proved to be present in the estuary due to a marine source and not from terrestrial weathering identifying it as a very poor choice as a normalising element to account for variable weathering.

Compared to estuarine sediments from long established industrialised rivers such as the Humber, Tees and Tyne in the UK and the Seine in France heavy metal pollution is not as acute. This is because these Western European rivers have a much longer legacy of industrialisation, and the that Pearl River drains a sub-tropical catchment with an average discharge that is 10^3 greater than that of the Humber (Cave *et al.,* 2003). This coupled with the significantly higher suspended sediment load suggests that the estuary may have an ability to subdue the concentrations of heavy metals and mask the anthropogenic signature.

An initial assessment of the ecotoxicological significance of heavy metal concentrates has proved inconclusive as the most polluted benthic environments of the PRE are in the low salinity/freshwater environment of the lower North River where foraminifera can not present.

References

Abrahim, G. M. S and Parker, R. J. (2008). Assessment of heavy metal enrichment factors and the degree of contamination in marine sediments from Tamaki Estuary, Auckland, New Zealand. *Environmental Monitoring and Assessment, 136,* 227-238.

Aggarwal, J., Habicht-Mauche, J and Juarez, C. (2008). Application of heavy stable isotopes in forensic isotope geochemistry: a review. *Applied Geochemistry, 23,* 2658-2666.

Albani, A., Barbera, R. S., and Donnici, S. (2007). Foraminifera as ecological indicators in the Lagoon of Venice, Italy. *Ecological Indicators, 7,* 239-253.

Álvarez-Iglesais, P., Quintana, B., Rubio, B and Pérez-Arlucea, M. (2007). Sedimentation rates and trace metal input history in intertidal sediments from San Simón Bay (Ría de Vigo, NW Spain) derived from ^{210}Pb and ^{137}Cs chronology. *Journal of Environmental Radioactivity, 98,* 229-250.

An,, Z. S., Porter, S. C., Kutzbach, J. E., Wu, X. H., Wang, S. M., Liu, X. D., Li, X. Q and Zhou, W. J. (2000). Asynchronous Holocene optimum of the East Asian Monsoon. *Quaternary Science Reviews, 19,* 743-762.

Anadón, P., Gliozzi, E and Mazzini, I. (2002). Paleoenvironmental Reconstruction of Marginal Marine Environments from Combined Paleoecological and Geochemical Analyses on Ostracods. In *The Ostracoda: Applications in Quaternary Research* (eds Holmes, J.A and Chivas, A. R). American Geophysical Union: USA, pp.227-247.

Anderson, T. J., Mikkelsen, O. A., Møller, A. L and Pejrup, M. (2000). Deposition and mixing depths in some European intertidal mudflats based on ^{210}Pb and ^{137}Cs activities. *Continental Shelf Research, 20,* 1569-1591.

Appleby, P. G and Oldfield, F. (1978). The calculation of ^{210}Pb dates assuming a constant rate of supply of unsupported ^{210}Pb to the sediment. *Catena, 5*, 1-8.

Beckman-Coulter. (2004). BR-9809A: LS™ 13 320 Series Laser Diffraction Particle Size Analyzer. Beckman-Coulter: USA., pp. 1-12.

British Gelogical Survey. (2005). *Britain beneath our feet - Copper in offshore sea-bed*

sediments.. Available:www.bgs.ac.uk/education/britainbeneath/off_copper.html

Last accessed 11th November 2008.

Birch, G. F., McCready, S., Long, E. R., Taylor, S. S and Spyrakis, G. (2008). Contaminant chemistry and toxicity of sediments in Sydney Harbour, Australia: spatial extent and chemistry-toxicity relationships. *Marine Ecology Progress Series, 363,* 71-87.

Boyle, E. A. (1981). Cadmium, Zinc, Copper, and Barium in foraminifera tests. *Earth and Planetary Science Letters, 53,* 11-35

Burrough, P. A and McDonnell, R. A. (1998). *Principals of Geographical Information Systems*. Oxford University Press: Oxford.

Carbonel, P. (1988) Ostracods and the transition between fresh and saline waters. In *Ostracoda in the Earth Sciences* (eds De Dekker, P., Colin, J-P and Peypouquet, J-P). Elsevier: Amsterdam, pp.157-175.

Cantwell, M. G., King, J. W., Burgess, R. M and Appleby, P. G. (2007). Reconstruction of contaminant trends ina salt wedge estuary with sediment cores dated using a multiple proxy approach. *Marine Environmental Research, 64,* 225-246.

Caurant, F., Aubail, A., Lahaye, V., Van Canneyt, O., Rogan, E., López, A., Addink, M., Churlaud, C., Robert, M and Bustamante, P. (2006). Lead contamination of small cetaceans in European waters – The use of stable isotopes for identifying the source of lead exposure. *Marine Environmetal Research, 62,* 131-148.

Cave, R. R., Ledoux, L., Turner, K., Jickells, T., Andrews, J. E and Davies, H. (2003). The Humber cathcment and its coastal area: from UK to European perspectives. *Science of the Total Environment, 314-316,* 31-52.

Changué-Goff, C., Nichol, S. L., Jenkinson, A. V and Heijnis, H. (2000). Signatures of natural catastrophic events and anthropogenic impact in an estuarine environment, New Zealand. *Marine Geology, 167*, 285-301.

Chau, K. W. (2006). Persistent organic pollution characterisation of sediments of the Pearl River estuary. *Chemosphere, 64*, 1545-1549.

Chen, S-S., Chen, L-F., Liu, Q-H and Tan, Q. (2005). Remote sensing and GIS-based integrated analysis of coastal changes and their environmental impacts in Lingding Bay, Pearl River Estuary, South China. *Ocean and Coastal Managment, 44(1),* 65-83.

Cheung, K. C., Leung, H. M and Wong, M. W. (2008). Metal Concentrations of Common Freshwater and Marine Fish from the Pearl River Delta, South China. *Archives of Environmental Contamination and Toxicology, 54,* 705-715.

Childs, C. (2004). Interpolating surfaces in ArcGIS spatial analyst.ESRI, USA, pp 32-35.

Cundy, A. B., Croudace, I. W., Cearreta, A and Irabien, M. J. (2003). Reconstructing historical trends in metal input inheavily-disturbed, contaminated estuaries: studies from Bilbao, Southampton Water and Sicily. *Applied Geochemistry, 18,* 311-325

Dashkalakis, K. D and O'Conner, T.P. (1995). Normalization and Elemental Sediment Contamination in the Coastal United States. *Environmental Science and Technology, 29 (2),* 470-477.

DeDeckker, P and Forester, R. M. (1988). The use of ostracods to reconstruct continental palaeoenvironmental records. In *Ostracoda in the Earth Sciences* (eds De Dekker, P., Colin, J-P and Peypouquet, J-P). Elsevier: Amsterdam, pp.175-200

Dong, L., Su, J., Wong, L. A., Cao, Z and Chen, J-C. (2004). Seasonal variation and dynamics of the Pearl River plume. *Continental Shelf Research, 24,* 1761-1777.

Durou, C., Smith, B. D., Roméo, M., Rainbow, P. S., Mouneyrac, C., Mouloud, M., Gnassia-Barelli, M., Gillet, P.,Deutch, B and Amiard-Triquet, C. (2007). From biomarkers to population responses in *Neris diversicolor*: Assessment of the stress in estuarine ecosystems. *Ecotoxicology and Environmental Safety, 66*, 402-411.

Dwyer, G. S., Cronin, T. M., Baker, P. A. (2002). Trace Elements in Marine Ostracods. In *The Ostracoda: Applications in Quaternary Research* (eds Holmes, J.A and Chivas, A. R). American Geophysical Union: USA, pp.205-225

Ebdon, D. (1985). *Statistics in Geography* (2nd Eds). Basil Blackwell Ltd: Oxford.

Elberling, B., Knudsen, K. L., Kristensen, P. H., and Asmund, G. (2003). Applying foraminiferal stratigraphy as a biomarker for heavy metal contamination and mining impact in a fiord in West Greenland. *Marine Environmental Research, 55,* 235-256.

Enright, M. J., Scott, E. E and Enright, Scott and Associates. (2006). *The Greater Pearl River Delta*. (4th ed). Invest Hong Kong of the HKSAR Government: Hong Kong, pp.5-10.

ESRI. (2006). *ArcGIS 9.1 Desktop Help*. Available: http://webhelp.esri.com/arcgisdesktop/9.1/index.cfm?TopicName=welcome Last accessed: 28th November 2008

Fan, F., Weng, Q and Wang, Y. (2007). Land Use and Land Cover Change in Guangzhou, China, from 1998 to 2003, Based on Landsat TM/ETM+ Imagery. *Sensors, 7,* 1323-1342.

Feng, H., Han, X., Zhang, W and Yu, L. (2004). A preliminary study of heavy metal contamination in Yangtze River intertidal zone due to urbanisation. *Marine Pollution Bulletin, 49,* 910-915.

Ferraro, L., Sprovieri, M., Alberico, I., Lirer, F., Prevedello, L and Marsella, E. (2006). Benthic foraminifera and heavy metal distribution: A case study from the Naples Harbour (Tyrrhenian Sea, Southern Italy). *Environmental Pollution, 142,* 274-287.

Folk, R.L and Ward, W.C. (1957) Brazos River bar: a study in the significance of grain size parame`ters. *Journal of Sedimentary Petrology*, *27*, 3-26.

Frontalini, F and Coccioni, R. (2008). Benthic foraminifera for heavy metal pollution monitoring: A case study from the central Adriatic Sea soast of Italy. *Estuarine Coastal and Shelf Science, 76,* 404-417.

Geslin, E., Denenay, J-P., Duleba, W and Bonetti, C. (2002). Morphological abnormalities of foraminiferal tests in Brazilian environments: comparison between polluted and non-poluted areas. *Marine Micropalaeontology, 45,* 151-168.

González, I., Águila, E and Galán, E. (2007). Partitioning, bioavailability and origin of heavy metals from the Nador Lagoon sediments (Morocco) as a basis for their managment. *Environmental Geology, 52,* 1581-1593.

Goodarzi, F., Huggins, F. E and Sanei, H. (2008). Assessment of elements, speciation of As, Cr, Ni and emitted Hg for a Canadian power plant burning bituminous coal. *International Journal of Coal Geology, 74 (1),* 1-12.

Harrison, P. J., Yin, K., Lee, J. H. W., Gan, J and Lui, H. (2008). Physical–biological coupling in the Pearl River Estuary. *Continental Shelf Research, 28,* 1405-1415.

Hayward, B. W., Grenfell, H. R., Nicholson, K., Parker, R., Wilmhurst, J., Horrocks, M., Swales, A and Sabaa, A. T. (2004). Foraminiferal record of human impact on intertidal estuarine environments in New Zealand's largest city. *Marine*

Micropaleontology, 53, 37-66.

Hiatt, V and Huff, J. E. (1975). The environmental impact of Cadmium: An overview. *International Journal of Environmental Studies, 7 (4),* 277-285.

Holmes, J. A and Chivas, A. R. (2002). Introduction. In *The Ostracoda: Applications in Quaternary Research* (eds Holmes, J.A and Chivas, A. R). American Geophysical Union: USA, pp.1-5.

Howarth, R. J., Evans. G., Croudace, I. W and Cundy, A. B. (2005). Sources and timing of anthropogenic pollution in the Ensenada de San Simo´n (inner Rı´a de Vigo), Galicia, NW Spain: an application of mixture-modelling and nonlinear optimization to recent sedimentation. *Science of the Total Environment, 340,* 149-176.

Hu, J., Peng, P., Jai, G., Mai, B and Zhang, G. (2006). Distribution and sources of organic carbon, nitrogen and their isotopes in sediments of the subtropical Pearl River estuary and adjacent shelf, Southern China. *Marine Chemistry, 98*, 274-285.

Ip, C. C. M., Li, X. D., Zhang, G., Farmer, J. G., Wai, O. W. H and Li, Y. S. (2004). Over one hundred years of trace metal fluxes in the sediments of the Pearl River Estuary, South China. *Environmental Pollution, 132,* 157-172.

Ip, C. C. M., Li, X. D., Zhang, G., Wong, C. S. C and Zhang, W. L. (2005). Heavy metals and Pb isotopic compostions of aquatic organisms in the Pearl River Estuary, South China. *Environmental Pollution, 138,* 494-504.

Ip, C. C. M., Li, X. D., Zhang, G., Wai, O. W. H and Li, Y. S. (2007). Trace metal distribution in sediments of the Pearl River Estuary and the surrounding coastal area, South China. *Environmental Pollution147 (2),* 311-323.

Jomes, R. W. (1994). *The Challenger Foraminifera.* Oxford University Press: Oxford.

Krishnaswami, S., Lal, D., Martin, J. M and Meybeck, M. (1971). Geochronology of lake sediments. *Earth and Planetary Science Letters, 11,* 407-414.

Lamb, A. L., Wilson, G. P and Leng, M. (2006). A review of coastal palaeoclimate and relative sea-level reconstructions using δ13C and C/N ratios in organic material. *Earth Science Review, 75,* 29-57.

Lamb, A. L., Vane, C. H., Wilson, G. P., Rees, J. G and Moss-Hayes, V. L. (2007). Assessing $\delta^{13}C$ and C/N ratios from organic material in archived cores as Holocene sea level and palaeoenvironmental indicators in the Humber Estuary, UK. *Marine Geology, 244,* 190-128.

Langer, M. R and Lipps, J. H. (2003). Foraminiferal distribution and diversity, Madang Reef and lagoon, Papau New Guinea. *Coral Reefs, 22,* 143-154.

Larson, M., Bellanca, R. Jönsson, L., Chen, C and Shi, P. (2005). A model of the 3D . circulation, Salinity Distribution, and Transport Pattern in the Pearl River Estuary, China. *Journal of Coastal Research, 21,* 896-908.

Lee, S. V and Cundy, A. B. (2000). Heavy Metal Contamination and Mixing Processes in Sediments from the Humber Estuary, Eastern England. *Estuarine, Coastal and Shelf Science, 53,* 619-636.

Lee, C. S. L., Li, X., Zhang, G., Peng, X and Zhang, L. (2005). Biomonitoring of trace metals in the atmosphere using moss (*Hypnum plumaeforme*) in the Nanling Mountains and the Pearl River Delta, Southern China. *Atmosperic Environment, 39,* 397-407.

Lee, C. S. L., Li, X-D., Zhang, G., Li, J., Ding, A-J and Wang, T. (2007). Heavy metals and Pb isotopic composition of aersols in urban and suburban areas of Hong Kong and Guangzhou, South China – Evidence of long-range transport of air contaminants. *Atmospheric Environment, 41,* 432-447.

Leung, Y., Lee, Y., Lam, K. C., Lin, K and Zeng, F-T. (2005). An environmental decision-support system for the management of water pollution in a tidal river network. *International Journal of Geographical Information Science, 19 (4)*, 483-500.

Li, X., Wai, O. W. H., Li, Y-S., Coles, B. J., Ramsey, M. H and Thornton, I. (2000). Heavy Metal Distribution in sediment profiles of the Pearl River Estuary, South China. *Applied Geochemistry, 15,* 567-581.

Li, X., Shen, Z., Wai, O. W. H. and Li, Y-S. (2001). Chemical Forms of Pb, Zn and Cu in the Sediment Profiles of the Pearl River Estuary. *Marine Pollution Bulletin, 42,* 215-223.

Li, Q-S., Wu, Z-F., Chu, B., Zhang, N., Cai, S-S and Fang, J-H. (2007). Heavy metals in coastal wetland sediments of the Pearl River Estuary, China. *Environmental Pollution, 149*, 158-164.

Liu, H., Probst, A and Liao, B. (2005). Metal contamination of soils and crops affected by the Chenzhou lead/zinc mine spill (Hunan, China). *Science of the Total Environment, 339 (1-3),* 153-166.

Lui, L., Li, F., Xiong, D and Song, C. (2006). Heavy metal contamination and their distribution in different size fractions of the surficial sediment of the Haihe

River, China. *Environmental Geology, 50,* 431-438.

Liu, M., Hou, L. J., Xu, S. Y., Ou, D. N., Yang, Y and Wang, Q. (2006). Organic carbon and nitrogen stable isotopes in the intertidal sediments from the Yangtze Estuary, China. *Marine Pollution Bulletin, 52,* 1625-1633.

Liu, W. and Deng, P. Y. (2007). Accumulation of Cadmium, Copper, Lead, and Zinc in the Pacific Oyster, *Crassostrea gigas,* Collected from the Pearl River Estuary, Southern China. *Bulletin of Environmental Contamination Toxicology, 78,* 535-538.

Lu, X. X., Zhang, S. R., Xie, S. P and Ma, P. K. (2007). Rapid Channel Incision of the lower Pearl River (China) since the 1990s as a conseuence of sediment depletion. *Hydrology and Earth Systems Sciences, 11*, 1897-1906.

Luo, X-l., Zeng, E. Y., Ji, R-Y and Wang, C-P. (2007). Effects of in-channel sand excavation on the hydrology of the Pearl River Delta, China. *Journal of Hydrology, 343,* 230-239.

Mackie, E. A. V., Leng, M. J., Lloyd, J. M and Arrowsmith, C. (2005). Bulk organic $\delta^{13}C$ and C/N ratios as palaeosalinity indicators within a Scottosh isolation basin. *Journal of Quaternary Science, 20 (4),* 303-312.

Mackie, E. A. V., Lloyd, J. M., Leng, M. J., Bentley, M. J and Arrowsmith, C. (2007). Assessment of $\delta^{13}C$ and C/N ratios in bulk organic matter as palaeosalinity indicators in Holocene and Lateglacial isolation basin sediments, northwest Scotland. *Journal of Quaternary Science, 22 (6),* 579-591.

Mackie, J. A., Natali, S. M., Levinton, J. S and Sañudo-Wilhelm, S. A. (2007). Declining metal levels at Foundry Cove (Hudson River, New York): Response to localised dredging or contaminated sediments. *Environmental Pollution, 149,* 141-148.

Malloy, K. J., Wade, D., Janicki, A., Grabe, S. A and Nijbroek, R. (2007). Development of a benthic index to assess sediment quality in the Tampa Bay Estuary. *Marine Pollution Bulletin, 54,* 22-31.

Mao, Q., Shi, P., Yin, K., Gan, J and Qi, Y. (2004). Tides and tidal currents in the Pearl River Estuary. *Continental Shelf Research, 24,* 1797-1808.

Maybeck, M., Lestel, L., Bonté, P., Moilleron, R., Colin, J. L., Rousselot, O., Hervé, D., de Pontevès, C., Grosbois, C and Thévenot, D. R. (2007). Historical perspective of heavy metals contamination (Cd, Cr, Cu, Hg, Pb, Zn) in the Seine River basin (France) following DPSIR approach (1950-2005). *Science of the Total*

Environment, 375, 204-231.

McBratney, A. B and Webster, R. (1986). Choosing functions for semi-variograms of soil properties and fitting them to sampling estimates. *Journal of Soil Science, 37*, 617-639.

Munksgaard, N. C., Batterham, G. J and Parry, D. L. (1998). Lead Isotope Ratios Determined by ICP-MS: Investigation of Anthropogenic Lead in Seawater and Sediment from the Gulf or Carpentaria. *Marine Pollution Bulletin, 36 (7),* 527-534.

Murray, J. (1971). *An atlas of recent British foraminiferids.* Heinemann Educational Books: London.

Murray, J. (2006). *Ecology and Applicatins of Benthic Foraminifera.* Cambridge University Press: Cambridge.

Nieto, J. M., Sarmiento, A. M., Olías, M., Canovas, C. R., Riba, I., Kalman, J and Delvalls, T. A. (2007). Acid mine drainage pollution in the Tinto and Odiel rivers (Iberian Pyrite Belt, SW Spain) and bioavailability of the transported metals to the Huelva Estuary. *Environment International, 33,* 445-455.

Nigam, R., Panchang, R and Banerjee, P. (2005). Foraminifera in Surface Sediments of Mondovi River Easuary: Indicators for mining pollution and High Sea Stand in Goa, India. *Journal of Coastal Research, 21,* 853-859.

Nigram, R., Saraswat, R and Panchang, R. (2006). Application of foraminifers in ecotoxicology: Retrospect, perspect and prospect. *Environmental International, 32,* 273-283.

Okudo, T., Katsuno, M., Naoi, D., Nakao, S., Tanaka, S., He, K., Ma, Y., Lei, Y and Jai, Y. (2008). Trends in hazardous trace metal concentrations in aerosols collected in Beijing, China from 2001 to 2006. *Chemosphere, 72,* 917-924.

Ouyang, T. P., Zhu, Z. Y., Kuang, Y. Q., Huang, N. S., Tan, J. J., Guo, G. Z., Gu, L. S and Sun, B. (2006). Dissolved trace elements in river water: spatial distribution and the influencing factor, a study for the Pearl River Delta Economic Zone, China. *Environmental Geology, 49 (5)*, 733-742.

Piper, D. Z., Ludington, S., Duval, J. S and Taylor, H. E. (2006). Geochemistry of bed and suspended sediment in the Mississippi river system: Provenance versus weathering and winnowing. *Science of the Total Environment, 362,* 179-204.

Ridgeway, J and Shimmield, G. (2002). Estuaries as Repositories of Historical Contamination and their Impact on Shelf Seas. *Estuarine, Coastal and Shelf*

Science, 55, 903-928.

Robbins, J. A. (1978). Geochemical and geophysical applications of radioactive lead. In *The Biogeochemistry of Lead in the Environment, Part A,* Nriagu, J. O. (ed). Elsevier - North Holland Biomedical Press, 285-393.

Rowlatt, S. M and Lovell, D. R. (1994). Lead, Zinc and Chromium in sediments around England and Wales. *Marine Pollution Bulletin, 28,* 324-329.

Ruiz, F., González-Regalado, M. L., Borrego, J., Abad, M and Pendón, J. G. (2004). Ostracoda and foraminifera as short-term tracers of environmental changes in very polluted areas: the Odiel Estuary (SW Spain). *Environmental Pollution, 129,* 49-61.

Schiff, K. C and Weisberg, S. B. (1999). Iron as a reference element for determining trace metal enrichment in South California coastal shelf sediments. *Marine Environmental Research, 48,* 161-176.

Schrőder-Adams, C. (2006). Estuaries of the past and present: A biofacies perspective. *Sedimentary Geology, 190*, 289-298.

Selvaraj, K., Mohan, V. R and Szefer, P. (2004). Evolution of metal conamination in coastal sediments of the Bay of Bengal, India: geochemical and statistical approaches. *Marine Pollution Bulletin, 49,* 174-185.

Sen Gupta, B. K. (2002). Introduction to modern Foraminifera. In Sen Gupta, B. K (eds) *Modern Foraminifera.* Kluwer: London, pp. 3-6.

Seto, K. C., Woodcock, C. E., Song, C., Huang, X., Lu, J and Kaufmann, R. K. (2002). Monitoring land-use change in the Pearl River Delta using Landsat TM. *International Journal of Remote Sensing, 23,* 1985-2004.

Shu, W. S., Ye, Z. H., Lan, C. Y., Zhang, Z. Q and Wong, M. H. (2001). Acidification of lead/zinc mine tailings and its effect on heavy metal mobility. *Environmental International, 26 (5-6),* 389-394.

Shu, W. S., Ye, Z. H., Lan, C. Y., Zhang, Z. Q and Wong, M. H. (2002). Lead, zinc and copper accumulation and tolerance in populations of *Paspalum distichum* and *Cynodon dactylon. Environmental Pollution, 120 (2),* 445-453.

Sit, V. S. F. (1984). *Resources and development of the Pearl River Delta*. Hong Kong: Wide Angle Press.

Smol, J. P. (2008). *Pollution of lakes and rivers: A palaeoenvironmental perspective*. Blackwell: Oxford.

Sonke, J. E., Sivry, Y., Viers, J., Freydier, R., Dejonghe, L., André, L., Aggarwal, J. K., Fontan, F and Dupré, B. (2008). Historical variations in the isotopic composition of atmospheric zinc deposition from a zinc smelter. *Chemical Geology, 252 (3-4),* 145-157.

Speelmans, M., Vanthuyne,D. R. J., Lock, K., Hendrickx, F., Du, L. G., Tack, F. M. G and Janssen, C. R. (2007). Influence of flooding, salinity and inundation time on the bioavailability of metals in wetlands. *Science of the Total Environment, 380,* 144-153

Stouff, V., Geslin, E., Debenay, J. P and Lesourd, M. (1990). Origin of morphological abnormalities in *Ammonia* (foraminifera): studies in laboratory and natural environments. *Journal of Foraminiferal Research, 29,* 152-170.

Souza, V. L. B., Hazin, C. A and Lima, R. A. (2007). Trace element dating by ^{210}Pb: Application to an estuarine lagoon. *Nuclear Instruments and Methods in Physics Research A, 580*, 690-693.

Su, J. (2004). Overview of the South China Sea circulation and its influence on coastal physical oceanography outside the Pearl River Estuary. *Continental Shelf Research, 24,* 1745-1760.

Taylor, S. R and McLennan, S. M. (1995). The geochemical evolution of the continental crust. *Reviews of Geophysics, 33 (2)*, 241-265.

Tylmann, W., Gołębiewski, R., Woźniak, P. P and Czarnecka, K. (2007). Heavy metals in sediments as evidence for recent pollution and quasi-estuarine processes: an example from lake Druzno, Poland. *Environmental Geology, 53*, 35-46.

University of Maryland. (1997-2008). *Landsat GeoCover at the Global Land Cover Facility.* Available: http://glcf.umiacs.umd.edu/portal/geocover/. Last accessed 20 March 2008.

US EPA (1994). *Method 200.8, Revision 5.4: Determination of trace elements in waters and wastes by inductively coupled plamsa – mass spectrometry.* EPA: Ohio, pp 17- 30.

US EPA. (1996). *Method 3052: Microwave digestion of siliceous and organically based matrices*. EPA: USA, pp.1-20

Vaalgamaa, S and Korhola, A. (2004). Searching for order in chaos:A sediment stratigraphical study of a multi-impacted bay of the Baltic Sea. *Estuarine, Coastal and Shelf Science, 59,* 319-332.

Vaalgamaa, S and Conley, D. J. (2008). Detecting environmental change in estuaries:

Nutrient and heavy metal distributions in sediment cores in estuaries from the Gulf of Finland, Baltic Sea. *Estuarine, Coastal and Shelf Science, 76,* 45-56.

Wai, O. W. H., Wang, C. H., Li, Y. S and Li, X. D. (2004). The formation mechanisms of turbidity maximum in the Pearl River estuary, China. *Marine Pollution Bulletin, 48,* 441-448.

Wang, P. (1985). *Marine Micropaleontology of China*. China Ocean Press: China

Wang, S., Cao, Z., Lan, D., Zheng, Z and Li G. (2008). Concentration distribution and assessment of several heavy metals in sediments of the west-four Pearl River Estuary. *Environmental Geology,* 55 (5), 963-975.

Wong, S. C., Li, X. D., Zhang, G., Qi, S. H and Min, Y. S. (2002). Heavy metals in agricultural soils of the Pearl River Delta, South China. *Environmental Pollution, 119*, 33-44.

Wong, C. S. C., Li X. D., Zhang, G., Qi, S.H and Peng, X. Z. (2003). Atmospheric deposition of heavy metals in the Pearl River Delta, China. *Atmospheric Environment, 37,* 767-776.

Wong C. S. C., Wu, S. C., Duzgoren-Aydin, N. S., Aydin, A and Wong, M. H. (2007). Trace metal conamination of sediments in an e-waste processing villiage in China. *Environmental Pollution, 145,* 434-442.

Xia, X. M., Li, Y., Yang, H., Wu, C. Y., Sing, T. H and Pong, H.K. (2004). Observations on the size and settling velocity distributions of suspended sediment in the Pearl River Estuary, China. *Continental Shelf Research, 24,* 1809-1826.

Yanko, V., Arnold, A. J. and Parker, W. C. (2002). Effects of marine pollution on benthic foraminifera. In *Modern Foraminifera* (eds Sen Gupta, B. K), Kluwer Academic Publishers, London. pp. 217-235.

Yang, Q. W., Shu, W. S., Qiu, J. W., Wang, H. B and Lan, C. Y. (2004). Lead in paddy soils and rice plants and its potential health risk around Lechang Lead/Zinc Mine, Guangdong, China. *Environmental International, 30 (7),* 883-889.

Yim, W. W. S and He, X. X. (1988). Holocene foraminifera in Hong Kong and their palaeoenvironmental significance. In *2nd Conference on Palaeoenvironment of East Asia from the mid-Tertiary.* Hong Kong, pp. 787-809.

Yim, W. W. S., Huang, G and Li, Q. Y. (1996). Hydrological Information on Hong Kong waters obtained from the study of holocene sediments. In *Coastal Infrastructure Development in Hong Kong – A Review. Proceedings Synopsis on Hydraulics of Hong Kong Waters.* Hong Kong Government: Hong Kong, pp. 97-113.

Yin, K and Harrison, P. J. (2007). Influence of the Pearl River estuary and vertical mixing in Victoria Harbour on the water quality in relation to eutrophication impacts in Hong Kong waters. *Marine Pollution Bulletin, 54,* 646-656.

Zhang, C and Wang, L (2001). Multi-element geochemistry of sediments from the Pearl River system, China. *Applied Geochemistry, 16,* 1251-1259.

Zhang, G. P., Liu, C. Q., Yang, Y. Q and Wu, P. (2004). Characterization of heavy metals and sulphur isotope in water and sediments of a mine-tailing area rich in carbonate. *Water Air and Soil Pollution, 155 (1-4),* 51-62.

Zhang, S-R., Lu, X. X., Higgitt, D. L., Chen, C-T., Sun, H and Han, J-T. (2007). Water chemistry of the Zhujiang (Pearl River): Natural Processess and anthropogenic influences. *Journal of Geophysical Research, 112* (F1)*,* F01011.

Zhang, S., Li, X. X., Higgitt, D. L., Chen, C-T. A., Han, J and Sun, H. (2008). Recent changes of water discharge and sediment load in the Zhujiang (Pearl River) Basin, China. *Global and Planetary Change, 60*, 365-380.

Zhao, H. T. (1990). Evolution of the Pearl River Estuary. China: Ocean Press, 365pp (in Chinese)

Zhou, H-Y., Peng, X-T and Pan, J-M. (2004). Distribution, source and enrichment of some chemical elements in sediments of the Pearl River Estuary, China. *Continental Shelf Research, 24,* 1857-1875

Zhou, J-M., Dang, Z., Cai, M-F and Lui, C-Q. (2007). Soil Heavy Metal Pollution Around the Dabaoshan Mine, Guangdong Province, China. *Pedosphere, 17 (5),* 588-594).

Zhu, B. Q. (1995). The mapping of geochemical provinces in China based on Pb isotopes. *Journal of Geochemical Exploration, 55,* 171-181.

Zhu, B. Q., Chen, Y. W and Peng, J. H. (2001). Lead isotope geochemistry of the urban environment in the Pearl River Delta. *Applied Geochemisty, 16,* 409-417.

Zong, Y., Lloyd, J. M., Leng, M. J., Yim, W. W-S and Huang, G. (2006). Reconstruction of Holocene monsoon history from the Pearl River Estuary, southern China, using diatoms and carbon isotope ratios. *The Holocene, 16,* 251-263.

Appendices

Appendix A – Matlab Coding and Results

Coding to calculate the the appropriate semivariogram for the spatial data based on the formula below:

$$\gamma(h) = \frac{1}{2n}\sum_{i=1}^{n}\{Z(xi) - Z(xi+h)\}^2$$ (Esri, 2006)

The equation was run as the following Matlab computation, with sampling interval of 100m and a buffer of 10m either side.

```
format long
Ag=dlmread('T:\Ash data\ash_samplepoints_new2.txt');
[M]=size(Ag,1); k=1;
s=1;
for p=1:500:150000
    N=0;
v=1;S1=zeros(M,1);R=zeros(500,1);S2=zeros(M,1);S3=zeros(M,1);S4=zeros(
M,1);meani=zeros(M,1);meanij=zeros(M,1);S10=zeros(M,1);S11=zeros(M,1);
S12=zeros(M,1);
    S13=zeros(M,1);P1=zeros(M,1);P2=zeros(M,1);P3=zeros(M,1);P4=zeros(
M,1);S5=zeros(M,1);S6=zeros(M,1);S7=zeros(M,1);S8=zeros(M,1);S9=zeros(
M,1);
    for i=1:M
        for j=1:M-i
            R(s)=sqrt((Ag(i,1)-Ag(i+j,1)).^2+(Ag(i,2)-Ag(i+j,2)).^2);

            if R(s)>p-100 && R(s)<p+100
                 S1(v)=S1(v)+((Ag(i,3)-Ag(i+j,3)).^2);
                 S4(v)=S4(v)+((Ag(i,4)-Ag(i+j,4)).^2);
                 S10(v)=S10(v)+((Ag(i,5)-Ag(i+j,5)).^2);
                 S11(v)=S11(v)+((Ag(i,6)-Ag(i+j,6)).^2);
                 S12(v)=S12(v)+((Ag(i,7)-Ag(i+j,7)).^2);
                 S13(v)=S13(v)+((Ag(i,8)-Ag(i+j,8)).^2);
%                 S2(v)=S2(v)+(Ag(i,5)*Ag(i+j,5));
%                 S9(v)=S9(v)+(Ag(i,4)*Ag(i+j,4));
%                 S3(v)=S3(v)+((Ag(i,5)-Ag(i+j,5))*(Ag(i,4)-
Ag(i+j,4)));
%                 S5(v)=S5(v)+abs(Ag(i,4)-Ag(i+j,4));
%                 S6(v)=S6(v)+abs(Ag(i,5)-Ag(i+j,5));
%                 S7(v)=S7(v)+sqrt(Ag(i,4)-Ag(i+j,4));
%                 S8(v)=S8(v)+sqrt(Ag(i,5)-Ag(i+j,5));
%
%
P1(N,1)=Ag(i,5);P2(N,1)=Ag(i+j,5);P3(N,1)=Ag(i,4);P4(N,1)=Ag(i+j,4);
                N=N+1;
            else continue
            end
          s=s+1;
        end
       v=v+1;
    end
    NN(k,1)=N;
```

```
    k=k+1;
%      meaniINT=mean(P1(1:N,1));
%      meanijINT=mean(P2(1:N,1));
%      meaniDEM=mean(P3(1:N,1));
%      meanijDEM=mean(P4(1:N,1));
      variogramCo(p,1)=0.5*sum(S1)/N;
      variogramPb(p,1)=0.5*sum(S4)/N;
      variogramTi(p,1)=0.5*sum(S10)/N;
      variogramFe(p,1)=0.5*sum(S11)/N;
      variogramAl(p,1)=0.5*sum(S12)/N;
      variogramCd(p,1)=0.5*sum(S13)/N;
%       crossvariogram(p,1)=(1/N)*sum(S3);
%       covarianceINT(p,1)=0.5*(1/N)*sum(S2)*meaniINT*meanijINT;
%       covarianceDEM(p,1)=0.5*(1/N)*sum(S9)*meaniDEM*meanijDEM;
%      madogramINT(p,1)=0.5*(1/N)*sum(S6)*meaniINT*meanijINT;
%      madogramDEM(p,1)=0.5*(1/N)*sum(S5)*meaniDEM*meanijDEM;
%      rodogramINT(p,1)=0.5*(1/N)*sum(S8)*meaniINT*meanijINT;
%      rodogramDEM(p,1)=0.5*(1/N)*sum(S7)*meaniDEM*meanijDEM;
end
%plot(variogramINT(:,1), 'DisplayName', 'variogramINT(1:45,1)',
'YDataSource', 'variogramINT(1:45,1)',xlabel('-\pi \leq \Theta \leq
\pi')); figure(gcf)

plot(variogramINT(1:500:99501,1), 'DisplayName',
'variogramINT(1:500:99501,1)', 'YDataSource',
'variogramINT(1:500:99501,1)'); figure(gcf)
set(gca,'Xtick',3001:500:99501);
%set(gca,'Xticklable',('3001','3501','4001'));
```

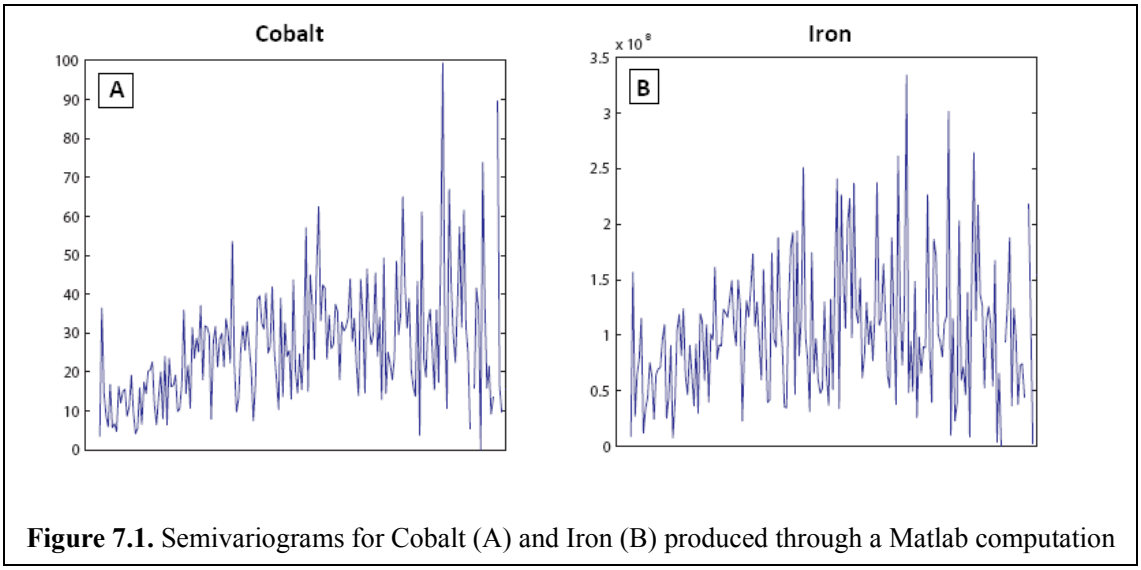

Figure 7.1. Semivariograms for Cobalt (A) and Iron (B) produced through a Matlab computation

This coding produced semivariograms (Co and Fe are shown below in fig. 7.1) which although highly variable, best equate to spherical semivariograms. A kriging function using a spherical semivariogram was used for spatial interpolation.

Appendix B – Surface Samples: Geochemical and Ecotoxicology Data

Geochemistry and Particle Size

Sample ID	Cr (mg/Kg)	Co (mg/Kg)	Cd (mg/Kg)	Ni (mg/Kg)	Cu (mg/Kg)	Zn (mg/Kg)	Ti (mg/Kg)
PE1	129	14.52	2.66	37.31	49.31	178.22	5129
PE2	172	21.87	4.28	65.96	102.92	299.93	6663
PE3	154	21.64	3.23	49.62	64.38	216.82	6197
PE4	124	12.73	0.12	35.78	46.45	167.03	4378
PE5	142	19.77	2.74	52.14	67.64	239.89	5790
PE6	124	20.20	2.36	46.06	60.18	167.70	6136
PE7	113	16.62	2.40	35.18	45.84	136.43	6205
PE8	160	21.54	3.46	63.20	92.57	275.08	7026
PE9	125	21.37	2.87	57.11	78.82	217.56	6553
PE10	127	17.18	1.19	37.03	46.57	133.91	6142
PE11	184	24.68	5.35	76.28	123.62	359.16	6836
PE12	128	20.64	2.73	42.50	59.82	152.51	7262
PE13	114	14.68	4.14	35.51	52.07	219.37	5145
PE14	117	16.16	2.01	41.24	47.48	143.94	4150
PE15	133	16.71	2.47	49.38	70.29	209.27	4924
PE16	88	12.34	1.63	25.77	26.48	105.33	3185
PE17	98	9.25	2.00	31.46	51.84	212.60	3101
PE18	128	18.67	1.93	41.70	41.14	168.35	4464
PE19	144	11.80	1.70	50.36	98.63	295.98	4428
PE20	280	21.03	6.16	112.08	216.32	699.87	5468
PE21	114	8.54	1.30	28.79	16.09	90.41	4513
PE22	114	8.01	1.27	26.48	16.04	81.88	4901
PE23	114	9.05	1.26	31.91	18.39	95.38	4906
PE24	125	9.85	1.33	35.06	19.63	103.56	4966
PE25	92	7.20	1.65	24.37	22.85	71.18	3742
PE26	104	8.32	1.84	27.85	16.38	93.37	4753
PE27	104	9.79	1.31	32.29	20.95	113.35	4802
PE28	95	10.52	1.57	31.12	21.52	94.61	4241
PE29	129	11.52	1.74	37.58	29.17	135.48	5499
PE30	109	9.95	1.50	29.25	22.53	110.42	4699

PE31	112	8.51	0.90	31.26	25.90	98.65	4770
PE32	94	7.42	1.89	24.77	17.54	79.85	4369
PE33	76	5.88	0.95	18.22	16.16	58.86	2671
PE34	106	8.88	1.61	29.52	22.25	90.85	4626
PE35	112	12.59	2.31	34.04	33.85	109.62	4835
PE36	85	5.96	1.33	21.77	19.63	81.32	2752
PE37	79	7.55	0.91	18.77	17.81	66.08	3170
PE38	158	12.91	2.26	38.41	26.70	118.48	5483
PE39	118	9.43	1.84	34.78	34.72	113.65	5145
PE40	132	10.18	1.93	36.08	36.32	124.66	5369
PE42	79.24	12.14	0.76	27.49	34.82	94.77	4465
PE45	65.39	8.60	0.61	18.22	27.97	92.58	2939
PE48	102.97	16.09	5.35	34.39	40.92	117.64	5345
PE50	102.54	16.05	0.70	35.82	37.31	120.89	4996
PE52	105.01	12.81	4.12	25.72	35.50	131.98	5539
PE54	128.97	24.12	2.44	48.18	76.29	148.81	9713
PE55	96.24	17.18	0.77	31.43	46.44	151.75	5380
PE56	90.11	15.72	0.32	31.30	39.47	105.60	5168
PE58	115.43	19.27	1.64	51.61	69.48	202.26	7038
PE59	126.04	20.28	2.36	47.23	67.53	241.19	6462
PE60	64.07	11.74	1.24	19.75	24.46	85.82	3278
PE61	46.96	5.72	2.16	11.15	12.28	44.24	2074
PE62	87.71	13.70	0.08	27.60	34.18	119.02	4977
PE63	124.96	19.07	1.36	51.91	76.88	211.84	6649
PE65	118.97	20.14	0.79	49.40	69.83	205.03	6514
PE66	149.07	20.61	0.57	51.04	59.24	162.86	6022
PE67	134.03	22.21	1.34	50.01	74.40	181.51	7534
PE68	102.58	16.99	5.89	38.69	54.77	180.94	6237
PE69	130.45	18.19	1.09	46.23	64.43	227.50	6253
PE70	116.16	18.01	0.14	43.80	56.65	166.95	6021
PE71	100.97	14.75	0.34	34.46	46.01	146.46	5044
PE73	124.36	18.31	0.52	42.51	58.94	157.21	6828
PE78	196.93	24.57	9.76	74.62	95.21	292.11	6216
PE79	141.63	16.78	4.03	50.35	65.40	201.83	6116

PE80	132.66	16.17	3.85	45.74	62.79	187.10	6166
PE81	142.72	17.54	4.11	50.29	64.65	199.05	6187
PE82	137.48	16.99	4.17	52.95	57.22	185.43	6045
PE83	131.76	15.91	4.85	42.98	57.76	178.25	5810
PE84	141.85	17.31	5.17	47.92	61.65	199.96	6094
PE85	125.87	15.41	3.96	38.66	56.42	144.92	5791
PE86	139.36	17.11	4.44	46.47	61.10	182.34	6099
PE87	121.02	15.04	4.84	35.25	43.74	146.54	5829
PE88	148.32	17.79	8.99	51.55	67.10	200.42	6450
PE89	115.15	19.51	4.77	52.01	68.30	204.95	7006
PE90	119.42	15.76	3.53	39.41	49.30	155.97	5874
PE91	108.90	14.32	3.68	33.31	37.21	128.95	5604
PE92	109.58	14.19	2.96	34.59	38.45	129.95	5501

Sample ID	**Fe (mg/Kg)**	**Al (mg/Kg)**	**Pb (mg/Kg)**	**Summer Salinity (‰)**	**Winter Salinity (‰)**
PE1	36112	20095	47.45	1.9	10.1
PE2	54091	23017	75.14	7.6	16.1
PE3	48384	26544	70.07	15.5	24.2
PE4	34736	26781	61.11	22.1	29.9
PE5	46693	28852	74.95	20.0	26.9
PE6	49730	41676	56.56	17.8	22.8
PE7	41792	27245	42.03	13.5	20.9
PE8	52436	30591	71.62	10.8	18.2
PE9	49500	25713	59.40	6.1	17.1
PE10	42924	28691	50.30	3.9	15.6
PE11	54484	29897	76.41	1.6	5.1
PE12	46172	25175	36.85	0.2	3.0
PE13	35288	27864	62.53	0.0	1.5
PE14	47340	23082	105.91	7.6	16.7
PE15	39199	20584	59.63	3.1	13.4
PE16	32257	22991	37.58	2.2	10.6
PE17	29184	18492	83.69	1.6	8.6
PE18	43047	25640	65.96	0.8	5.7
PE19	36500	24372	87.14	0.3	4.8
PE20	47591	22324	168.01	0.0	2.7

PE21	32365	40370	18.42	33.7	32.8
PE22	35119	49024	17.38	33.8	33.1
PE23	35699	45227	16.88	33.8	33.2
PE24	36384	43290	18.25	33.7	33.2
PE25	25021	38567	23.06	33.7	33.2
PE26	32076	34681	19.63	32.8	32.1
PE27	36896	34566	20.48	32.8	32.1
PE28	37185	30483	23.18	30.0	32.2
PE29	40346	40297	23.08	30.9	31.8
PE30	33780	22396	22.53	32.4	31.8
PE31	33692	28212	22.36	29.1	31.7
PE32	26727	31874	22.11	30.7	32.0
PE33	19687	31061	21.48	31.0	32.1
PE34	31824	30590	22.58	29.3	31.3
PE35	33608	24228	39.69	29.8	31.2
PE36	18682	22234	22.34	29.2	31.1
PE37	34701	19843	28.65	28.6	30.9
PE38	54363	34192	34.25	28.6	30.9
PE39	36875	39985	28.34	21.7	28.0
PE40	38392	29985	35.15	15.8	24.9
PE42	28715	21415	32.21	0.2	3.0
PE45	23954	22614	31.65	-0.2	-0.1
PE48	40227	23361	40.54	-0.1	0.8
PE50	41318	18888	32.01	0.0	2.0
PE52	31030	20103	29.84	0.0	4.0
PE54	53479	20671	35.96	2.0	5.8
PE55	38937	21236	47.90	4.0	10.0
PE56	38400	24555	34.90	4.0	9.0
PE58	49841	23319	55.22	8.0	16.0
PE59	49464	24332	81.12	10.0	22.0
PE60	27240	21999	34.18	14.0	24.5
PE61	14178	14784	21.15	9.0	19.0
PE62	30382	22126	33.86	6.0	16.0
PE63	49376	21595	61.55	8.2	18.0

PE65	48490	25476	66.77	9.7	18.5
PE66	45413	27873	60.80	9.5	18.0
PE67	56243	25464	56.47	10.5	20.5
PE68	42957	23156	59.83	14.5	22.5
PE69	50110	32292	73.38	16.5	25.0
PE70	45751	26890	50.94	20.0	28.2
PE71	38146	26711	55.35	19.0	29.0
PE73	50964	28658	54.61	15.5	25.0
PE78	52267	26796	91.79	13.5	21.8
PE79	48842	30941	65.56	15.2	24.6
PE80	51328	35090	65.79	18.2	26.0
PE81	50329	31066	65.67	15.8	24.9
PE82	46276	27842	61.96	18.6	27.4
PE83	45904	29959	58.89	22.0	29.8
PE84	47911	34416	62.77	20.3	28.2
PE85	42514	30980	50.06	24.0	30.9
PE86	47514	39666	62.31	25.4	32.2
PE87	41472	30712	47.17	27.5	32.4
PE88	51916	38267	66.04	20.0	30.7
PE89	53737	33294	69.40	25.0	32.0
PE90	44925	49253	55.27	26.2	32.6
PE91	39363	30144	44.80	28.2	33.2
PE92	41543	44819	48.53	28.4	33.4

Sample ID	Sand (%)	Silt (%)	Clay (%)	Channel Depth (m)
PE1	32.9	54.3	12.8	4.4
PE2	24.6	46.8	28.6	6.9
PE3	22.3	51.6	26.1	5.0
PE4	35.7	42.8	21.5	4.8
PE5	18.9	52	29.1	4.0
PE6	16.8	55	28.2	5.8
PE7	30.8	51.4	17.8	4.8
PE8	19.9	54.7	25.4	2.8
PE9	24	53.9	22.1	2.1

PE10	12.5	57	30.5	5.0
PE11	12.1	66.6	21.3	2.2
PE12	44	42.8	13.2	4.0
PE13	34.2	54	11.8	3.2
PE14	8.4	59.2	32.4	3.8
PE15	22.6	53.5	24	10.5
PE16	33.3	47.2	19.5	2.5
PE17	42.8	42.2	15	2.1
PE18	34.9	44.4	20.7	2.4
PE19	35.5	50	14.5	2.3
PE20	23.7	52.1	24.2	2.1
PE21	17.3	63.9	18.8	24.0
PE22	14.4	63.9	21.6	25.0
PE23	19.8	55.6	24.6	28.0
PE24	3.4	68.7	27.8	31.0
PE25	21.3	61.1	17.6	21.0
PE26	16.5	66.1	17.4	14.0
PE27	9.9	64.1	26	14.0
PE28	23.5	58.4	18.1	14.0
PE29	15.8	59.4	24.8	8.0
PE30	2.6	66.5	31	35.0
PE31	6.8	60.4	32.8	8.0
PE32	8.3	75.9	15.8	6.0
PE33	29	49.2	21.7	20.0
PE34	18.9	56.2	24.9	11.0
PE35	13.9	56.8	29.3	14.0
PE36	24.9	52.6	22.4	5.0
PE37	47.8	37	15.2	20.0
PE38	11.9	59.9	28.2	8.0
PE39	4	63.8	32.3	4.0
PE40	13.8	62.9	23.3	3.0
PE42	53.6	38.2	8.2	2.2
PE45	65.6	27.1	7.3	1.8
PE48	24.8	54.5	20.7	2.3

PE50	8.3	61	30.7	3.2
PE52	20.5	66.6	12.9	4.1
PE54	6.6	70.8	22.6	6.0
PE55	55.8	37	7.3	8.0
PE56	20.6	52.2	27.2	3.5
PE58	12.5	58.3	29.2	10.0
PE59	12.7	63.4	23.9	15.0
PE60	63.2	28.2	8.6	18.0
PE61	42.5	39.5	17.9	16.0
PE62	37.8	51	11.2	8.0
PE63	9.3	63.7	27	5.5
PE65	12.8	52.7	34.5	5.0
PE66	22	46.9	31.1	3.5
PE67	7.1	54.6	38.3	13.0
PE68	19.9	61.6	18.4	12.0
PE69	12.5	54.1	33.3	13.5
PE70	15.7	53	31.3	20.0
PE71	15.8	55.8	28.4	13.0
PE73	18.4	52.7	28.9	15.0
PE78	20.3	46.5	33.2	6.2
PE79	9	58.6	32.5	5.3
PE80	13.7	51.1	35.2	5.8
PE81	16.1	52.6	31.3	5.3
PE82	16.9	54.9	28.2	7.0
PE83	14.7	55.6	29.7	6.0
PE84	15.4	55.1	29.5	6.8
PE85	19.6	55.2	25.2	8.5
PE86	17.1	54.2	28.7	6.0
PE87	20.9	58.9	20.2	8.5
PE88	16	53.8	30.2	6.3
PE89	14.8	59.6	25.6	8.5
PE90	18.6	57.1	24.3	8.5
PE91	16.9	63.3	19.8	11.5
PE92	15.9	62.6	21.5	14.0

Foraminifera Ecotoxicology

Sample ID	Benthic Zone	Total Tests	Total Deformed	Deformations (%)
PE23	1	231	3	1.3
PE28	1	264	4	1.51
PE37	2	243	3	1.28
PE40	2	246	4	1.63
PE64	4	85	1	1.18
PE72	3	204	3	1.47
PE78	4	75	0	0
PE81	5	93	2	2.15
PE88	3	76	1	1.32
PE90	5	233	2	0.86

Appendix C – Short Core Analysis

Core PRE 2: Heavy Metal Concentrations (mg/Kg)

Depth (cm)	Cr	Co	Ni	Cu	Zn	Cd	Pb
0	94	14.77	31.25	38.48	131	0.22	50.91
2	110	17.15	39.91	46.41	148	0.25	52.12
4	108	16.29	36.91	44.77	142	0.25	51.45
6	109	16.21	36.15	42.82	140	0.23	51.37
8	107	16.18	37.09	44.15	143	0.24	50.21
10	89	14.68	32.12	38.10	135	0.21	45.90
12	114	17.16	38.05	45.09	139	0.32	48.89
14	117	17.97	40.97	52.70	150	0.25	49.28
16	113	17.43	40.68	50.92	149	0.24	49.35
18	113	16.99	39.29	46.56	145	0.25	50.29
20	105	16.18	37.12	43.11	137	0.24	47.14
22	116	17.20	40.56	48.76	145	0.25	45.11
24	119	17.62	41.66	49.90	146	0.30	48.81
26	117	16.78	38.36	47.90	139	0.26	46.81
28	112	17.94	40.20	48.59	142	0.28	45.57
30	122	18.43	43.22	51.53	147	0.35	50.85
32	107	16.59	36.07	44.26	135	0.22	46.85
34	119	18.01	39.75	48.35	147	0.27	57.72
36	109	16.66	38.95	44.72	136	0.21	48.86
38	112	16.98	39.24	47.87	138	0.24	49.91

Core PRE 3: Heavy Metal Concentrations (mg/Kg)

Depth (cm)	Pb	Cd	Co	Cu	Ni
0	77.96	0.22	15.71	43.25	36.44
2	75.66	0.21	14.72	37.16	33.90
4	56.55	0.24	16.37	41.97	37.64
6	52.24	0.20	15.25	39.62	35.47

8	51.16	0.19	14.02	34.72	31.46
10	48.98	0.20	14.06	37.12	31.91
12	54.33	0.21	14.90	36.97	33.70
14	50.12	0.20	13.93	34.80	36.03
16	51.33	0.20	14.17	35.54	32.01
18	53.50	0.17	14.27	35.74	32.52
20	51.97	0.17	13.84	35.10	31.61
22	62.35	0.22	16.45	41.16	37.71
24	53.23	0.19	14.29	35.14	32.06
26	53.67	0.25	13.87	34.50	30.92
28	56.26	0.23	15.35	37.82	35.22
30	53.84	0.22	14.34	36.96	32.96
34	54.02	0.16	14.33	36.66	34.09
38	57.45	0.19	15.20	42.33	36.48
42	55.19	0.21	14.98	39.54	36.08
46	53.71	0.16	14.32	37.85	34.04
50	51.72	0.22	13.58	34.97	31.10
58	52.48	0.22	13.92	34.48	32.35
66	60.28	0.28	14.43	161.42	62.69
74	53.56	0.24	15.39	54.14	39.07
82	53.71	0.23	13.04	147.89	44.71
90	59.30	0.23	12.22	127.22	44.29
98	55.45	0.19	11.36	158.52	48.22

Depth (cm)	**Zn**	**Cr**	**Al**	**Fe**
0	143	110	11332	22953
2	133	97	12575	21975
4	145	116	11975	24334
6	137	104	9789	22376
8	127	99	11444	20584
10	129	97	10568	20847
12	135	111	12278	22362
14	126	95	10398	20507
16	130	101	11582	20981

18	131	99	13043	21451
20	127	100	12832	20861
22	151	119	12411	24526
24	131	95	11463	21175
26	127	102	11171	21198
28	140	100	10598	23416
30	139	80	11803	21785
34	137	103	12197	21871
38	147	101	12926	23529
42	149	101	9891	22751
46	139	103	12934	21785
50	128	99	11624	20121
58	131	97	9786	20797
66	210	123	10894	20584
74	146	107	9506	22132
82	178	121	11447	19196
90	173	129	11435	18137
98	181	131	14768	18609

Core PRE 4: Heavy Metal Concentrations (mg/Kg)

Depth (cm)	Pb	Co	Cu	Ni
0	93.72	19.02	71.62	56.02
6	68.87	18.86	68.12	53.86
8	72.19	19.77	74.41	61.50
10	69.97	18.87	69.60	55.25
12	76.68	18.82	69.34	53.32
14	72.69	19.62	70.61	53.15
16	60.38	18.83	60.98	46.57
18	69.04	18.79	67.56	44.90
20	68.66	19.02	63.99	50.58
22	52.20	20.26	64.55	51.54
24	51.50	20.45	61.48	49.39
26	50.50	20.70	60.74	49.00

28	49.22	19.98	60.50	48.37
30	51.27	20.13	61.73	49.48
32	50.19	20.38	61.59	49.18
34	50.21	20.32	61.52	49.78
36	47.74	20.41	59.78	47.62
38	45.44	19.05	56.71	45.02
40	49.72	20.44	61.41	49.05
44	41.48	20.18	62.15	48.17
48	38.80	22.15	71.16	52.71
52	39.80	21.37	66.78	50.98
56	38.37	21.12	64.93	49.73
60	39.82	21.55	66.34	52.15
68	42.65	21.19	63.41	51.09
76	37.60	21.59	65.98	49.57
84	39.00	21.78	68.78	51.26

Depth (cm)	**Zn**	**Cr**	**Al**	**Fe**
0	256	135	11866	25237
6	253	134	10257	24892
8	267	146	11879	25998
10	256	128	9553	25470
12	253	130	11103	24968
14	254	135	11385	25961
16	194	128	10283	25223
18	192	119	13144	25203
20	231	128	11655	25324
22	182	135	12560	27129
24	170	135	11410	27475
26	169	133	10907	27628
28	168	132	12142	27256
30	170	134	10443	27371
32	170	135	11896	27277
34	169	136	11727	27348
36	164	131	10347	26440

38	188	124	10300	25181
40	172	135	10079	27078
44	157	125	8541	26304
48	160	143	10501	28687
52	159	139	10845	28400
56	156	134	10929	27297
60	161	143	11205	28369
68	162	141	11492	28378
76	154	128	8589	27530
84	157	141	11181	27966

Core PRE 2: Carbon and Nitrogen Bulk Composition (%) and C/N Ratio

Depth (cm)	C	N	C/N
0	1.098	0.246	4.462914
2	1.241	0.246	5.048007
4	1.101	0.234	4.711168
6	0.850	0.214	3.977549
8	0.990	0.193	5.124741
10	0.825	0.171	4.815528
12	0.991	0.149	6.651007
14	0.987	0.102	9.684004
16	0.997	0.153	6.532591
18	0.898	0.145	6.203729
20	0.827	0.131	6.311569
22	0.892	0.132	6.747826
24	0.845	0.128	6.581549
26	0.840	0.120	7.025105
28	0.961	0.112	8.562138
30	0.893	0.115	7.772075
32	0.714	0.104	6.897151
34	1.027	0.107	9.63679
36	0.897	0.107	8.379262
38	0.901	0.098	9.155917

Core PRE 3: Carbon and Nitrogen Bulk Composition (%) and C/N Ratio

Depth (cm)	C	N	C/N
0	0.799	0.040	20.01754
2	0.813	0.051	15.94118
4	0.897	0.043	21.01639
6	0.887	0.044	20.1959
8	0.881	0.038	23.3634
10	0.824	0.032	25.84013
12	0.862	0.031	27.46497
14	0.796	0.039	20.45244
16	0.921	0.034	27.09412
18	0.890	0.033	26.87311
20	0.973	0.038	25.47382
22	1.040	0.044	23.47856
24	1.113	0.037	30.25272
26	0.946	0.036	26.06887
28	0.991	0.036	27.7619
30	0.985	0.041	24.14461
34	0.984	0.033	29.8303
38	0.919	0.031	29.65161
42	0.831	0.031	26.88673
46	1.018	0.034	30.20475
50	0.788	0.032	24.32099
58	0.784	0.023	33.78448
66	1.061	0.034	30.93294

Core PRE 4: Carbon and Nitrogen Bulk Composition (%) and C/N Ratio

PRE4	C	N	C/N
0	2.094	0.112	18.64648
6	1.250	0.107	11.68037
8	1.245	0.112	11.1586
10	1.231	0.110	11.18764

12	1.170	0.107	10.89106
14	1.234	0.109	11.36464
16	1.156	0.095	12.17483
18	1.280	0.098	13.05456
20	1.219	0.103	11.88499
22	1.134	0.101	11.26279
24	1.103	0.095	11.60863
26	1.078	0.099	10.90091
28	1.016	0.097	10.53161
30	1.032	0.095	10.90755
32	1.110	0.094	11.82215
34	1.020	0.088	11.55606
36	0.881	0.071	12.41268
38	0.969	0.069	14.04493
40	1.021	0.069	14.81858
44	0.979	0.074	13.20783
48	0.893	0.062	14.3141
52	0.905	0.063	14.36984
56	0.903	0.059	15.42906
60	0.871	0.053	16.37782
68	0.912	0.065	14.12229
76	0.873	0.045	19.31195
84	0.868	0.039	22.3162

Carbon and Nitrogen Bulk Composition (%) and C/N Ratio: Quality Control

Blanks

	Area signal (mV.s)	
	N	**C**
Calibration Blank	218	522
Sample blank 1	286	490
Sample blank 2	358	380

Sample blank 3	268	440

CRM

	N (%)	C (%)
ref values	0.46	6.52
crm (B2150)	0.4616	6.4012
% recovery	100.35	98.2
crm (B2150)	0.4696	6.5080
% recovery	102.09	99.82

AQC

	%N	%C
aqc 1	16.16	42.09
% bias	99.34	100.60
aqc 2	16.15	41.87
% bias	99.27	100.08

Repeats

	%N	%C
PRE2/14	0.1019	0.9868
PRE2/14REPEAT	0.10225	1.004
% relative difference	0.34	1.73

	%N	%C
PRE4/32	0.0939	1.1101
PRE4/32REPEAT	0.0938	1.0826
% relative difference	0.11	2.51

Core PRE 2: Stable Pb Isotope Composition

Depth (cm)	^{206}Pb	^{207}Pb	^{208}Pb	^{204}Pb	$^{206}Pb/^{207}Pb$	$^{208}Pb/^{207}Pb$
0	0.2525	0.2102	0.5240	0.0130	1.2014	2.4933
2	0.2522	0.2107	0.5238	0.0130	1.1970	2.4866
4	0.2523	0.2102	0.5243	0.0130	1.2006	2.4948
6	0.2525	0.2103	0.5240	0.0130	1.2005	2.4913
8	0.2525	0.2102	0.5242	0.0130	1.2014	2.4941
10	0.2528	0.2100	0.5238	0.0130	1.2040	2.4944
12	0.2525	0.2100	0.5238	0.0130	1.2024	2.4944
14	0.2525	0.2105	0.5235	0.0130	1.1995	2.4869
16	0.2533	0.2097	0.5235	0.0130	1.2083	2.4968
18	0.2533	0.2102	0.5235	0.0130	1.2054	2.4909
20	0.2527	0.2102	0.5240	0.0130	1.2022	2.4933
22	0.2530	0.2102	0.5235	0.0130	1.2038	2.4909
24	0.2535	0.2100	0.5233	0.0130	1.2071	2.4921
26	0.2528	0.2100	0.5238	0.0130	1.2040	2.4944
28	0.2533	0.2098	0.5238	0.0130	1.2073	2.4964
30	0.2520	0.2095	0.5250	0.0130	1.2029	2.5060
32	0.2523	0.2098	0.5250	0.0130	1.2025	2.5020
34	0.2527	0.2100	0.5238	0.0130	1.2032	2.4944
36	0.2523	0.2098	0.5247	0.0130	1.2025	2.5004
38	0.2525	0.2100	0.5240	0.0130	1.2024	2.4952

Core PRE 3: Stable Pb Isotope Composition

Depth (cm)	^{206}Pb	^{207}Pb	^{208}Pb	^{204}Pb	$^{206}Pb/^{207}Pb$	$^{208}Pb/^{207}Pb$
0	0.2517	0.2108	0.5242	0.0130	1.1937	2.4862
2	0.2515	0.2103	0.5245	0.0132	1.1957	2.4937
4	0.2522	0.2100	0.5245	0.0130	1.2008	2.4976
6	0.2525	0.2098	0.5242	0.0130	1.2033	2.4980
8	0.2522	0.2102	0.5247	0.0130	1.1998	2.4964
10	0.2522	0.2100	0.5243	0.0130	1.2008	2.4968

12	0.2520	0.2102	0.5243	0.0130	1.1990	2.4948
14	0.2522	0.2100	0.5247	0.0130	1.2008	2.4984
16	0.2527	0.2098	0.5242	0.0130	1.2041	2.4980
18	0.2525	0.2098	0.5247	0.0130	1.2033	2.5004
20	0.2523	0.2102	0.5243	0.0130	1.2006	2.4948
22	0.2520	0.2100	0.5248	0.0130	1.2000	2.4992
24	0.2522	0.2102	0.5248	0.0130	1.1998	2.4972
26	0.2513	0.2100	0.5255	0.0130	1.1968	2.5024
28	0.2515	0.2098	0.5257	0.0130	1.1986	2.5052
30	0.2513	0.2098	0.5258	0.0130	1.1978	2.5060
34	0.2520	0.2098	0.5250	0.0130	1.2010	2.5020
38	0.2512	0.2098	0.5255	0.0130	1.1970	2.5044
42	0.2517	0.2102	0.5250	0.0130	1.1975	2.4980
46	0.2512	0.2102	0.5255	0.0130	1.1951	2.5004
50	0.2517	0.2103	0.5250	0.0130	1.1965	2.4960
58	0.2512	0.2105	0.5255	0.0130	1.1932	2.4964
66	0.2508	0.2102	0.5257	0.0130	1.1935	2.5012
74	0.2515	0.2103	0.5257	0.0130	1.1957	2.4992
82	0.2513	0.2098	0.5255	0.0130	1.1978	2.5044
90	0.2518	0.2098	0.5255	0.0130	1.2002	2.5044
98	0.2515	0.2097	0.5258	0.0130	1.1995	2.5079

Core PRE 4: Stable Pb Isotope Composition

Depth (cm)	^{206}Pb	^{207}Pb	^{208}Pb	^{204}Pb	^{206}Pb/^{207}Pb	^{208}Pb/^{207}Pb
0	0.2503	0.2108	0.5253	0.0130	1.1874	2.4917
6	0.2508	0.2108	0.5255	0.0130	1.1897	2.4925
8	0.2508	0.2112	0.5250	0.0130	1.1878	2.4862
10	0.2520	0.2105	0.5243	0.0130	1.1971	2.4909
12	0.2510	0.2110	0.5245	0.0130	1.1896	2.4858
14	0.2513	0.2108	0.5243	0.0130	1.1921	2.4870
16	0.2518	0.2105	0.5245	0.0130	1.1964	2.4917
18	0.2515	0.2110	0.5245	0.0130	1.1919	2.4858

20	0.2512	0.2108	0.5245	0.0130	1.1913	2.4877
22	0.2525	0.2102	0.5243	0.0130	1.2014	2.4948
24	0.2520	0.2102	0.5248	0.0130	1.1990	2.4972
26	0.2525	0.2102	0.5245	0.0130	1.2014	2.4956
28	0.2518	0.2103	0.5248	0.0130	1.1973	2.4952
30	0.2523	0.2102	0.5247	0.0130	1.2006	2.4964
32	0.2522	0.2098	0.5245	0.0130	1.2017	2.4996
34	0.2523	0.2102	0.5242	0.0130	1.2006	2.4941
36	0.2523	0.2100	0.5247	0.0130	1.2016	2.4984
38	0.2523	0.2100	0.5243	0.0130	1.2016	2.4968
40	0.2522	0.2103	0.5243	0.0130	1.1989	2.4929
44	0.2533	0.2098	0.5235	0.0130	1.2073	2.4948
48	0.2535	0.2097	0.5242	0.0130	1.2091	2.5000
52	0.2530	0.2097	0.5243	0.0130	1.2067	2.5008
56	0.2530	0.2093	0.5240	0.0130	1.2086	2.5032
60	0.2528	0.2098	0.5243	0.0130	1.2049	2.4988
68	0.2528	0.2097	0.5245	0.0130	1.2059	2.5016
76	0.2530	0.2095	0.5245	0.0130	1.2076	2.5036
84	0.2530	0.2098	0.5242	0.0130	1.2057	2.4980

Stable Pb Isotope Composition: Quality Control

AQC

		^{206}Pb	^{207}Pb	^{208}Pb	^{204}Pb		^{206}Pb	^{207}Pb	^{208}Pb	^{204}Pb
aqc	Ratio Mean	1	0.913	2.155	0.059	average ratio fraction	0.24	0.22	0.52	0.01
Certified value (SRM 981)		1	0.915	2.168	0.059		0.24	0.22	0.52	0.01
	% diff	100.0	99.8	99.4	99.9	% diff	100.4	100.1	99.7	98.2
aqc	Ratio Mean	1	0.912	2.161	0.059	average ratio fraction	0.24	0.22	0.52	0.01

Certified value (SRM 981)		1	0.915	2.168	0.059		0.24	0.22	0.52	0.01
	% diff	100.0	99.7	99.7	99.9	% diff	100.2	100.0	99.9	98.2
aqc	Ratio Mean	1	0.917	2.181	0.059	average ratio fraction	0.24	0.22	0.53	0.01
Certified value (SRM 981)		1	0.915	2.168	0.059		0.24	0.22	0.52	0.01
	% diff	100.0	100.3	100.6	99.9	% diff	99.7	99.9	100.3	98.2
aqc	Ratio Mean	1	0.918	2.175	0.058	average ratio fraction	0.24	0.22	0.52	0.01
Certified value (SRM 981)		1	0.915	2.168	0.059		0.24	0.22	0.52	0.01
	% diff	100.0	100.4	100.3	98.2	% diff	99.9	100.2	100.1	98.2

Repeats

Sample ID		$^{206}Pb/^{206}Pb$	$^{207}Pb/^{206}Pb$	$^{208}Pb/^{206}Pb$	$^{204}Pb/^{206}Pb$
PRE 2_ 02	Ratio Mean	1.0000	0.8350	2.0780	0.0520
	Ratio %RSD	0.0000	0.3850	0.2180	0.7720
PRE 2_ 02 Repeat	Ratio Mean	1.0000	0.8310	2.0780	0.0530
	Ratio %RSD	0.0000	0.7810	0.6970	0.8890
	% relative diff		0.48	0.00	1.90
PRE 2_ 08	Ratio Mean	1.0000	0.8330	2.0770	0.0520
	Ratio %RSD	0.0000	0.4350	0.4110	0.5680
PRE 2_ 08 Repeat	Ratio Mean	1.0000	0.8310	2.0700	0.0520
	Ratio %RSD	0.0000	0.5010	0.3890	0.6160
	% relative diff		0.24	0.34	0.00

PRE 2_ 10	Ratio Mean	1.0000	0.8310	2.0720	0.0530
	Ratio %RSD	0.0000	0.5900	0.4440	0.4830
PRE 2_ 10 Repeat	Ratio Mean	1.0000	0.8320	2.0710	0.0530
	Ratio %RSD	0.0000	0.1170	0.4010	0.4920
	% relative diff		0.12	0.05	0.00
PRE 3_ 98	Ratio Mean	1.0000	0.8350	2.0930	0.0530
	Ratio %RSD	0.0000	0.1540	0.2410	0.4480
PRE 3_ 98 Repeat	Ratio Mean	1.0000	0.8330	2.0900	0.0530
	Ratio %RSD	0.0000	0.2650	0.2940	0.5480
	% relative diff		0.24	0.14	0.00
PRE 4_ 06	Ratio Mean	1.0000	0.8400	2.0950	0.0530
	Ratio %RSD	0.0000	0.1440	0.2660	0.3740
PRE 4_ 06 repeat	Ratio Mean	1.0000	0.8410	2.0960	0.0530
	Ratio %RSD	0.0000	0.2900	0.3140	0.3620
	% relative diff		0.12	0.05	0.00

Sample ID		^{206}Pb	^{207}Pb	^{208}Pb	^{204}Pb
PRE 2_ 02	average ratio fraction	0.2522	0.2107	0.5238	0.0130
PRE 2_ 02 Repeat	average ratio fraction	0.2523	0.2097	0.5243	0.0130
	% relative diff	0.07	0.48	0.10	0.00
PRE 2_ 08	average ratio fraction	0.2525	0.2102	0.5242	0.0130
PRE 2_ 08 Repeat	average ratio fraction	0.2528	0.2102	0.5235	0.0130
	% relative diff	0.13	0.00	0.13	0.00

PRE 2_ 10	average ratio fraction	0.2528	0.2100	0.5238	0.0130
PRE 2_ 10 Repeat	average ratio fraction	0.2530	0.2103	0.5237	0.0130
	% relative diff	0.07	0.16	0.03	0.00
PRE 2_ 36	average ratio fraction	0.2518	0.2100	0.5248	0.0130
PRE 2_ 36 Repeat	average ratio fraction	0.2523	0.2098	0.5247	0.0130
	% relative diff	0.20	0.08	0.03	0.00
PRE 3_ 98	average ratio fraction	0.2513	0.2098	0.5260	0.0130
PRE 3_ 98 Repeat	average ratio fraction	0.2515	0.2097	0.5258	0.0130
	% relative diff	0.07	0.08	0.03	0.00
PRE 4_ 06	average ratio fraction	0.2508	0.2108	0.5255	0.0130
PRE 4_ 06 repeat	average ratio fraction	0.2507	0.2110	0.5252	0.0130
	% relative diff	0.07	0.08	0.06	0.00

Core PRE 3: ^{210}Pb and ^{137}Cs Activity

SAMPLE						
ID	**Upper Depth (cm)**	**Lower Depth (cm)**	**Mid Depth (cm)**	**Segment Size (cm)**	**Core**	**Dry Bulk Density (g/cm^3)**
1B	0.00	2.00	1.00	2.00	PRE 3	0.23
2B	8.00	10.00	9.00	2.00	PRE 3	0.23
3B	16.00	18.00	17.00	2.00	PRE 3	0.24
4B	24.00	26.00	25.00	2.00	PRE 3	0.21
5B	32.00	34.00	33.00	2.00	PRE 3	0.21
6B	40.00	42.00	41.00	2.00	PRE 3	0.22

7B	48.00	50.00	49.00	2.00	PRE 3	0.21
8B	56.00	58.00	57.00	2.00	PRE 3	0.22
9B	64.00	66.00	65.00	2.00	PRE 3	0.19
10B	72.00	74.00	73.00	2.00	PRE 3	0.24
11B	80.00	82.00	81.00	2.00	PRE 3	0.22
12B	88.00	90.00	89.00	2.00	PRE 3	0.19
13B	96.00	98.00	97.00	2.00	PRE 3	0.18

ACTIVITIES								
ID	**^{137}Cs**	**Error (1σ)**	**Total ^{210}Pb**	**Error (1σ)**	**^{214}Pb [^{226}Ra] (supported ^{210}Pb)**	**Error (1σ)**	**Excess ^{210}Pb (Unsupported ^{210}Pb)**	**Error (1σ)**
	(mBq/g)	**(mBq/g)**	**(mBq/g)**	**(mBq /g)**	**(mBq/g)**	**(mBq/g)**	**(mBq/g)**	**(mBq/g)**
1B	0.01	0.01	69.47	2.98	44.12	1.26	25.35	2.12
2B	0.01	0.01	44.25	2.83	48.37	1.21	-4.12	2.02
3B	0.02	0.02	46.04	4.74	46.61	2.07	-0.57	3.40
4B	0.01	0.01	48.15	3.90	44.66	1.19	3.49	2.55
5B	0.02	0.02	50.43	4.70	46.15	1.45	4.28	3.07
6B	0.02	0.02	55.32	5.09	53.51	2.03	1.81	3.56
7B	2.74	0.41	51.54	4.18	55.88	2.01	-4.34	3.09
8B	0.01	0.01	44.81	3.81	43.57	1.08	1.24	2.45
9B	0.01	0.01	46.66	4.06	51.42	1.63	-4.76	2.84
10B	2.21	0.32	56.41	3.28	55.64	1.54	0.78	2.41
11B	0.68	0.35	52.15	4.23	47.79	1.32	4.37	2.77
12B	0.94	0.38	65.38	4.59	67.32	1.98	-1.94	3.29
13B	2.08	0.35	70.30	4.18	76.59	1.87	-6.29	3.03

Core PRE 4: ^{210}Pb and ^{137}Cs Activity

SAMPLE						
ID	Upper Depth (cm)	Lower Depth (cm)	Mid Depth (cm)	Segment Size (cm)	Core	Dry Bulk Density (g/cm^3)
1A	0.00	2.00	10.00	2	PRE 4	0.14
2A	7.00	9.00	8.00	2	PRE 4	0.19
3A	14.00	16.00	15.00	2	PRE 4	0.17
4A	21.00	23.00	22.00	2	PRE 4	0.19
5A	28.00	30.00	29.00	2	PRE 4	0.21
6A	35.00	37.00	36.00	2	PRE 4	0.20
7A	42.00	44.00	43.00	2	PRE 4	0.22
8A	49.00	51.00	50.00	2	PRE 4	0.23
9A	56.00	58.00	57.00	2	PRE 4	0.24
10A	63.00	65.00	64.00	2	PRE 4	0.22
11A	70.00	72.00	71.00	2	PRE 4	0.21
12A	77.00	79.00	78.00	2	PRE 4	0.22
13A	84.00	86.00	85.00	2	PRE 4	0.18

ACTIVITIES								
ID	^{137}Cs (mBq/g)	Error (1σ) (mBq/g)	Total ^{210}Pb (mBq/g)	Error (1σ) (mBq /g)	^{214}Pb [^{226}Ra] (supported ^{210}Pb) (mBq/g)	Error (1σ) (mBq/g)	Excess ^{210}Pb (Unsupported ^{210}Pb) (mBq/g)	Error (1σ) (mBq/g)
1A	1.22	0.29	76.80	2.90	41.31	0.87	35.49	1.89
2A	1.67	0.30	77.75	3.11	41.1	0.91	36.65	2
3A	1.88	0.49	62.61	4.53	36.11	1.35	26.49	2.94
4A	3.39	0.34	69.30	3.89	34.53	1.05	34.77	2.47
5A	2.41	0.55	67.95	3.76	40.15	1.55	27.81	2.66
6A	4.15	0.38	66.98	3.29	44.80	1.50	22.18	2.40
7A	1.36	0.54	54.79	4.20	38.20	1.26	16.59	2.73
8A	0.03	0.59	51.50	4.21	40.02	1.69	11.48	2.95
9A	2.17	0.37	49.06	3.77	40.10	1.75	8.96	2.76

10A	0.52	0.40	42.19	3.59	35.97	1.02	6.22	2.31
11A	0.71	0.75	40.77	3.55	39.36	1.40	1.40	2.48
12A	1.22	0.29	40.52	3.12	38.73	1.40	1.79	2.26
13A	0.03	0.77	32.89	3.95	30.61	1.04	2.28	2.50